FOR PUBLIC RELEASE
PL/PA 16 DEC 96

Sensor and Simulation Notes
Note 156

18 September 1972

# A Technique for Simulating the System Generated Electromagnetic Pulse Resulting from an Exoatmospheric Nuclear Weapon Radiation Environment

Carl E. Baum
Air Force Weapons Laboratory

## Abstract

This note discusses a new EMP simulator concept, one for simulating the system generated EMP in exoatmospheric regions. It uses a pulsed photon source (Bremsstrahlung or otherwise) illuminating a space system in a vacuum chamber. There are various important features which improve the simulation quality. This type of simulator can use electron backscatter reduction from the tank walls as well as use electron repelling grids. The photons can be appropriately collimated to remove those not incident on the space system and "get lost" holes can be used to reduce backscatter from the vacuum tank associated with the main photon beam in the case of high energy photons. The required vacuum in the chamber is related to the electron collisions with the gas and to electrical breakdown. The electromagnetic interactions of the space system with the test chamber are rather important. These include capacitance to the chamber walls, cavity resonances, and reflection of higher frequencies from the cavity walls. Capacitance is associated with the chamber size. Cavity resonances can be damped and high frequency reflections reduced by the use of appropriate lossy materials near the cavity walls. Various figures of merit can be defined to quantitatively characterize the deviation of various simulator parameters from those of the environment being simulated.

DI 96-1615

## Foreword

This note has been long overdue. I began writing it over a year ago at which time I wrote what are roughly the first three sections. The antiquity of this note became apparent when I picked it up more recently to finish it and noticed that I was listed as Captain on the draft. Unfortunately too many other reports interferred with the completion of this report until recently. The general concept for this type of simulator is then over a year old as are the major features which go together to make up this type of simulator. Some of the quantitative information (regarding damping and reflection reduction) is of recent origin but the general concepts are older. In a recent note on the various types of EMP simulators I discussed the major features very briefly.[1] This note is the detailed note discussing this type of simulator. I would like to thank Sgt. Robert Marks of AFWL and Terry Brown and Joe Martinez of Dikewood for the computer calculations for the numbers in sections V through IX. Some of these calculations gave clues to simplifying the analytic expressions and make certain numerical calculations unnecessary.

Table of Contents

List of Tables

## List of Illustrations

# I. Introduction

The nuclear electromagnetic pulse (EMP) comes in several varieties. Depending on the type of situation of concern the EMP can have different characteristics in its spatial distribution and in its time domain waveforms and frequency domain spectra. Furthermore the interaction of the EMP with objects of interest can be strongly dependent on the conductivity of any source region in contact with it and the electron transport around it even in a vacuum.[2] Consider some general space vehicle such as a satellite as shown in figure 1.1. Let us divide the EMP cases into two basic types: source region and non source region. Figure 1.1A shows the source region case where the nuclear weapon detonation point has a clear line of sight to the space vehicle so that an intense pulse of $\gamma$ rays and X rays travels at the speed of light and produces high energy electrons by interaction with the object thereby creating the source region in the vicinity of the object. This is the system generated EMP. Of course there are EMP signals propagated from the detonation point to the space vehicle but due to the small size of the source region these signals are not very large, at least from an EMP standpoint.[3,4] In contrast to this situation figure 1.1B shows the case that a large EMP source region in the atmosphere of the earth radiates an EMP out to the space system. The detonation point may be deep in the atmosphere or, of greater interest, it may be a high altitude detonation with a quite large atmospheric source region with a propagation path missing the earth's surface and reaching the space vehicle after passing through a portion of the ionosphere. This propagated and dispersed EMP is not considered in this note, but there are techniques to simulate this which will hopefully be considered in some future notes.

Considering then the general case shown in figure 1.1A we have the general problem of the system generated EMP plus other effects associated with the nuclear radiation (of all types). For this case there are TRE phenomena in the system electronics associated with the same $\gamma$ rays and X rays (travelling at the speed of light to the space vehicle) which also produce the system generated EMP. While our considerations here are primarily concerned with simulating the system generated EMP using high energy photons, TRE interactions inevitably accompany such simulation.

In the system generated EMP it is the presence of the system itself in the photon flux which produces the EMP source region. As illustrated in figure 1.2 the $\gamma$ rays and X rays from the nuclear detonation travel from the nuclear detonation at the speed of light and are essentially unattenuated on the way to the space vehicle; the pulse width (time spread) is also essentially the same as at the detonation position. On interacting with the space vehicle these photons produce various effects such as the direct TRE effects on the electronic

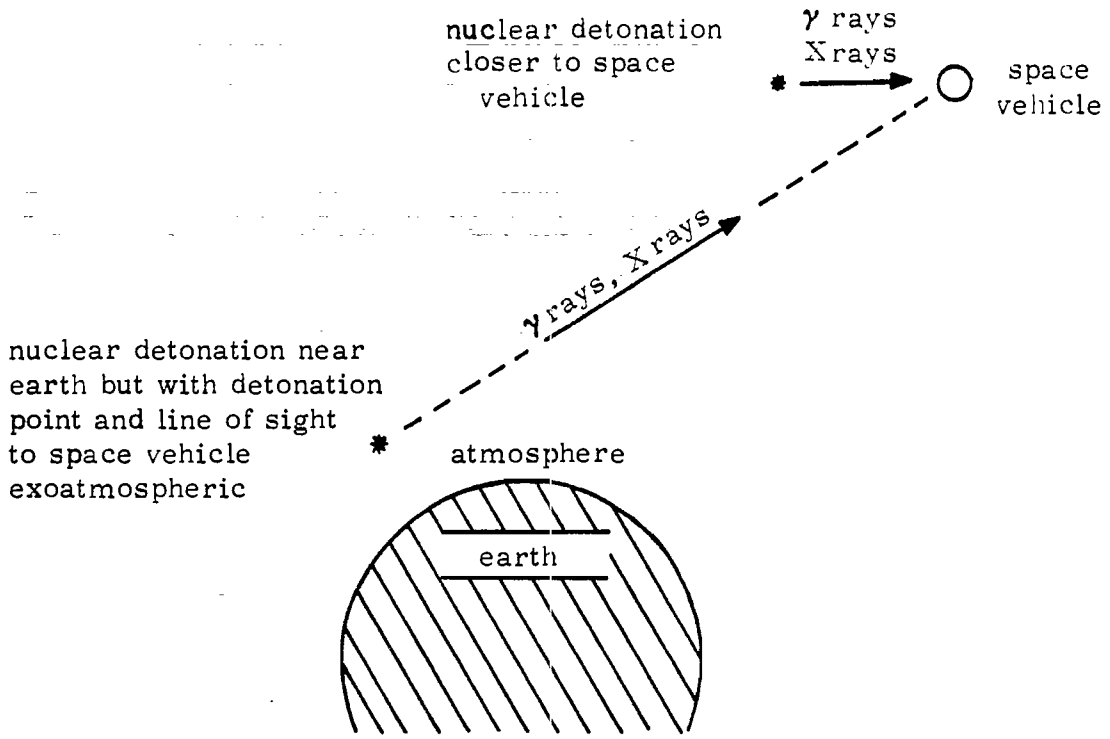


A. System generated EMP from nuclear radiation

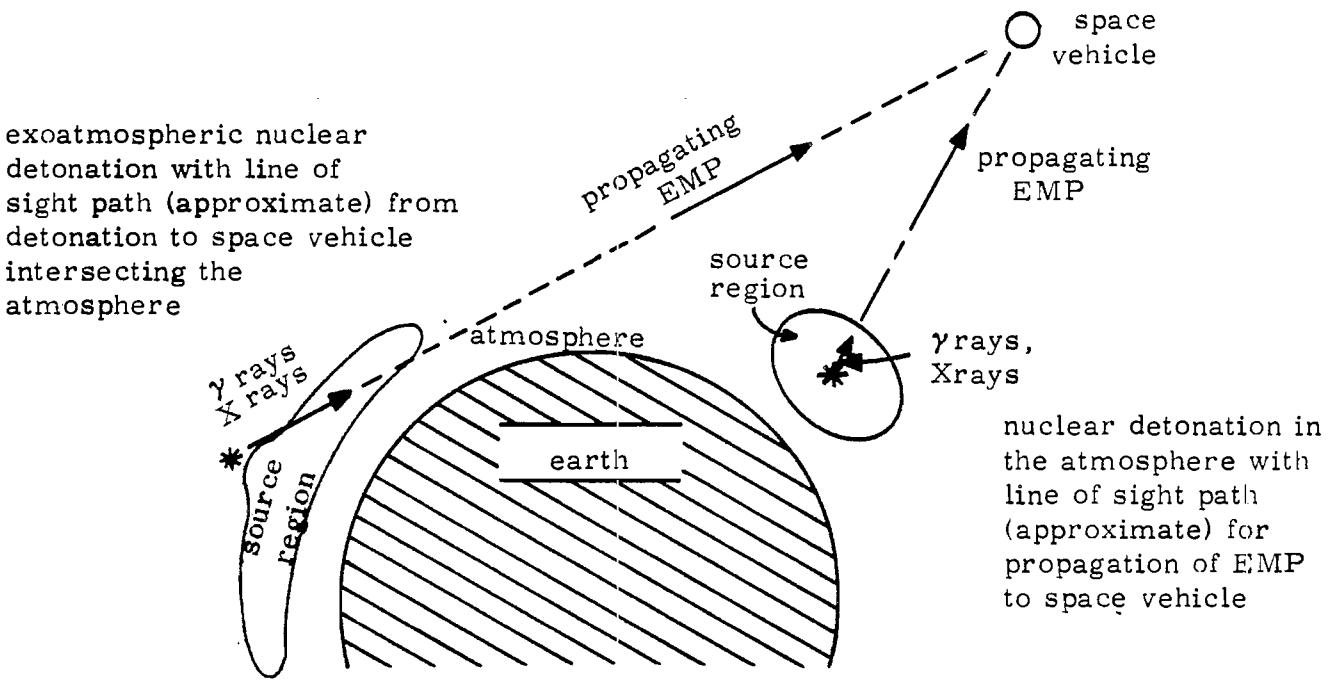


B. EMP propagated from atmospheric source region

Figure 1.1 Two Basic Types of Nuclear EMP on a Space Vehicle

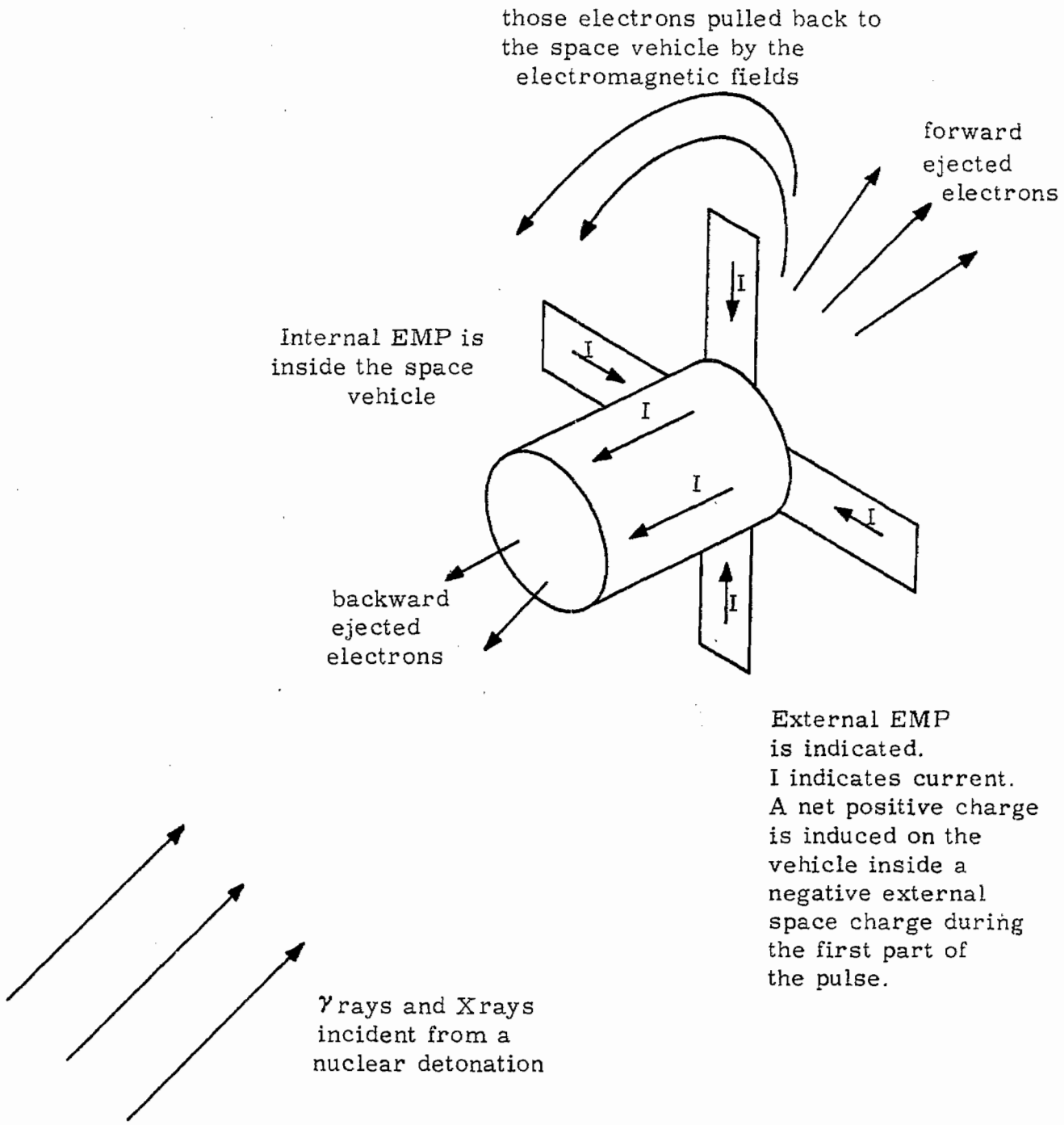


Figure 1.2 System Generated EMP on a Space Vehicle

components in the space system. Of concern in this note are the high energy electrons emitted in various directions from the various parts of the space system and the associated electric and magnetic fields and current and voltage densities which produce currents and voltages at various places of concern in the system. This phenomenon is the system generated EMP which can often be split into two types: external and internal. The internal EMP is associated with the high energy electrons driven into the inner cavities of various kinds in the system. For the internal EMP the electromagnetic geometry is determined principally by the space system itself, particularly if there is little penetration of electromagnetic signals to or from the system exterior so that the internal electromagnetic phenomena can be treated as occurring in one or more closed cavities. For the external system generated EMP, however, the space around the system is also quite important. Thus for a simulation test with $\gamma$ rays and/or X rays incident on the space system the proximity of other objects around the system which can influence the fields etc. can be quite important and has a significant impact on the simulator design.

There are other particles which travel from near the nuclear detonation to the space system such as neutrons and high energy electrons. However these particles arrive quite spread out in time so that the pulse width, rise time, etc. are large compared to transit times of interest on the space system and large compared to the $\gamma$ ray and X ray pulse widths. The spread in pulse width is also accompanied by a decrease in pulse amplitude. The associated electromagnetic transients on the space system are then also significantly reduced making these particle fluxes less significant from an EMP standpoint. While one could include various such particle fluxes in a simulator of this type these are lower order questions, such as particularly in the case of neutrons which introduces other complications such as radioactive activation of the simulator site and the system under test.

In simulating the system generated EMP on a space vehicle the space vacuum is quite important so as to give the same nonlinear electron transport in and around the space vehicle. In this note we consider a simulation approach for which the space system is essentially at the earth's surface. Thus some kind of vacuum test chamber to contain the space system is required. This chamber is the "space" part of the simulator, but it has many other features besides vacuum which significantly affect the simulation. The chamber scatters photons and electrons produced by a photon source such as a flash X-ray machine or a nuclear weapon. The photon source is, of course, the other fundamental part of the simulator and could be one or more flash X-ray machines or even a nuclear weapon, say in an underground test context. Besides reducing the photon and electron scattering from the chamber walls there are various electromagnetic effects of the cavity which can interfere with the

simulation. For example the cavity can resonate just like any microwave cavity except that the lowest cavity modes are somewhat lower in frequency because the vacuum chamber needed is a rather large cavity. At somewhat higher frequencies associated with the size of the space vehicle and the electron cloud produced around it the space vehicle can act as a radiator and the chamber should not reflect too much of this radiated signal back to the space vehicle. Thus the chamber will have to be impedance loaded to make it look more like free space. The presence of the chamber walls even increases the capacitance of the space vehicle and so the chamber will have to be somewhat large compared to the vehicle to avoid too much of a capacitance increase.

This note defines a simulation technique for the system generated EMP for space systems which, because of the photon source, also simulates part of the TRE environment as well. There are many aspects of this kind of a simulator and various of these are briefly discussed in this note. This is just a first note on the subject which will hopefully serve to introduce the reader to the basic concepts involved. Many detailed design calculations and optimizations can profitably be done. This type of simulator was very briefly introduced in a previous note.[1]

The type of simulator discussed here is one which attempts to reproduce the nuclear weapon environment ($\gamma$ rays and X rays) under the conditions found in space outside the atmosphere and over the entire space vehicle. As such it is a rather complete simulation. On the other hand it is not a perfect simulation quantitatively because of various limitations associated with chamber size, photon spectrum, etc. These limitations are, however, quantitative and a matter of degree so that one can make various aspects of the simulator match the real situation being simulated within definable tolerances; this of course impacts cost and time.

In this note various important aspects of the simulation technique are discussed. First we consider some aspects of the photon simulation including possible sources, electron removal, reduction of photon and electron scattering from the chamber, and some implications regarding the vacuum. Second we consider some techniques for reducing electromagnetic interaction of the vacuum chamber which affects the EMP on the space system. Third we briefly consider some other aspects of such a simulator for some details of the environment and operation of the space system in the simulator. Finally we consider some overall design options for a simulation facility layout for this kind of a system-generated-EMP simulator.

## II. Some Aspects of the Photon and Electron Environment

First let us look at the photon source which is going to initiate electron motion on and thereby in the vicinity of the space system. There are various designs of such sources that one might consider. Some basic questions regarding the photon source can be posed in terms of the incident photon environment produced over the test volume occupied by the space vehicle. Comparing various aspects of this environment (in terms of the photons directly or in terms of the electrons knocked off a space vehicle or other simplified object) to those associated with $\gamma$ rays and X rays from typical exoatmospheric nuclear detonations one can estimate how complete certain features of the simulation are in each case considered.

For the photon environment there is the general problem of making it intense enough over the entire space system. Suppose this environment is to be simulated as a photon flux passing through some cross section area $A_S$ which might typically be circular with radius $r_S$. This area can be thought of as the area of a cross section area of a cylinder with the cylinder axis parallel to the photon direction from the bomb to the space system. The space system is contained entirely within the cylinder. Of course the photons reaching the space system can be better thought of as in a cone, but this cone is very nearly a cylinder near the space system since the photons are travelling very nearly parallel at typical large distances from the bomb r (compared to $r_S$) of interest.

If U is the entire energy released by the nuclear detonation* then the energy released as prompt $\gamma$ rays and as X rays which go far from the detonation position can be represented as

$$U_\gamma \equiv f_\gamma U \ , \quad U_x \equiv f_x U \tag{2.1}$$

The fractional energy in gamma rays $f_\gamma$ may typically be a few tenths of a percent which is somewhat less than say 3.5% which is the fractional energy released as gamma rays in a typical fission.[5] On the other hand most of the energy comes out in the form of X rays so that $f_x$ is close to one, say .7 or .8. The $\gamma$ ray spectrum is the fission spectrum plus that associated with neutron interactions with various materials and has an average photon energy in the few MeV range. The average photon energy of the X rays is much lower. Considered together the $\gamma$ rays and X rays give a photon spectrum which covers a broad range of photon energies peaking toward the low energy end of this spectrum. Since the electrons emitted from the materials

*All units are rationalized MKSA. While yields may be mentioned in tons or energies in eV they must still be put into formulas in terms of joules.

(making up the space system) have energies which are a significant fraction of the photon energies, then the emitted electron spectrum is very dependent on the incident photon spectrum. The electron trajectories in the presence of the electromagnetic fields generated in and around the space vehicle are dependent on the electron energy. If the fields generated are sufficiently large the problem is then nonlinear making it desirable for a simulator to have as nearly the same photon spectrum and photon pulse time history as a nuclear weapon, and since photon spectrum can depend on the weapon design perhaps more than one photon spectrum for simulation testing would be desirable.

For relating the $\gamma$ ray and X ray energies to typical weapons we have

$$1 \text{ ton} \equiv 10^9 \text{ calories}$$
$$1 \text{ calorie} \approx 4.1868 \text{ J} \qquad (2.2)$$

so that

$$1 \text{ ton} \approx 4.1868 \times 10^9 \text{ J} \qquad (2.3)$$

As an example then one might take $U = 10^{16}$ J for the yield, corresponding to an approximately 2.4 megaton weapon. Suppose as shown in figure 1.1 the nuclear detonation is exoatmospheric with line of sight also exoatmospheric to a satellite in synchronous orbit so that the distance from the center of the earth is about 40 Mm. Let this distance also be the distance from the detonation point to the satellite. Also let $f_\gamma = .002$ and $f_x = .8$ to further specify the example.

In free space the photon energy per unit area falls off as $U/(4\pi r^2)$ where r is the distance from the detonation point. Thus the energy flux per unit area from $\gamma$ rays and from X rays can be written as

$$\phi_\gamma = \frac{U_\gamma}{4\pi r^2} = f_\gamma \frac{U}{4\pi r^2}$$
$$\phi_x = \frac{U_x}{4\pi r^2} = f_x \frac{U}{4\pi r^2} \qquad (2.4)$$

In these equations any asymmetry in the weapon output is not included. Of course the $\gamma$ rays and X rays will not be uniformly

radiated into each increment of solid angle. If $\vec{e}_r$ is the unit vector in the r direction then these results can include factors which are functions of $\vec{e}_r$ which are normalized so that the integral over the full solid angle ($4\pi$) is unity; the present approximation just has a uniform $1/(4\pi)$ as this factor. The same applies to the formulas that follow in that $\vec{e}_r$ is not included in such functions as photon spectrum, etc. To include effects of weapon asymmetry one may explicitly include $\vec{e}_r$ and integrals over the solid angle, or one may use the present results referred to any particular direction (i.e., particular $\vec{e}_r$) with bomb yield, etc. adjusted accordingly.

The space system as seen from the weapon lies in an area $A_s$ through which the simulator is to put photons. Taking $A_s$ as circular with $A_s = \pi r_s^2$ we then have $\gamma$-ray and X-ray energies required as

$$\Phi_\gamma = \phi_\gamma A_s = f_\gamma U \frac{1}{4}\left(\frac{r_s}{r}\right)^2$$

$$\Phi_x = \phi_x A_s = f_x U \frac{1}{4}\left(\frac{r_s}{r}\right)^2 \qquad (2.5)$$

Similarly one can define a total energy flux per unit area as

$$\phi_o = \frac{U}{4\pi r^2} \qquad (2.6)$$

which gives a total energy referred to $A_s$ written as

$$\Phi_o = \phi_o A_s = U \frac{1}{4}\left(\frac{r_s}{r}\right)^2 \qquad (2.7)$$

For our example case let $r_s = 5$ m and assume that this includes solar panels and anything else associated with the space system in the circular area $A_s$. Our example case for comparing simulator performance (which will crop up throughout the note) can then be summarized as

$$\text{Example weapon and space system} \begin{cases} U = 10^{16} \text{ J}, \quad f_\gamma = .002, \quad f_x = .8 \\ r = 40 \text{ Mm}, \quad r_s = 5 \text{ m} \end{cases} \qquad (2.8)$$

This implies

$$\text{Example weapon and space system} \begin{cases} \phi_o \simeq .5\ \mathrm{J\,m^{-2}}, & \Phi_o \simeq 40\ \mathrm{J} \\ \phi_\gamma \simeq 10^{-3}\ \mathrm{J\,m^{-2}}, & \Phi_\gamma \simeq 8 \times 10^{-2}\ \mathrm{J} \\ \phi_x \simeq .4\ \mathrm{J\,m^{-2}}, & \Phi_x \simeq 30\ \mathrm{J} \end{cases} \tag{2.9}$$

Certainly from an energy viewpoint such numbers look quite tractable, even for a rather inefficient conversion of electron beam energy to photon energy in a flash X-ray machine.

Not only might one consider the energy flux associated with the photons; there are various other characteristics of the photon flux which have significance to our simulation problem. In its most general form the photons can be represented by a time dependent spectrum $s_p$ with the normalization

$$\int_{-\infty}^{\infty}\int_{o}^{\infty} s_p(\psi_p,t)\,d\psi_p dt \equiv 1 \tag{2.10}$$

The subscript p is used to denote photons (and similarly e for electrons) and $\psi$ is used for particle energy (units are joules in formulas). The units of $s_p$ are then $(\mathrm{Js})^{-1}$. The time variable implies evaluation of $s_p$ at some position in space, or for our problem this could be taken as retarded time

$$t^* \equiv t - \frac{r}{c} \tag{2.11}$$

since we are neglecting any atmospheric or other effects on the photons propagating to the space system. While the limits on the integrals are over $-\infty < t < \infty$ and $0 \leq \psi_p < \infty$ these can be reduced to only those values of t and $\psi_p$ for which the spectrum function is non zero. Note that the spectrum function is written as a scalar; we are assuming that the photons are randomly polarized with a uniform distribution in polarization angle. A purely energy spectrum can also be defined as

$$S_p(\psi_p) \equiv \int_{-\infty}^{\infty} s_p(\psi_p,t)\,dt \tag{2.12}$$

which is then automatically normalized as

$$\int_0^\infty S_p(\psi_p)\,d\psi_p = 1 \tag{2.13}$$

Having defined a spectrum function various parameters can be defined such as an average photon energy in a time dependent sense as

$$\psi_{p_{avg}}(t) \equiv \frac{\int_0^\infty \psi_p s_p(\psi_p,t)\,d\psi_p}{\int_0^\infty s_p(\psi_p,t)\,d\psi_p} \tag{2.14}$$

Since $s_p$ is the number of photons per unit energy and per unit time then

$$n_p(t) \equiv \int_0^\infty s_p(\psi_p,t)\,d\psi_p \tag{2.15}$$

is the distribution function for the number of photons per unit time normalized as

$$\int_{-\infty}^\infty n_p(t)\,dt = 1 \tag{2.16}$$

The average photon energy for the entire photon pulse can then be defined as

$$\begin{aligned}\bar{\psi}_{p_{avg}} &\equiv \int_{-\infty}^\infty \psi_{p_{avg}}(t)\,n_p(t)\,dt \\ &= \int_{-\infty}^\infty \int_0^\infty \psi_p s_p(\psi_p,t)\,d\psi_p\,dt \\ &= \int_0^\infty \psi_p S_p(\psi_p)\,d\psi_p \end{aligned} \tag{2.17}$$

These spectral considerations can be applied to the $\gamma$ rays and X rays separately simply by using the subscripts $\gamma$ and X in place of p. The distinction between $\gamma$ rays and X rays is based on the physical processes of their generation in the nuclear weapon. From the viewpoint of the space system, however, both are just photons and distinction can only be made on the basis of the energies $\psi_p$ of the individual photons. One might then also define a fractional energy of the bomb yield in photons as

$$f_p \equiv f_x + f_\gamma \simeq f_x \tag{2.18}$$

which is then approximately .8 for our example case. If one wishes an arbitrary split can be made in the photon spectrum at a $\psi_p$ of roughly 100 keV, calling those of lower energy X rays and those of higher energy $\gamma$ rays.[6]

The average $\gamma$-ray energy $\bar{\psi}_{\gamma_{avg}}$ is roughly 1 MeV and the detailed spectrum is affected by the weapon design as evidenced by the fact that only a small fraction of the $\gamma$ rays escape. The temperature inside the nuclear detonation is of the order of 10 keV corresponding to a 15 keV average particle energy (3/2 times the temperature expressed in terms of energy).[6] Again the detailed spectrum of the X rays escaping from the weapon is affected by the weapon design as is discussed in various classified reports as well as reference 6. While in this note we do not consider the detailed aspects of $\gamma$-ray and X-ray spectra, the photon spectrum used in a simulator for the system generated EMP will have a significant influence on the current and charge generated on the space system.

As an example of an analytic spectrum function that is often used consider the Planck or black body spectrum which we designate by $S_b$ (time independent). Let $\psi_o$ be the temperature of the effective black body radiator (which is 2/3 of the mean energy in a simple case). With $\psi_b$ as the photon energy, the number of photons in an incremental energy interval has the distribution function[7]

$$S_b(\psi_b) = B\psi_b^2\left[e^{\psi_b/\psi_o} - 1\right]^{-1} \tag{2.19}$$

Note that the distribution function for photon energy (instead of number of photons) has a $\psi_b^3$ factor instead of $\psi_b^2$. This distribution is also often used in terms of incremental wavelength (instead of incremental energy, or equivalently frequency) in which case a $\psi_b^5$ term appears instead of $\psi_b^3$ for the energy distribution.

Here we need the Riemann zeta function defined by[8]

$$\zeta(\alpha) \equiv \sum_{k=1}^{\infty} k^{-\alpha} \qquad (\mathrm{Re}(\alpha) > 1)$$

$$= \frac{1}{\Gamma(\alpha)} \int_0^{\infty} \frac{\nu^{\alpha-1}}{e^{\nu} - 1} d\nu \qquad (\mathrm{Re}(\alpha) > 1) \tag{2.20}$$

From the normalization condition of equation 2.13 we have

$$1 = B \int_0^{\infty} \psi_b^2 \left[ e^{\psi_b/\psi_o} - 1 \right] d\psi_b$$

$$= B\psi_o^3 \int_0^{\infty} \left( \frac{\psi_b}{\psi_o} \right)^2 \left[ e^{\psi_b/\psi_o} - 1 \right] d\left( \frac{\psi_b}{\psi_o} \right)$$

$$= B\psi_o^3 \Gamma(3)\zeta(3) = 2B\psi_o^3 \zeta(3) \tag{2.21}$$

Thus our distribution function for photon number per unit energy is

$$S_b(\psi_b) = \frac{\psi_b^2}{2\zeta(3)\psi_o^3} \left[ e^{\psi_b/\psi_o} - 1 \right]^{-1} \tag{2.22}$$

For reference we have

$$\zeta(3) = 1.202 \cdots$$

$$\zeta(4) = \frac{\pi^4}{90} = 1.082 \cdots \tag{2.23}$$

$$\frac{\zeta(4)}{\zeta(3)} = .900 \cdots$$

The average photon energy for the black body distribution is

$$\bar{\psi}_b = \int_o^\infty \psi_b S_b(\psi_b)\, d\psi_b$$

$$= \frac{\psi_o}{\Gamma(3)\zeta(3)} \int_o^\infty \left(\frac{\psi_b}{\psi_o}\right)^3 \left[e^{\psi_b/\psi_o} - 1\right]^{-1} d\left(\frac{\psi_b}{\psi_o}\right)$$

$$= \frac{\Gamma(4)}{\Gamma(3)} \frac{\zeta(4)}{\zeta(3)} \psi_o = 3 \frac{\zeta(4)}{\zeta(3)} \psi_o \simeq (2.70 \cdots)\psi_o \qquad (2.24)$$

The peak of the black body spectrum (for photon number per unit energy) is found from

$$\frac{d}{d\psi_b} S_b(\psi_b) = \frac{1}{2\zeta(3)\psi_o^3} \left\{ 2\psi_b \left[e^{\psi_b/\psi_o} - 1\right]^{-1} - \frac{\psi_b^2}{\psi_o} e^{\psi_b/\psi_o} \left[e^{\psi_b/\psi_o} - 1\right]^{-2} \right\} \qquad (2.25)$$

Setting this to zero and calling the value of $\psi_b$ for this peak as $\psi_{b_o}$ we have

$$0 = \left[2 - \frac{\psi_{b_o}}{\psi_o}\right] e^{\psi_{b_o}/\psi_o} - 2 \qquad (2.26)$$

which gives

$$\frac{\psi_{b_o}}{\psi_o} \simeq 1.6 \qquad (2.27)$$

as the spectrum peak. Note that this is less than the average photon energy.

Spectra like the black body distribution for X rays or the fission spectrum for $\gamma$ rays or actual measured or calculated weapon spectra can be used for detailed transport calculations to describe the photon interaction with the space system. The results can be compared with those produced by the photons from a flash X-ray machine. Of course an X-ray machine does not give the exact same spectrum as a nuclear weapon. In particular it is difficult and inefficient for an X-ray machine using the standard Bremsstrahlung production from an electron beam on a target to produce a photon spectrum with an average photon energy even approaching that from the weapon X rays. It is typically much higher, even in the MeV range, but the hundreds

of keV range can and has been done with accompanying loss of efficiency.

In order to compare various flash X-ray machines as photon sources for our simulator one can define several characteristics of the photon flux and see how they compare to the weapon flux. These characteristics or figures of merit should be based on the various physical effects of significance which result from the incident photon flux. We have already mentioned the total photon energy illuminating the space system in the area $A_S$. However other large scale parameters can also be considered. These parameters can be thought of as weighted averages of the photon spectrum with the weighting chosen according to the physics of particular important phenomena associated with the photon interaction. Thus one may reduce the consideration of the exact details of the photon spectrum and flux to a few numbers which characterize some of its most important features.

One of the macroscopic parameters of the photons from the weapon is the dose rate which is the power deposited in the system of interest on a per unit mass basis. This has units of watts/kilogram abbreviated W/kg (preferred to rads/s or roentgens/s). Integrating this over the entire radiation pulse gives the dose in J/kg (which is also the same as $(m/s)^2$ or a speed squared). The dose and dose rate can be important for TRE interactions as an example. Another example would be the local energy deposited in a material simply from the viewpoint of local heating and associated shock wave generation (at sufficiently large dose levels).

Now the dose and dose rate are not only functions of the photon spectrum, but also of the atomic element or elements comprising the material. Furthermore the dose and dose rate can vary as a function of position in the object (i.e. space system) due to changes in the material composition and/or attenuation and scattering of the photons. To estimate the dose rate one can take a mean free path for photon absorption in typical materials. Of course this varies somewhat between materials for any given photon energy, but if this is expressed in terms of a mass type of cross section ($m^2/kg$) then the material density is factored out and the results only depend somewhat insensitively on the atomic number (Z) of the material, at least in the few MeV range where Compton scattering is dominant. Since for dose we are interested in the energy absorbed by the medium then we do not want the total photon collisions per unit mass but instead the photon energy deposited. Thus we want the mass absorption coefficient instead of the mass linear attenuation coefficient.

Call this mass absorption coefficient $M(\psi_p)$ with units $m^2/kg$. For any given atomic number Z one can calculate or look up this quantity as a function of $\psi_p$ the photon energy.[9] This

quantity could be subscripted to indicate what Z or Z combination this applies to. For low Z materials in the middle of the Compton region, say 1 MeV, M will be like .003 $m^2/kg$. For higher photon energies pair production takes over (not very important for our cases). For lower photon energies the photoelectric process with an absorption coefficient proportional to roughly $Z^4/\psi_p^3$ takes over.[9] Thus at the very low photon energies M is greatly increased and is very Z dependent.

One can define a mean mass absorption coefficient using a given photon spectrum as

$$\bar{M}_{p_{avg}} \bar{\psi}_{p_{avg}} \equiv \int_o^\infty M(\psi_p)\psi_p S_p(\psi_p)\,d\psi_p \tag{2.28}$$

where the weight factor $\psi_p$ is used because we are weighting energy absorption. Here we have used the time independent spectrum although the time dependent form may be used as well to give

$$M_{p_{avg}}(t)\psi_{p_{avg}}(t) \equiv \frac{1}{n_p(t)} \int_o^\infty M(\psi_p)\psi_p s_p(\psi_p,t)\,d\psi_p \tag{2.29}$$

For a given Z or Z combination the mean mass absorption coefficient is then one useful macroscopic parameter to characterize the photons from the weapon or from another kind of X-ray source.

Call the dose rate waveform d(t) normalized such that

$$\int_{-\infty}^{\infty} d(t)\,dt = 1 \tag{2.30}$$

The total dose is then $d_{p_o}$ (and similarly for $\gamma$ rays and X rays). This is related to the number of photons per unit area $n_{p_o}$ as

$$d_{p_o} = \int_o^\infty n_{p_o} M(\psi_p)\psi_p S_p(\psi_p,t)\,d\psi_p = \bar{M}_{p_{avg}} \bar{\psi}_{p_{avg}} n_{p_o}$$

$$d_{p_o} d(t) = \int_o^\infty n_{p_o} M(\psi_o)\psi_p s_p(\psi_p,t)\,d\psi_p = M_{p_{avg}}(t)\psi_{p_{avg}}(t) n_{p_o} n_p(t) \tag{2.31}$$

where subscripts, as before, allow one to separate the contributions from various parts of a photon spectrum. Note these doses are incident doses in that no attenuation or other alteration of the incident photon spectrum is included.

To get a feel for what the total dose is for our example case consider various photon energies and the associated mass absorption coefficients for aluminum (using ref. 9) and the associated doses for our $10^{16}$ J bomb at 40 Mm distance. For simplicity pick a monoenergetic photon spectrum and use that energy for the calculations. Using just the total bomb energy at each photon energy with $\phi_{p_o} \approx .4$ J $m^{-2}$ as the incident photon energy flux per unit area for our example case gives the following table.

| Photon energy | Photon number flux per unit area ($n_{p_o}$) | Approximate mass absorption coefficient in aluminum ($M_{p_{Al}}$) | Approximate dose ($d_{p_o}$) | Approximate average dose rate ($\bar{d}_{p_{Al}}$) |
|---|---|---|---|---|
| 10 keV | $3.1 \times 10^{14}$ $m^{-2}$ | 2.4 $m^2/kg$ | .96 J/kg | $.96 \times 10^{8}$ W/kg |
| 100 keV | $3.1 \times 10^{13}$ $m^{-2}$ | .0038 $m^2/kg$ | .0015 J/kg | $1.5 \times 10^{5}$ W/kg |
| 1 MeV | $3.1 \times 10^{12}$ $m^{-2}$ | .0026 $m^2/kg$ | .001 J/kg | $1 \times 10^{5}$ W/kg |
| 10 MeV | $3.1 \times 10^{11}$ $m^{-2}$ | .0018 $m^2/kg$ | .0007 J/kg | $.7 \times 10^{5}$ W/kg |

Table 2.1 Approximate Dependence of Photon Number Flux per Unit Area and Dose on Photon Energy for Monoenergetic Photons from Example Weapon

As one can readily see the incident dose does not vary markedly over the energy range 100 keV to 10 MeV. However in going from 100 keV down to 10 keV (and even lower) there is a very significant change in the dose (associated with the photoelectric process). Thus from a dose viewpoint (for a given incident energy flux per unit area) the low end of the spectrum (below about 100 keV) can be quite important. The actual incident dose for our example weapon depends on the detailed characteristics of the photon spectrum and may be referred to other materials besides aluminum. This dose would seem, however, to be one useful comparison between a nuclear weapon (such as our example weapon) and a flash X-ray machine or other photon source as part of a simulator. Besides the total incident dose one might similarly compare the incident dose rates based on the time history of the photon number and energy, comparing peaks, rise times, etc. For our example weapon we might take a characteristic time of $10^{-8}$ seconds as a rough number for estimates.

Dividing the dose by this time ($t_p$) gives an average dose rate during the pulse as

$$\bar{d}_p \equiv \frac{d_{p_o}}{t_p} \tag{2.32}$$

which is included in table 2.1.

As included in table 2.1 another useful number to characterize the photons is the number of photons per unit area. This is distinguished from the total energy per unit area of the photons. Let $n_{p_o}$ be the total (time integrated) number of photons per unit area at the space system, and similarly for $n_{x_o}$ and $n_{\gamma_o}$. Then $n_{p_o} S_p(\psi_b)$ is the number of photons per unit area per unit energy, $n_{p_o} n_p(t)$ is the number of photons per unit area per unit time, and $n_{p_o} s_p(\psi_p, t)$ is the number of photons per unit area per unit energy per unit time. This number of photons per unit area is related to the photon energy per unit area $\phi_{p_o}$ as

$$\phi_{p_o} = \int_o^\infty \psi_p n_{p_o} S_p(\psi_p)\, d\psi_p = n_{p_o} \bar{\psi}_{p_{avg}}$$

$$n_{p_o} = \frac{\phi_{p_o}}{\bar{\psi}_{p_{avg}}} \tag{2.33}$$

Similarly in a time dependent sense we can write

$$\phi_{p_o} \phi_p(t) = \int_o^\infty \psi_p n_{p_o} s_p(\psi_p, t)\, d\psi_p = \psi_{p_{avg}}(t) n_{p_o} n_p(t)$$

$$n_{p_o} n_p(t) = \frac{\phi_{p_o} \phi_p(t)}{\psi_{p_{avg}}(t)} \tag{2.34}$$

where $\phi_p(t)$ is the photon power per unit area waveform normalized so that

$$1 = \int_{-\infty}^{\infty} \phi_p(t)\, dt \tag{2.35}$$

This gives the time dependent photon number per unit area as

$$n_{p_o} \bar{n}_p(t) = \phi_{p_o} \frac{\phi_p(t)}{\psi_{p_{avg}}(t)} \tag{2.36}$$

These formulas can all be applied to X rays and $\gamma$ rays by substituting X and $\gamma$ respectively for p throughout. In addition to the energy per unit area and dose one can also look at the photon number per unit area to compare a nuclear weapon (as in our example case) to some other photon source for our simulator. Relating the energy flux per unit area to the dose gives

$$\begin{aligned} d_{p_o} &= \bar{M}_{p_{avg}} \phi_{p_o} \\ d_{p_o} d(t) &= M_{p_{avg}}(t) \phi_{p_o} \phi_p(t) \end{aligned} \tag{2.37}$$

The mass absorption coefficient then provides a direct relation between the two kinds of quantities.

One reason to consider the number of photons per unit area is because this quantity is related to the number of electrons emitted per unit area of the surfaces on the space system. It is this emitted charge which is the source for the system generated EMP. Each photon from the weapon or other source arriving at the space system produces some number of electrons $\eta(\psi_p)$. These electrons have some distribution in energy $\psi_e$ and solid angle $\Omega_e$ with respect to the incoming photons described by some distribution function $g(\psi_p, \psi_e, \Omega_e)$ normalized such that

$$\int_o^\infty \int_{\text{all } \Omega_e} g(\psi_p, \psi_e, \Omega_e) d\Omega_e d\psi_e = 1 \tag{2.38}$$

Of course there can be some variation in $\eta$ and g depending on the specific system geometry and materials and the position on any particular surface of the system from which the electrons are being emitted. There is also some time delay for the electrons to emerge from the materials but this is neglected in our considerations.

Since there is much possible variation in the system geometry then some simple geometry would help in comparing the electron spectra associated with various photon spectra. Let us choose a simple flat plate example of uniform thickness,

uniform material composition, and perpendicular to $\vec{e}_r$ (the direction of propagation of the photons). Furthermore let the flat plate be large enough that edge effects can be ignored and treat the problem on a per-unit-area basis. Such a geometry quite naturally divides the electrons into two categories, the forward scattered and back scattered electrons which can be denoted by subscripts f and b respectively on quantities such as the fractional numbers of electrons and the distribution functions for energy and direction. There is still the question of what plate thickness to choose for the standard of comparison. Since we are interested in the effects associated with large current densities of these electrons then perhaps a thin plate, one electron range thick at the maximum electron energy associated with a photon of energy $\psi_p$, would be appropriate.

Since the photon mean free path is generally much larger than the range of an electron produced by that photon for most energies and materials of interest then we might consider an unattenuated photon flux in the material for this calculation of the electrons escaping from both sides. This avoids the issue of how thick to make the plate as long as it is thick enough to have reached the final equilibrium electron spectrum. Of course the photon mean free path is a strong function of $\psi_p$ at low photon energies (in the X-ray region) so that for a given plate thickness which is thicker than the largest electron range (associated with the largest energy photons) the plate can be many photon mean free paths thick at the low X-ray energies giving a significant photon attenuation. Neglecting photon attenuation in the plate then can lead to a significant overestimate of the number of low energy forward scattered electrons while having negligible effect on the backscattered electrons. Thus our present definition neglecting photon attenuation can be a useful way to compare electron yields from different photon spectra, but it does not give all the answers. For other comparisons one can just leave the plate thickness as a parameter in the problem.

Note that once the electron has left the system surface it is not followed any farther for the present comparison technique. Further collisions of the electron with the system surfaces can produce yet more electrons coming from the surfaces. In the case of large photon fluxes per unit area the current density leaving the system can be large enough to make the problem nonlinear, altering the electron trajectories. It would be desirable to make photon spectrum comparisons before having to solve the nonlinear electron trajectories as a simpler way to understand something about the adequacy of the photon spectrum from a source of interest.

The dose comparison for the photon spectrum depends on the choice of a material, particularly affecting the results for low photon energies of interest. For the electron yield calculations one also needs to choose a material or regard this

choice as a parameter in the comparison. For first order comparisons one might choose a common material such as aluminum. Then an infinite homogeneous thick aluminum slab (for example) neglecting photon attenuation would form a basis for comparing photon spectra (and numbers) on the basis of electron number yield, energy, and direction. This type of comparison specification can be applied to the dose comparison as well.

Having defined a technique for comparing electron yields (such as, for example, the one discussed above) one can then consider various quantitative features of the electrons produced. This characterizes some important features of the electrons in a few numbers. The fractional number of electrons (or electron yield) produced by the incident photon spectrum is found by averaging over $\eta(\psi_p)$ for both time and energy as

$$\bar{\eta}_{p_{avg}} \equiv \int_o^\infty \eta(\psi_p) S_p(\psi_p)\, d\psi_p \tag{2.39}$$

This can be considered an electron generation efficiency. A related time dependent electron efficiency can be defined as

$$\eta_{p_{avg}}(t) \equiv \frac{1}{n_p(t)} \int_o^\infty \eta(\psi_p) s_p(\psi_p, t)\, d\psi_p \tag{2.40}$$

so that

$$\bar{\eta}_{p_{avg}} = \int_{-\infty}^\infty \eta_{p_{avg}}(t) n_p(t)\, dt = \int_{-\infty}^\infty \int_o^\infty \eta(\psi_p) s_p(\psi_p, t)\, d\psi_p dt \tag{2.41}$$

Typical electron fractions are somewhat dependent on the incident photon spectrum as well as the material of interest. Again aluminum is used as the material for making comparisons. In reference 6 an estimate is made of the electron fraction associated with incident X rays, giving an electron fraction of about $5 \times 10^{-4}$ at a $\psi_p$ of 30 keV with a dependence of about $\psi_p^{-1}$ far from absorption edges. Another reference summarizes some of the spectra and electron fractions for incident X rays showing the increasing electron fractions for low photon energies.[10] For $\psi_p$ about 5 keV the electron fraction can be a few percent. The photoelectric process which dominates the low energy photon interaction has a large influence on this kind of electron fraction variation. Going to higher energies for $\gamma$ rays in the few MeV range the dominant photon interaction is by the Compton process. The electron fraction for such photon energies is about $7 \times 10^{-3}$ (as in reference 6). Various of the theoretical

notes deal with electron fluxes in air associated with MeV photons. Calculations have been made for various photon spectra giving, for example, an electron fraction for forward scattering of $3 \times 10^{-3}$ for a fission $\gamma$-ray spectrum.[11]

The electron fraction discussed here has been for electrons emitted from both sides of the assumed infinite slab of aluminum. One can use $\eta_f(\psi_p)$ for a forward scattered fraction and $\eta_b(\psi_p)$ for a backscattered electron fraction. For low photon energies for which the photoelectric process is dominant the electrons are made to move initially at about a right angle to the incident photons. This results in roughly equal magnitudes for $\eta_f$ and $\eta_b$, each roughly half of $\eta$. As the photon energy is increased the Compton process takes over and the electrons are ejected predominantly in the forward direction. This results in $\eta_f$ approaching $\eta$ while $\eta_b$ becomes a small fraction of $\eta$.

Having the electron fraction in various forms we can look at the total number of electrons and associated current density. The number of electrons per square meter leaving the slab from both sides can be written in time dependent form as

$$n_{e_o} n_e(t) = n_{p_o} \int_o^\infty \eta(\psi_p) s_p(\psi_p, t) d\psi_p = \eta_{p_{avg}}(t) n_{p_o} n_p(t) \qquad (2.42)$$

where the electron emission waveform is normalized so that

$$\int_{-\infty}^{\infty} n_e(t) dt = 1 \qquad (2.43)$$

The total electron emission per unit area is then

$$n_{e_o} = n_{p_o} \int_{-\infty}^{\infty} \eta_{p_{avg}}(t) n_p(t) dt = n_{p_o} \int_o^\infty \eta(\psi_p) S_p(\psi_p) d\psi_p$$

$$= \bar{\eta}_{p_{avg}} n_{p_o} \qquad (2.44)$$

The current density, taking all leaving electrons from both sides as contributing with the same sign to this current density (even though oppositely directed) is just

$$J_e(t) = -e\, n_{e_o}\, n_e(t) \tag{2.45}$$

$$e = 1.602 \cdots \times 10^{-19}\ C$$

where e is the magnitude of the electron charge and $J_e$ is the net current density leaving. The total charge per unit area emitted is

$$q_e = \int_{-\infty}^{\infty} J_e(t)\,dt = -e\, n_{e_o} \tag{2.46}$$

If one wishes, the electrons per unit area, current density, and charge per unit area can be separated in forward and backward components with subscripts f and b respectively simply by using $\eta_f(\psi_p)$ and $\eta_b(\psi_p)$ in the integrals.

The number of electrons per unit area can also be related to the incident photon energy per unit area (which can be conveniently measured) from equation 2.33 as

$$n_{e_o} = \frac{\bar{\eta}_{p_{avg}}}{\bar{\psi}_{p_{avg}}}\,\phi_{p_o} \tag{2.47}$$

which requires that one know the average photon energy and average electron fraction. In a time dependent form this is

$$n_{e_o}\, n_e(t) = \frac{\eta_{p_{avg}}(t)}{\psi_{p_{avg}}(t)}\,\phi_{p_o}\,\phi_p(t) \tag{2.48}$$

The current density and the associated charge emitted from the surfaces of a space system are clearly important effects of the incident photons from an EMP point of view. This places great importance on the average electron fraction. If the photons are specified in terms of energy flux per unit area then the average photon energy is also very important. Sometimes the incident photons may be specified in terms of dose. Then from equations 2.37 we can write

$$n_{e_o} = \frac{\bar{\eta}_{p_{avg}} d_{p_o}}{\bar{\psi}_{p_{avg}} \bar{M}_{p_{avg}}} \tag{2.49}$$

$$n_{e_o} n_e(t) = \frac{\eta_{p_{avg}}(t) d_{p_o}(t)}{\psi_{p_{avg}}(t) M_{p_{avg}}(t)}$$

In such a case it is also important to know the mass absorption coefficient.

While the time dependent current density of electrons emitted from the space system is one of the most important parameters to consider in designing a simulator for the system generated EMP on a space vehicle, other parameters also affect the resulting EMP. The resulting current and charge densities in the space inside and outside of the space system depend not only on the emitted charge but also on the subsequent spatial and temporal behavior of the electrons. This subsequent behavior depends on the energy and direction of the emitted electrons as well as the number of electrons. Remember that for large numbers of electrons the problem is nonlinear. Thus one must be concerned (for the larger current levels in particular) with the average energy of the emitted electrons and how this compares to the energies associated with the position changes of the electrons in the electromagnetic fields. The vector and scalar potentials may be more convenient for considerations of the electron energy $\psi_e$. For example in the static limit only those electrons with $\psi_e/e$ greater than or equal to the negative of the scalar potential of the space system with respect to infinity can possibly escape from the space system. While the average electron energy does not completely characterize the interaction of the electrons with the fields it still is a first order way to compare different electron spectra for the fields they will produce.

Again for our infinite aluminum plate one can separate the electrons into forward and backscattered parts and consider an average energy for each with appropriate subscripts added to the following results. With the electron fraction $\eta(\psi_p)$ and distribution function $g(\psi_p,\psi_e,\Omega_e)$ (normalized as in equation 2.38) we have the time dependent spectrum of the electrons emitted at each time as

$$s_{e_p}(\psi_e,\Omega_e,t) = \frac{\int_o^\infty \eta(\psi_p)\, g(\psi_p,\psi_e,\Omega_e)\, s_p(\psi_p,t)\, d\psi_p}{\int_{-\infty}^{\infty}\int_o^\infty \int_{all\ \Omega_e}\int_o^\infty \eta(\psi_p)\, g(\psi_p,\psi_e,\Omega_e)\, s_p(\psi_p,t)\, d\psi_p d\Omega_e d\psi_e dt}$$

$$= \frac{1}{\bar{\eta}_{p_{avg}}} \int_o^\infty \eta(\psi_p)\, g(\psi_p,\psi_e,\Omega_e)\, s_p(\psi_p,t)\, d\psi_p \qquad (2.50)$$

with the normalization

$$\int_{-\infty}^{\infty}\int_o^\infty \int_{all\ \Omega_e} s_{e_p}(\psi_e,\Omega_e,t)\, d\Omega_e d\psi_e dt = 1 \qquad (2.51)$$

In a time independent sense this is

$$S_{e_p}(\psi_e,\Omega_e) = \int_{-\infty}^{\infty} s_{e_p}(\psi_e,\Omega_e,t)\, dt$$

$$= \frac{1}{\bar{\eta}_{p_{avg}}} \int_o^\infty \eta(\psi_p)\, g(\psi_p,\psi_e,\Omega_e)\, S_p(\psi_p)\, d\psi_p \qquad (2.52)$$

with the normalization

$$\int_o^\infty \int_{all\ \Omega_e} S_{e_p}(\psi_e,\Omega_e)\, d\Omega_e d\psi_e = 1 \qquad (2.53)$$

Adding subscripts f and b with the normalizations over $2\pi$ steradians or half a sphere

$$\int_{\Omega_e \text{ forward}} g_f(\psi_p,\psi_e,t)\,d\Omega_e = 1$$

$$\int_{\Omega_e \text{ backward}} g_b(\psi_p,\psi_e,t)\,d\Omega_e = 1 \qquad (2.54)$$

and using the presumably known $\eta_f$ and $\eta_b$ where

$$\eta_f + \eta_b = \eta \qquad (2.55)$$

then $s_{e_{pf}}(\psi_e,\Omega_e,t)$, $s_{e_{pb}}(\psi_e,\Omega_e,t)$, $S_{e_{pf}}(\psi_e,\Omega_e)$, and $S_{e_{pb}}(\psi_e,\Omega_e)$ are all readily obtained in the same manner as above. Note that this also involves calculating $\eta_{p_{f_{avg}}}(t)$ and $\eta_{p_{b_{avg}}}(t)$ as well as $\bar{\eta}_{p_{f_{avg}}}$ and $\bar{\eta}_{p_{b_{avg}}}$.

Figure 2.1 shows an infinite slab which is perpendicular to the direction of incidence of randomly polarized photons (with uniformly distributed polarization angle). Considering the electrons emitted from some incremental area of the slab then by symmetry their directional distribution is uniform with respect to $\phi_e$ and only depends on $\theta_e$ where $\theta_e$ is the angle from a normal to the slab $\hat{n}$ and $\phi_e$ is the azimuthal angle around this normal from some arbitrary reference axis parallel to the slab. Forward scatter has $0 \leq \theta_e < \pi/2$ and backscatter has $\pi/2 < \theta_e \leq \pi$. The electron distribution function for this slab geometry can be written as

$$g(\psi_p,\psi_e,\Omega_e) = g_s(\psi_p,\psi_e,\theta_e) \qquad (2.56)$$

where g is still considered on a per-unit-solid-angle basis. The normalization is now

$$\int_o^{\pi}\int_o^{2\pi} g_s(\psi_p,\psi_e,\theta_e)\,\sin(\theta_e)\,d\phi_e d\theta_e = 2\pi\int_o^{\pi} g_s(\psi_p,\psi_e,\theta_e)\,\sin(\theta_e)\,d\theta_e$$

$$= 1 \qquad (2.57)$$

since the incremental solid angle is just

$$d\Omega_e = \sin(\theta_e)\,d\phi_e d\theta_e \qquad (2.58)$$

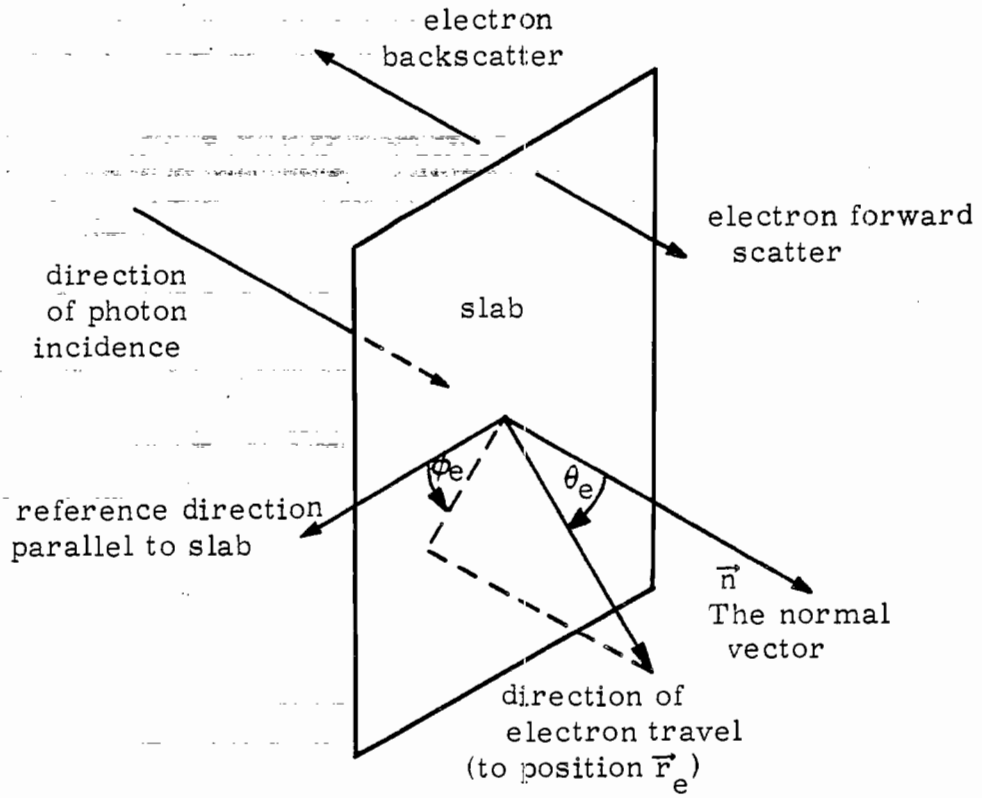


Figure 2.1 Slab Model for Photon Interaction

Subscripts f and b can be used with $g_s$ as well as with g.

Besides the electron energy being considered one might consider something about the electron direction as well. One might look at the average velocity to see how fast the charge is moving away from the slab. For $0 < \theta_e < \pi/2$ the average velocity of the forward scattered electrons is reduced in magnitude because they are not all travelling parallel to the normal vector $\vec{n}$ (or along $\theta_e = 0$). The velocity of an individual electron is given by

$$\vec{v}_e(\psi_e,\theta_e,\phi_e) = \left[1 - \left(\frac{m_e c^2}{\psi_e}\right)^2\right]^{1/2} c\,\vec{e}_{r_e} \tag{2.59}$$

where

$$m_e c^2 \simeq .511 \text{ MeV}$$

$$c = \frac{1}{\sqrt{\mu_o \varepsilon_o}} \simeq 2.998 \times 10^8 \text{ m/s} \tag{2.60}$$

and where $m_e$ is the electron rest mass, c is the speed of light in vacuum, $\mu_o$ is the permeability of free space, $\varepsilon_o$ is the permittivity of free space, and $\vec{e}_{r_e}$ is a unit vector in the direction of electron travel. For the slab model we have the average electron velocity for the forward scattered electrons at the time of electron emission as

$$\vec{v}_{e_{f_{avg}}}(t) = \frac{c\vec{n}}{n_{e_f}(t)} \int_o^\infty \int_{\Omega_e}_{\text{forward}} \left[1 - \left(\frac{m_e c^2}{\psi_e}\right)^2\right]^{1/2} \cos(\theta_e)\, s_{e_{p_f}}(\psi_e,\Omega_e,t)\, d\Omega_e\, d\psi_e$$

$$= \frac{2\pi c\vec{n}}{\bar{\eta}_{p_{f_{avg}}}\, n_{e_f}(t)} \int_o^\infty \int_o^\infty \int_o^{\pi/2} \left[1 - \left(\frac{m_e c^2}{\psi_e}\right)^2\right]^{1/2} \cos(\theta_e)\, \eta_f(\psi_p)\, g_{s_f}(\psi_p,\psi_e,\theta_e)$$

$$\sin(\theta_e)\, s_p(\psi_p,t)\, d\theta_e\, d\psi_e\, d\psi_p \tag{2.61}$$

and similarly for the backscattered electrons by changing subscripts f to b and changing the limits on the $\theta_e$ integration to $\pi/2 \leq \theta_e \leq \pi$. By integrating over $-\infty < t < \infty$ after multiplying by $n_{ef}(t)$ (or $n_{eb}(t)$) time independent averages are also obtained. Remember that $n_{ef}(t)$ and $n_{eb}(t)$ are normalized so that the complete time integral is one.

The average electron energy is a significant fraction of the energy of the photons producing the electrons. For low energy photons for which photoelectric interaction is important the initial electron energy is most of the photon energy but it loses energy on moving through the slab. Those that leave the slab can then have roughly half of the photon energy on the average. At higher photon energies for which the Compton process is dominant the electron is initially produced at a significant fraction of the photon energy, say half, making the escaping electrons still have say a quarter of the incident photon energy. Thus average electron energy is closely related to average photon energy and in the example problem using monoenergetic photons in table 2.1 the electron energy would have about the same variation as the photon energy. In considering a distributed photon spectrum, however, the variation of the electron fraction $\eta(\psi_p)$ has some influence, weighting the electron energy toward those $\psi_p$ values having the larger $\eta$. The average electron velocity is strongly influenced by the electron energy and therefore by the photon energy in line with the above discussion. However, the velocity is not simply proportional to the energy, shifting the averaging somewhat. The electron angular distribution as a function of $\theta_e$ also varies with $\psi_p$ and $\psi_e$, also shifting the averaging process somewhat. Still these are generally small factors compared to the dominant influence of the photon energy and even electron fraction dependence on photon energy.

In this section various aspects of the incident photon spectrum and number per unit area have been considered from the viewpoint of average quantities associated with resulting effects of the photon interaction. This reduces the photons to some discrete numbers such as energy flux per unit area, number per unit area, average photon energy, average mass absorption coefficient, dose, average electron fraction, number of electrons per unit area, average electron energy, average electron velocity, and photon pulse characteristic time. Note that many of these quantities require the definition of an idealized space system such as an aluminum slab one electron range thick and perhaps neglecting photon attenuation in the slab. Many more characteristic numbers can be defined if one wishes. In general it will be a difficult task to exactly reproduce the desired nuclear weapon photon spectrum in a simulator using say a flash X-ray machine. However one must have some way of judging if he is even getting close or which parameters are being exceeded and which are deficient. This allows for progressive

improvement in the simulation. The parameters discussed here are rather natural ones and these with their associated formalism (as elaborated above) should form a useful basis for characterizing photon sources for both calculational (design) purposes and experimental measurements.

## III. Some Aspects of the Photon and Electron Simulation

A photon source for the simulator must illuminate a space system with a photon flux over some area $A_s$ ($= \pi r_s^2$) which we take as circular (for convenience) with radius $r_s$. One part of the simulator design is this photon source. The total simulator involves much more than just the photon source, such as the vacuum tank to hold the space system and various equipment associated with the vacuum system. Thus one might even have more than one X-ray machine, for example, for different photon sources. One might also start out with a not very large flash X-ray machine and as time goes on replace this machine with progressively better machines.

There are various types of pulsed photon sources one might use for such a simulator. In order to closely approximate the desired weapon photon spectrum and time history one might use a small nuclear device in an underground test context. Due to the required vacuum system for the space system environment an underground test could be rather difficult. The lack of repeatability on any short time scale limits the usefulness of such tests. Nevertheless duplicating the weapon X-ray spectrum can be very difficult for a large flash X-ray machine because of the comparatively low photon energy for which such X-ray machines are quite inefficient given the present state of the art. Thus one cannot completely dismiss the possibility of nuclear weapon sources for the simulator. While most of the discussion of the simulator design assumes the use of flash X-ray machine sources the same design features for the remainder of the simulator can be applied for the most part in the case of a nuclear weapon source or other type of pulsed photon source.

First consider the localized source which we might call a point source as shown in figure 3.1A. Such a source would be typical of presently existing flash X-ray machines. A high energy electron beam strikes a localized target where photons are generated primarily as bremsstrahlung. To gain high conversion efficiency the electrons are made to strike the target with several (or even 10 or 15) MeV energy. This produces bremsstrahlung with a few MeV energy which are predominantly forward scattered. This produces a cone of photon radiation leaving the "point" source. The photon spectrum has typical energies in the same range as the $\gamma$-ray spectrum of a nuclear weapon. The relative number of low energy photons is, however, small compared to the relative number of nuclear weapon X rays. Nevertheless such machines exist and obtaining large fluxes of low energy photons in short pulses is difficult by comparison. Thus such types of flash X-ray machines are interesting for use with the simulator, at least initially. As time goes on one might try to improve the quality of the simulation by using better designs of X-ray machines for this kind of simulator.

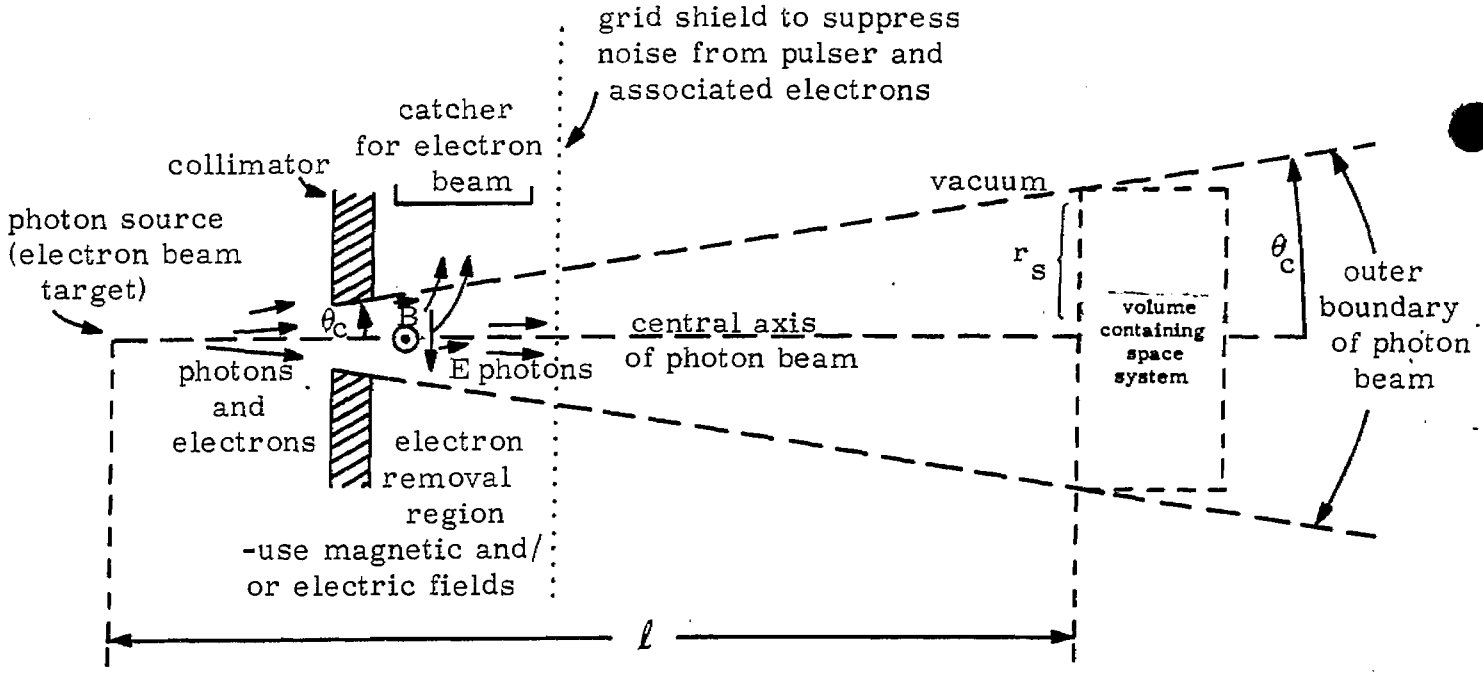


A. Point source

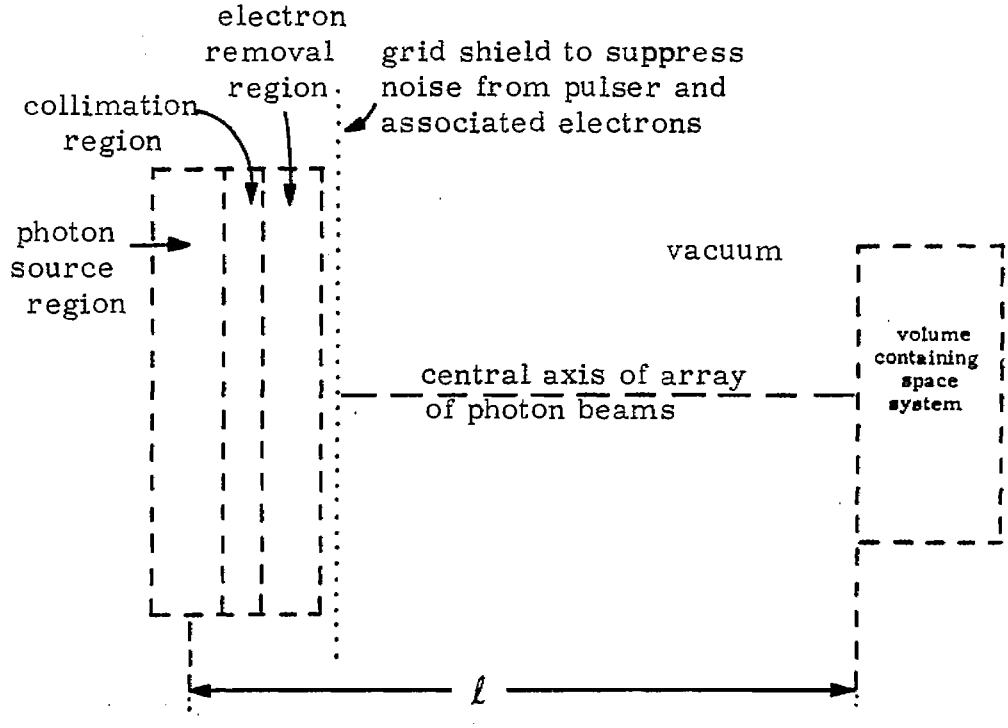


B. Distributed source

Figure 3.1 Two Kinds of X-Ray Sources

Typical high photon energy point sources for this kind of simulator can be characterized by some half cone angle $\theta_c$ as in figure 3.1A. This angle is chosen so that for $0 \leq \theta \leq \theta_c$ the photon flux has some desired degree of uniformity. Collimate the photon cone at this angle to get rid of unwanted photons that can interact with the simulator structure but are not going to be used to interact with the space system. If $\ell$ is the distance to the space system from the approximate point source then the photon simulation radius $r_s$ is just

$$r_s = \ell \tan(\theta_c) = \ell\theta_c[1 + O(\theta_c^2)] \quad \text{for } \theta_c \to 0 \tag{3.1}$$

Then given $r_s$ because of the size of the space system this point source can be positioned so as to just illuminate all the space system. Given the total photon number, energy, etc. in this cone then the maximum densities (on a per unit area basis) available from this source are fixed basically by dividing by $A_s$.

For comparison to our example $10^{16}$ J weapon at 40 Mm distance as in equations 2.8 and 2.9 and table 2.1 we have picked $r_s = 5$ m. Let us also briefly look at typical large flash X-ray machines. For sake of discussion consider the operating characteristics of the Hermes II machine.[12] This produces a 70 ns wide bremsstrahlung pulse from an electron beam with electron energies of roughly 10 MeV giving a 4000 rad dose (in water) at 1 m from the tantalum target. At 9° off the beam axis the photon dose is down to about .6 of the axial value. Thus for our example machine (neglecting dose conversion from water and noting that 1 rad is 100 erg/gm or $10^{-2}$ J/kg) we then take

$$\text{example machine} \begin{cases} \theta_c \simeq .05\ \pi \simeq .157 \text{ radians} \\ d_{p_o} \simeq 40\ \ell^{-2} \text{ J/kg} \end{cases} \tag{3.2}$$

Given the $r_s$ value we have

$$\text{example machine and space system} \begin{cases} r_s = 5 \text{ m} \\ \ell \simeq 31.5 \text{ m} \\ d_{p_o} \simeq .04 \text{ J/kg} \end{cases} \tag{3.3}$$

Comparing this dose to what appears in table 2.1 we see that this is more dose than our example weapon would give if all photons were 100 keV but less dose than it would give if all photons were 10 keV. Thus a Hermes II type machine looks in the ballpark as far as dose is concerned, but this neglects many subtleties. The weapon has a distributed photon spectrum for which the dose (or perhaps the dose that penetrates to a certain depth of aluminum) must be evaluated.

There are, of course, various other comparisons between the example machine (with space system) and the example weapon (with chosen distance). For example the photon pulse from Hermes II has a pulse width of 70 ns while for our example weapon we use a nominal 10 ns for a characteristic time. The average photon energy for our example machine is a few MeV while the weapon photon spectrum is dominated by the X rays with much lower energy. The same discrepancy is then also noted for the average energy of the electrons emitted from the space system (using the previously discussed slab model) due to the close relation of the energy of the emitted electrons to the energy of the incident photons. Considering the average electron velocity a 1 MeV (not including rest mass) electron has a speed of about .94 c while a 10 keV electron has a speed of about .2 c. Of course there is some difference in the direction of the emitted electrons but the relative speeds are somewhat closer than the relative energies.

Convert the dose to energy per unit area through a mass absorption coefficient. Taking an average photon energy[13,14] of 1.6 MeV we have a mass absorption coefficient of about .0025 $m^2/kg$. Then the energy per unit area and number of photons per unit area are

$$\text{example machine and space system} \begin{cases} \phi_{p_o} \simeq 16 \text{ J/m}^2 \\ n_{p_o} \simeq 1 \times 10^{14} \text{ m}^{-2} \end{cases} \tag{3.4}$$

Comparing the number of photons per unit area to the results for the example weapon in table 2.1 the comparison is not unfavorable except for very low average weapon photon energies. One would come to a similar conclusion about the comparative number of electrons per unit area emitted from the idealized space system (slab model). The energy per unit area is much larger than that for the example weapon (equations 2.9). Thus our example machine for some parameters exceeds the example weapon while for other parameters the example machine is deficient. Thus existing flash X-ray technology can do a partial simulation of the weapon photons to the required levels. However, some aspects are not closely simulated indicating that

further development of such X-ray machine technology is needed to better tailor the photon spectrum. The above results indicate that some parameters can even be reduced if needed (such as the photon energy flux) in the process of better tailoring the photon spectrum. In building a simulator for the system generated EMP on space systems one might even begin testing with a particular X-ray source and then change it for something better as tests become more detailed and sophisticated and better X-ray source technology is available.

One of the directions one might pursue in developing better flash X-ray machines for this application is the distributed photon source concept as illustrated in figure 3.1B. This kind of simulator does not require large photon fluxes over small areas. The space system is generally quite large compared to the usual exposure volumes used in TRE tests with flash X-ray machines. Why start with a very intense photon flux over some small area and then expand it to a large test area? By spreading out the photon source over dimensions comparable to the space system size the photon intensity near the distributed source need be no larger on the average than the photon intensity at the space system. One might even tailor the direction and intensity of the photons coming out of the source to improve the uniformity in spectrum, numbers, and direction at the space system. Having a much larger photon source area one can generate more photons, generate a better photon spectrum, and/or have a better time history of the photon pulse. There is now more space in which to cram electron beams, anodes, etc. allowing one to improve various aspects of the photon output.

This kind of photon source might typically be an array of small sources (cathodes, electron beams, and anodes) arranged in a pattern of unit cells which fit together as simple planar geometric figures such as squares, regular hexagons, and equilateral triangles. Each cell can have its own return current paths, returning the beam current, thereby isolating an electron beam in one cell from those in other cells. Thus an array of photon sources can reduce the problem of generating high current electron beams and make it easier to lower the electron energy in the beams and thereby lower the average energy of the bremsstrahlung, although at a decrease in conversion efficiency. One might integrate all these individual sources into a more continuous source provided return currents are distributed throughout the electron beam which is travelling toward the bremsstrahlung target. Such current paths, say on small wires, can effectively isolate one part of the beam from another. Such added current paths can be oriented such that some are parallel to the electron beams while others are perpendicular to the beams to effectively alter some of the macroscopic features of the ratio of electric and magnetic fields associated with the beams (or beam array). The added current paths might then be oriented at some optimally chosen angle to achieve

similar effects. If standing waves of the electron beam in such a structure are troublesome one might introduce some random variations in the positions of such current paths depending on the details of the problem. Figure 3.2 shows some various neutralizing current path geometries one might consider. Of course for some cases one may not drift the beam but position the cathodes fairly close to the anodes so that while the magnetic field neutralization is needed the electric field neutralization is avoided. However if the cathodes, or some of them, are far behind the anodes to reduce packing problems and/or to spread out the cathodes over a larger area than the anode array (thereby having a convergent electron beam array) then beam drifting is required and gases, metallic conductor arrays, and/or some combination of the two might be profitably used. In addition a magnetic field parallel to the beam may help in controlling it. In a beam array such a guide field may need to be periodically reversed to keep the guide magnetic field lines closed on themselves so as not to significantly fringe out to the space system.

The cathodes and anodes can also be designed to fit into the distributed photon source array. The cathodes can be separated from one another or some other technique can be used to allow the return current paths to pass through the cathode region so as to isolate portions of the electron beam array from one another. Each cathode might be further segmented in various designs such as are used to obtain good field emission characteristics as required for the beam admittance (or perhaps here admittance per unit area).

Perhaps more significantly the anode can be split up in several ways to improve the conversion efficiency from electrons to photons, particularly low energy photons. This can be achieved by using multiple anodes for the electron beam to pass through consecutively, each anode being only an appropriate fraction of an electron range thick. The direction to the target would be off at some angle from the beam so that the low energy photons which are produced somewhat isotropically only have to travel part way through one of the anode foils on the way to the space system. This is compared to each electron in the beam which passes through a large number of anode foils. Another way to achieve this effect is to make the electron beam make multiple passes through a single thin foil. If the passes are all through the same area then the local space charge density is increased, limiting the current density somewhat. The multiple pass might be achieved through electric fields by pulsing the anodes positive with respect to the cathodes which are electrically grounded to the pulser body. One might have two cathodes to each anode, one on either side producing two electron beams travelling in opposite directions. If one of the cathodes is in the way of the desired photons it could be made essentially transparent by making it look like a screen where most of the cross section area would be holes. To this dual

indicates the position of an electron beam.

• indicates the position of a current return conductor.

⊙ and ⊗ indicate patterns of alternate directions for guide magnetic fields in adjacent cells for cases of triangular and square cells. These require additional coils or permanent magnets. For hexagonal cells alternating directions can be accomplished in groups of cells.

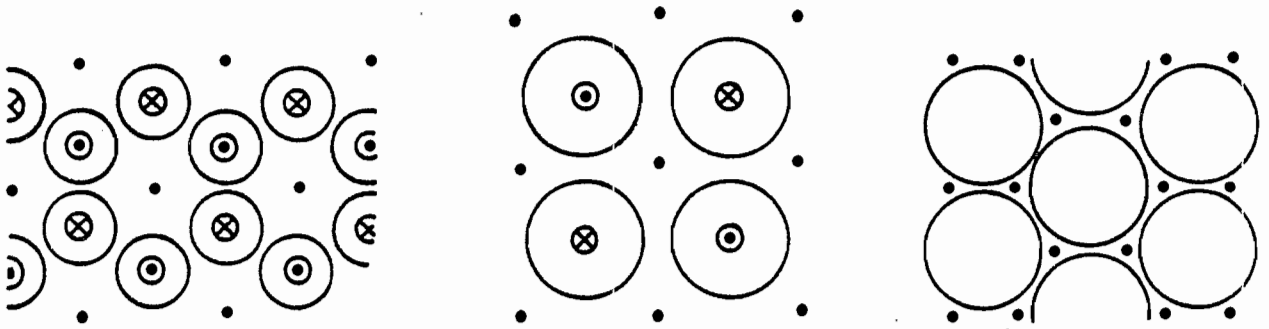

triangular cells | square cells | hexagonal cells

A. Some geometries for return current paths together with beams in arrays

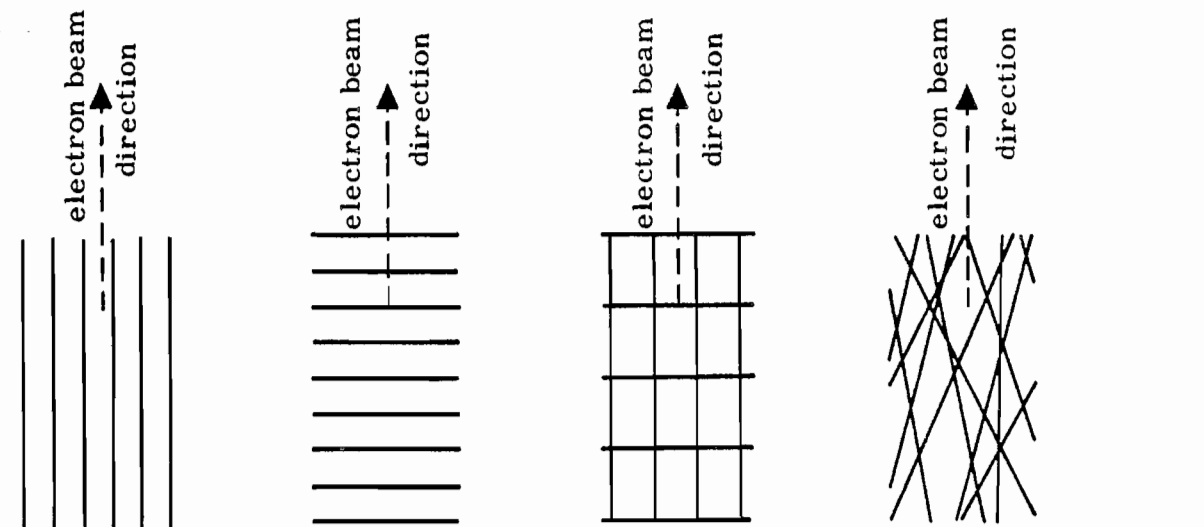


B. Current and charge neutralization conducting paths distributed in electron beams

Figure 3.2 Discrete Current and Charge Neutralization Conductors in Electron Beams and Beam Arrays

cathode arrangement one could also add a guide magnetic field as well as various additional beam directing conductors and gases. Figure 3.3 shows some of these numerous possibilities.

Magnetic fields can also be used to make multiple pass anodes. One can simply make the electrons race around as in a cyclotron by using a magnetic field perpendicular to the electron beam. The electrons could be made to strike the same foil once or twice in one circular path. One or more special entrances for the electron beam(s) would be needed to inject the electron beam(s) into the transverse magnetic field. In such a scheme multiple foils could also be used and the approximate electron paths need not be circular (or spiral as a better approximation) but might be helical (with a spiral decay). Another scheme might have oppositely directed magnetic fields on opposite sides of a foil, both fields being parallel to the foil, by having the foil itself at least transiently carry part of the guide-field-producing current. Such a combination of guide magnetic fields would make the electrons circle in opposite directions on opposite sides of the foil and thereby make the electron cloud drift along the foil as the electrons passed back and forth through it. Clearly there are many schemes for making electrons make multiple passes through thin foils so as to reduce the attenuation of those low energy photons produced in the anodes which are headed toward the target. Perhaps some combination of electric and magnetic field geometries with foil geometries such as those above will prove optimum.

As part of an optimum anode design one can control the relative distances that electrons and photons of interest travel through anode foils. Since the space system is in one general direction from the anodes then the anode foils can be aligned such that their surfaces are approximately perpendicular to this direction. The photons of interest then have a minimum foil thickness to traverse. However the electrons in the beams need not travel in this same direction. Their paths through each anode can be significantly larger than the foil thickness by striking the anode at some optimum grazing incidence angle. Thereby the electrons can deposit a greater fraction of their energy while still keeping the foil thin to allow more of the low energy photons to escape in the direction of interest. The ratio of electron travel distance through the foil to the foil thickness is then greater than one and can be thought of as one of several possible figures of merit for the anode array design.

Since the lowest energy photons that propagate to the space system come from the last part of the foil thickness (because of the high photon attenuation in the foil at sufficiently small photon energy) then the foil might even be laminated or composed of several thinner foils. The foil nearest the space system would be chosen to have atomic number Z to optimize to production of the very lowest energy photons. The next foil back would be designed with slightly higher energy photon

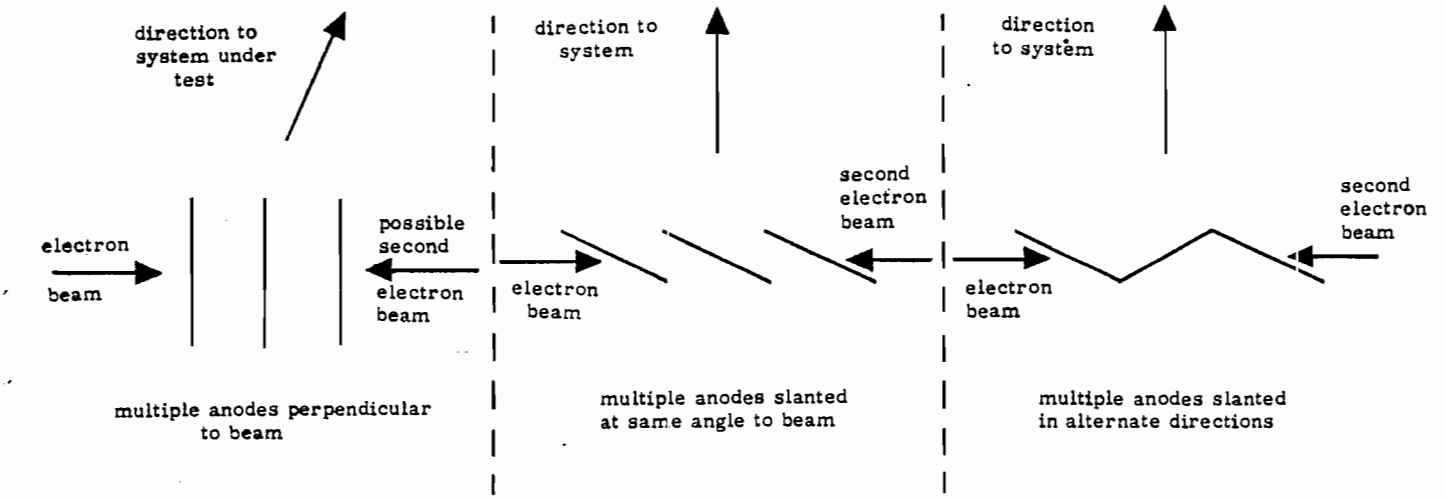


A. Multiple thin anodes

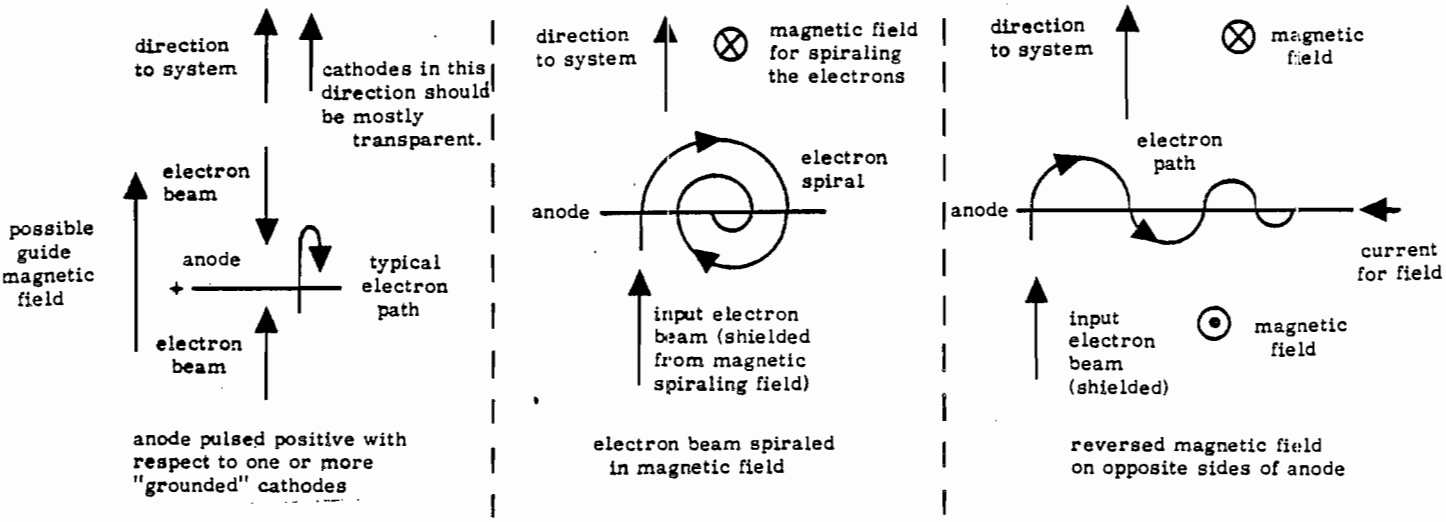


B. Multiple pass of electron beam through one anode

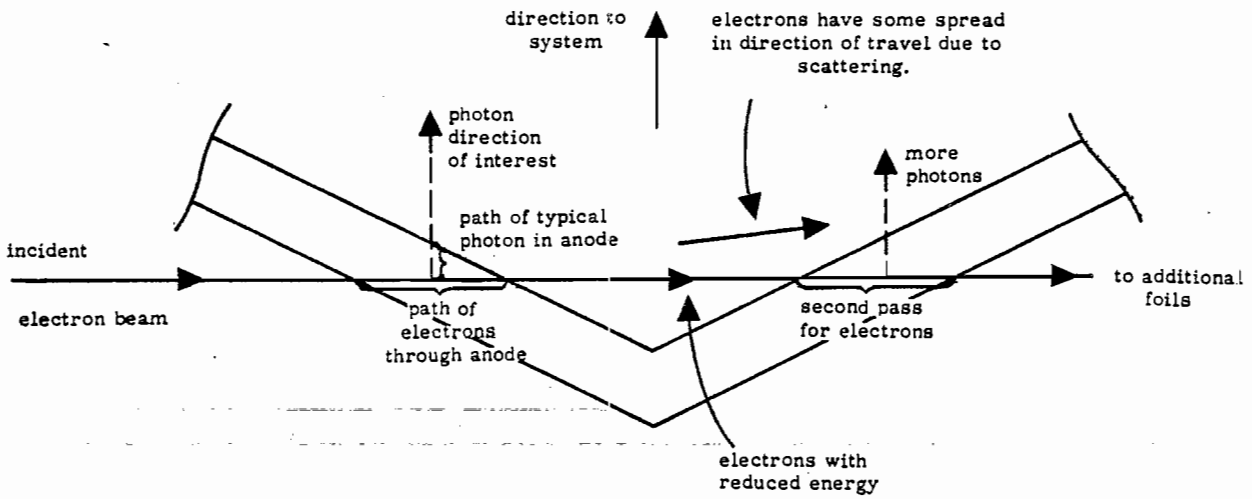


C. Increasing ratio of electron to photon travel distance in anode

Figure 3.3 Anode Geometries for Increasing Electron To Photon Conversion Efficiency

production in mind, and so on with successive layers. It is not clear how much improvement if any one can achieve this way but it is something to consider.

Now we don't want photons going everywhere with all directions in this simulator. We wish to illuminate only the space system, and illuminate it with photons travelling in approximately one direction. A technique which should then be considered is collimation. First consider collimation in the case of a single point source as illustrated in figure 3.1A. The concept of collimation is rather straightforward in this case. At some position between the idealized point source and the space system place a thick photon attenuator with a hole in it which allows only those photons directed toward the space system to pass through the hole, the rest being severely attenuated. There is some scattering of photons off the "edge" of the collimator hole but such scattering can be considered in the detailed design of the collimator. Multiple collimator assemblies can be considered so as to improve the overall collimation. Generally one would like the collimator assembly to be fairly close to the photon source so that the collimator assembly does not approach the space system so closely so as to make the other items which come after the collimator be placed unnecessarily close to the space system and thereby increase some of the electromagnetic distortion associated with the presence of the simulator structure.

If one uses the distributed source type of photon generator as shown in figure 3.1B then the collimation problem is somewhat more complex. If one attempts to collimate the photon beam as a whole then the distributed photon source must be moved far away if it is to look like a point source for a collimator to effectively remove the photons not directed at the space system while removing no photons which are directed at the space system. Such a collimator for the whole beam then does not look very attractive because a far away photon source means small efficiency in getting photons to the space system. If one notes that the distributed photon source can be made of many small sources, such as indicated by the patterns shown in figure 3.2, then the collimation can be done fairly close to the distributed source. Each small photon source can be collimated in a manner like that shown in figure 3.1A for a single source. Each small source would then send a photon beam through a collimator at its own optimally chosen angle to illuminate the space system (and very little more than this).

One of the undesirable byproducts of the photon source is electrons directed toward the space system. These need to be deflected away from the space system such that they do not enter the test chamber. Note that one cannot simply stop these with a slab of material because the photons knock electrons off such a slab to replace the removed electrons. Perhaps the

current of such electrons can be reduced, at least for the low energy electrons by having a very thin layer of low Z (atomic number) material as the last material on the photon source. This layer would be one electron range thick at some appropriate small electron energy. This layer should be thin enough to not appreciably attenuate the low energy photons.

The removal of the electrons in the photon beam can be accomplished by static electric and/or magnetic field distributions. One method would use a negatively charged grid with respect to the photon source and the vacuum chamber to turn the electrons back. Of course the grid potential has to be larger in magnitude than the largest electron energy divided by the electron charge. Note that between the grid wires the potential does not have as great a magnitude as on the wires. While the photons themselves knock electrons off the grid this is a comparatively small number because of the small wire size in the grid.[15] Of course one can also minimize the electron emission from the grid by minimizing the atomic number of the grid material and by the use of low atomic number coatings on the grid wires. How effective this technique is depends on the energy of the photons and electrons being generated. For electrons in the 100 keV range this technique should be rather effective. However, for megavolt electrons the required grid potential becomes rather large. In such cases magnetic deflection may be more interesting and transverse electric fields may also be useful. For a distributed source such transverse magnetic and/or electric fields may need to be periodically reversed in the photon source array so that polarities of the transverse electron removal fields reverse between adjacent small photon sources. Certainly one does not want a large magnetic field from the photon source to appear at the space system. A similar technique for turning back the electrons from the photon source is to operate the anode(s) and other parts of the photon source(s) at a positive potential with respect to the vacuum tank etc. This technique can also be combined with the negative electron repelling grid.

There is in general a fair amount of electrical noise signals generated by the photon source. This should be shielded from the space system without much intervening material (which would emit electrons due to the photon environment). A grid with wires running in two or more directions so as to interlace with conducting connections forms such a shield. This grid can also be the electron repelling grid.

This grid concept is also useful for reducing the electron backscatter (due to both incident photons and incident electrons) from the walls of the vacuum tank. As shown in figure 3.4 there are various grid schemes possible. Such a grid structure can completely surround the space system with the innermost grid forming an approximate Faraday cage surrounding the space system and keeping out external electromagnetic

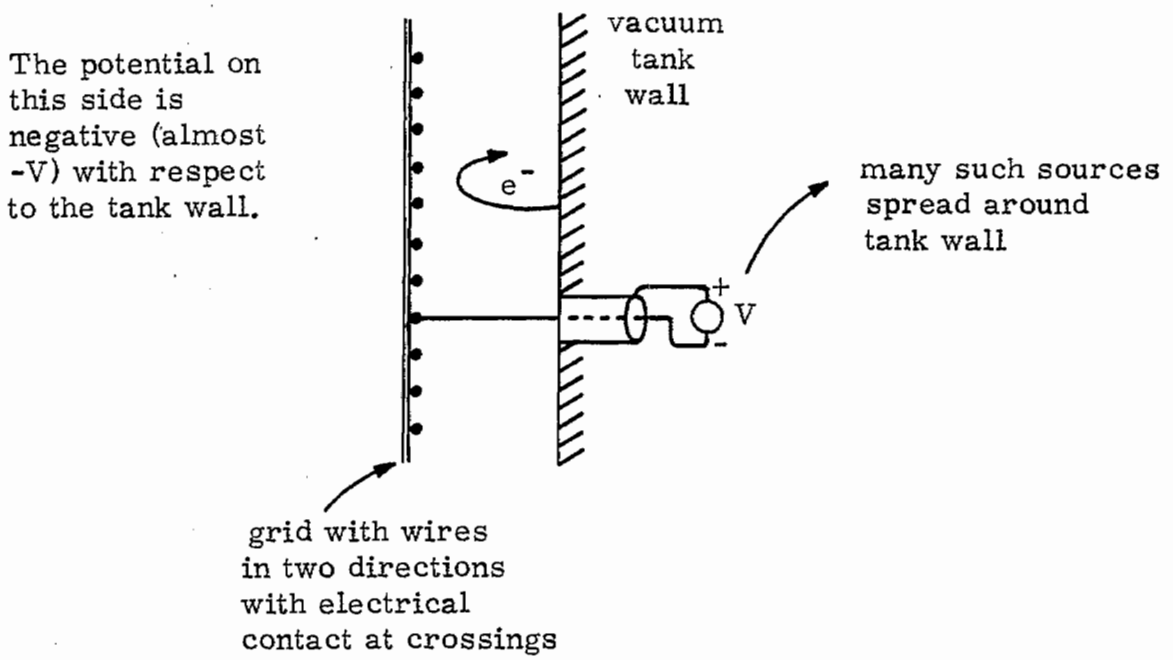


A. Single negative grid near vacuum tank wall

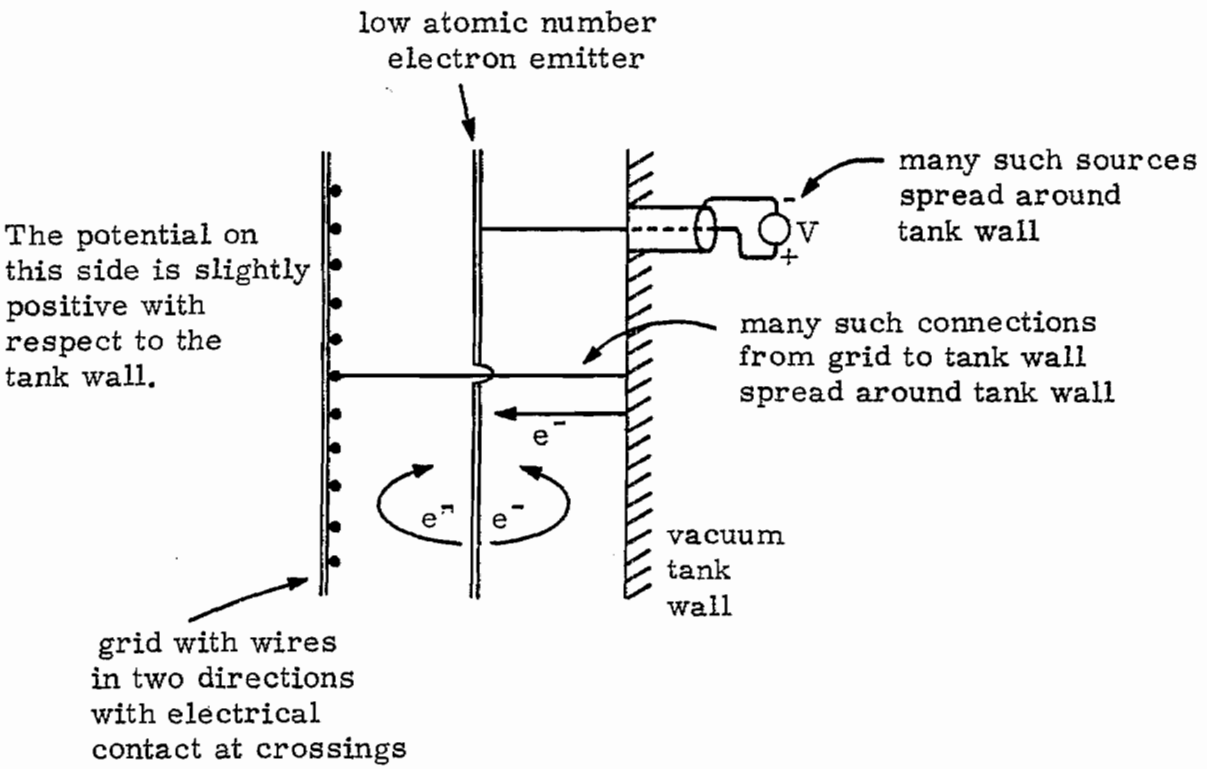


B. Positive electron-emitting surface between tank wall and grounded grid

Figure 3.4 Electron Trapping Grid Structures

signals. While this makes the volume internal to the grid a resonant cavity one can place electromagnetic damping structures inside this volume as discussed later in this note. The volume behind the innermost grid can also support resonances but these can also be damped with resistive loading in positions to intercept the transient signals such as at the power supplies which charge the grids. Resistors can also be placed in the grid structures or extra electron emitters themselves, except for the innermost grid since the innermost grid is intended to be an approximate Faraday cage. Various other structures for electromagnetic damping, such as those to be discussed later, can also be placed outside the innermost grid and inside the vacuum tank if desired.

Figure 3.4A shows the case of a single grid at negative potential inside the vacuum tank. This is perhaps the simplest type of structure for repelling the electrons from the walls yet not turning back the electrons arriving from the space system. The space system is then at some negative potential (not quite the negative grid potential) given by the potential of the test volume before the photon pulse arrives provided that the space system was at the vacuum tank potential before charging the grid and leakage currents to or from the space system can be neglected or compensated for. One disadvantage of this technique is that if one wishes to transmit electrical signals on conducting wires from the inner volume near the inner grid to outside the vacuum tank then conducting wires cannot be used without introducing large potentials (in magnitude) into the inner volume and/or at the vacuum tank on the wires of interest. Note that the tank wall can be coated on the inside with low atomic number material to reduce the electron emission.

An alternate grid structure is that shown in figure 3.4B. In this case the innermost grid is electrically shorted to the vacuum tank wall. Between this grid and the tank wall there is a low atomic number electron emitter plate maintained at a positive potential with respect to the grid and tank wall. This emitter intercepts the electrons emitted from the tank wall; the potential turns back the electrons emitted from this special emitter toward the emitter (up to some maximum energy not quite the magnitude of the electron charge times the bias potential). This emitter need not be a continuous sheet; there should be holes through it for electrical connections. It could be a "venetian blind" type of structure to try to have the direction of maximum electron emission not toward the grid; it must, however, be opaque to electrons coming from the tank wall over most of its area. This general type of electron trapping structure has the advantage of allowing electrical signal paths (wires) to pass from the tank wall to the grid without a potential change. However, the potential of the inner volume is not quite that of the grid due to the influence of the electron emitter structure between the grid and tank wall.

In these various electron trapping schemes there are connections which must be made between the various layers (grids, emitters, tank wall) to maintain them at certain relative potentials. When the photons and electrons arrive at these structures there will be a significant fast transient electromagnetic pulse throughout these structures. The grid structures etc. must have a high frequency response for maintaining the desired potentials throughout the pulse within some tolerance. The various connections between the layers (shorts and power supply connections) should then be placed closer than the fastest times in the pulse. The lead and power supply impedances should also be sufficiently small so as to not limit the response time for maintaining the desired potentials.

The effectiveness of the grid system for reducing electron backscatter depends on the electron (and photon) energies. If the electron energy is low because of the photon source being designed to give only low energy photons then the grid system can be quite effective in trapping the electrons. On the other hand if high energy (say MeV) photons are emitted by the photon source then the required grid potentials can get to be quite large. If, however, the grid is used at a lower potential then one can still trap the corresponding lower energy electrons.

For trapping the high energy electrons and photons as well one can use a get-lost hole. As indicated in figure 3.5 such a "hole" would be located so as to intercept the photons directly from the source which pass through the space system. If the hole is sufficiently deep compared to its diameter then the resulting electrons and photons scattered from the walls of the hole are attenuated geometrically before returning to the test volume. One could still have the grid system covering the inside of the remainder of the vacuum tank and cover the get-lost hole as well for extra electron removal and to complete the inner approximate Faraday cage. Inside the hole which intercepts the main photon beam one can place additional electric and magnetic field distributions to bend the electron paths back to the walls. It is this portion of the tank wall in direct illumination of the photon beam (except for some attenuation from the space system) which is most significant from the point of view of electron and photon backscatter.

The question of the energy of the incident photons is fairly important in determining the number and energy of the electrons emitted from the space system materials. The photon spectrum from photon sources such as flash X-ray machines will be limited by technology (which should improve with time). One might try to compensate for undesirable aspects of the photon spectrum by coating parts of the space system with materials of appropriate atomic number to shift the electron spectrum and/or numbers in the desired direction. Such materials should also be chosen so as not to interfere with the electrical characteristics of the system.

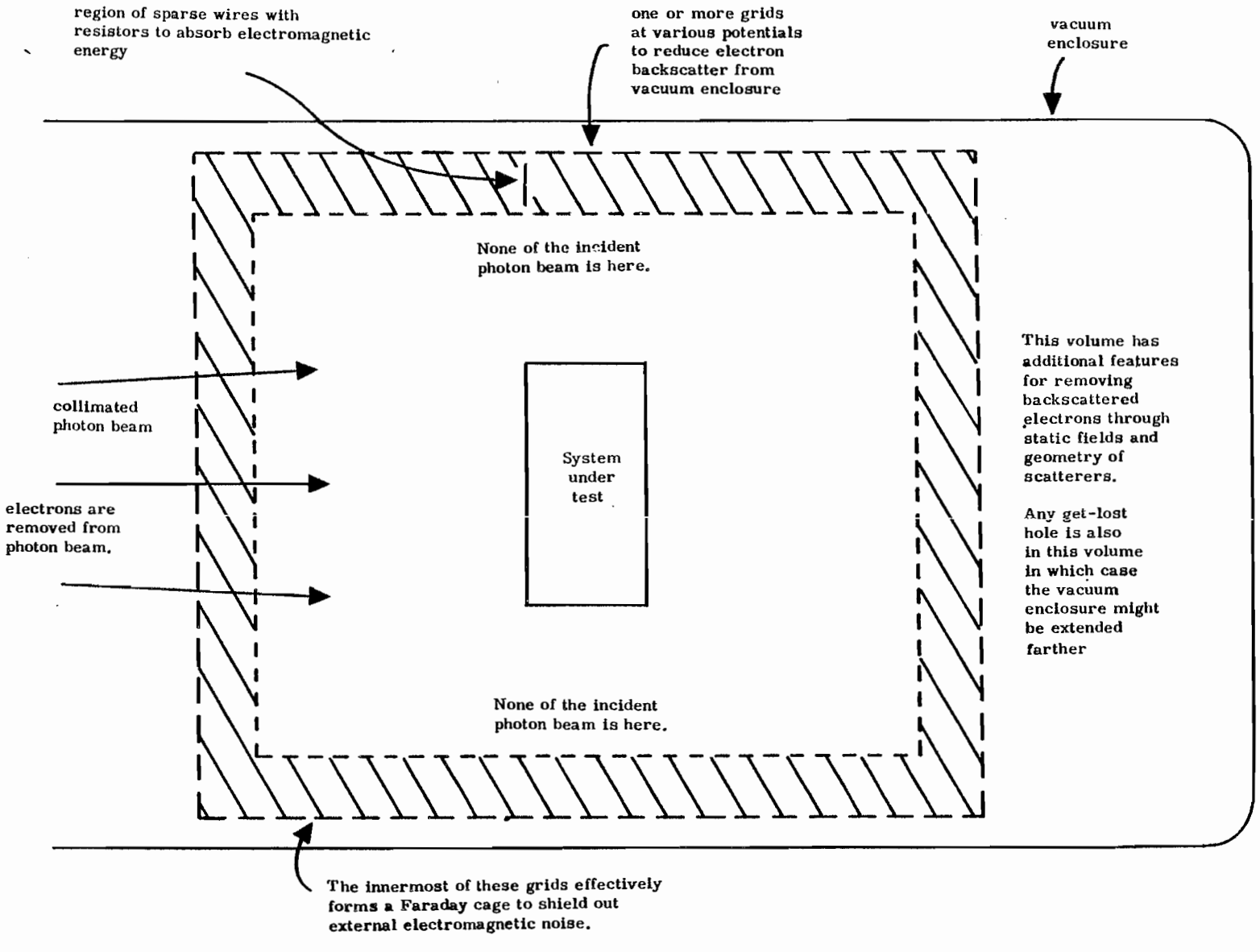


Figure 3.5 Photons From a Pulsed Photon Source Driving an Exoatmospheric System in a Test Chamber with Properties Approximating Free Space

Figure 3.5 gives a rough overall view of the test chamber geometry, showing the photons incident from one side with the special backscatter reduction system (including get-lost hole) on the opposite side. The grid system surrounds the space system and isolates it from the vacuum tank wall. The electromagnetic damping structure is inside the grid structure to couple to the fields in the test volume; this is discussed in later sections. The test chamber is evacuated to simulate space conditions. However, some residual gas is left because vacuum systems are not perfect. How good a vacuum is required depends on several factors which will now be briefly indicated.

First the residual gas should be small enough that the number of electrons produced by photon interaction with the gas is small compared with the number knocked off the space system. Viewed another way only a small fraction of the photons from the photon source should scatter off the gas molecules. This implies that the photon mean free path (for first scatter) be large compared to the maximum dimension of the test volume. Second the trajectories of the electrons knocked off the space system should not be altered by scattering in the gas. This means that the typical electron ejected from the space system should on the average scatter significantly less than once in travelling across the test volume. For this purpose a scatter is counted as such if it makes any significant change in the electron's energy or direction. Third the number of low energy conduction electrons (ionization) generated in the background gas by scattering of the high energy electrons (and photons) should be small compared to the number of electrons knocked off the space system. This implies that each high energy electron knocked off the space system should on the average produce much less than one electron-ion pair in the background gas in travelling across the test chamber.

There are other effects associated with the background gas and the associated drifting of the low energy electrons in it. In particular the space system is charged positive by the photon pulse and the charge is eventually neutralized in space by ions and low energy electrons.[6] In the type of simulator considered here this could be accomplished by the introduction of low energy electrons from electron guns connected to the tank wall and/or inner grid with appropriate power supplies. The number and time history of such electrons would have to be appropriately controlled. There is also the problem of electrical breakdown in the background gas because of the grid potentials and the transient fields associated with the system generated EMP. The background gas number density should be small enough to avoid such breakdown by allowing the lower energy electrons moving under the influence of the fields to travel across the test volume while producing negligible additional ionization due to collisions.

There are thus various complex physical processes associated with the background gas which must be considered in the design. Some of the more important of these have been briefly discussed here. Much should be done to quantify these effects in detail for use in designing specific simulators of the present general type.

One more characteristic of the space around a space system of interest is the presence of a background magnetic field such as that due to the earth. Depending on the position of the space system the amplitude of this field can vary considerably. In particular as the space system altitude is increased away from the earth (say to synchronous altitude) the earth's magnetic field decreases significantly. The presence of such a magnetic field can significantly alter the trajectories of the electrons knocked off the space system. A simulator (for the system generated EMP on space systems) which is located on the earth surface will then need to compensate for the local earth's magnetic field and produce the ambient magnetic field desired on the space system. This can be accomplished by constructing large coils around the vacuum tank with optimally chosen positions and currents. Appropriate power supplies are needed to drive the currents in such a coil system unless superconducting coils (or permanent magnets) are used. Note that if permeable steel is used for the vacuum tank then the permeability of the steel and the geometry of the tank influence the coil currents and positions required for cancelling the earth's magnetic field.

## IV. Some Electromagnetic Features of the Test Chamber

Thus far the simulator has been discussed from the point of view of the photon and electron transport associated with the various spectra and materials and how this corresponds to a nuclear weapon and a space system in space. Other aspects of the ambient space environment such as the earth's magnetic field also influence the electron motion and have been briefly discussed. In this section we consider one of the most important aspects of the simulator design, namely its electromagnetic performance in simulating the electromagnetic conditions of space as far as the space system response to the system generated EMP is concerned. The problem is the presence of the vacuum tank, backscatter reduction grids, and other large objects associated with the simulator which interact with the transient currents on the space system and thereby change the response of the space system.

Starting with the vacuum tank, if it is metal then it scatters the fields associated with the currents on the space system and in the space around the space system. One could try to reduce the scattering from the vacuum tank by segmenting the tank walls with insulators at some increase in problems of maintaining a vacuum. One might also try to make a dielectric vacuum tank to reduce its electromagnetic interaction with the fields. However, if there are grid structures surrounding the system to reduce electron backscatter, these grid structures strongly interact with the transient electromagnetic fields. In particular if the innermost grid is an approximate Faraday cage (for noise suppression) then the vacuum tank walls are somewhat shielded from the space system (except for the electrons passing through the grid) and the innermost grid, not the tank walls, is the most important for its electromagnetic influence on the space system.

Assuming then an approximate inner conducting boundary, such as the innermost grid (or tank wall if impedance loaded grids are used), then one must account for the interaction of this boundary with the space system. Such interaction should be reduced to acceptable levels. The next several sections consider some aspects of this interaction and some techniques for reducing it.

## V. Capacitance Between the Space System and the Test Chamber

One of the distortions of the space system response associated with the walls of the test chamber is the increased capacitance of the space system. This is a low frequency parameter. In free space far from any other objects the space system has a certain capacitance to infinity. The electrons knocked off the space system charge it to some positive potential with respect to infinity. Inside the test chamber the space system capacitance is increased thereby decreasing the potential of the space system for the same number of electrons escaping to the walls. This lower potential means that electrons of lower energy can escape to the walls thereby increasing the charge left on the space system after the low energy electrons have returned to the space system. The presence of the electron cloud affects this capacitance. In this note we only consider the capacitance without the electron cloud around the space system. Note that in calculating the capacitance the presence of grids and lossy damping systems should be counted as part of the test chamber walls; these items can increase the capacitance and such effects should be included.

A simple first estimate of this capacitance increase can be obtained by considering a spherical capacitor as shown in figure 5.1. The potential between the concentric conducting spherical shells is just

$$V = \frac{Q}{4\pi\epsilon_o r} \tag{5.1}$$

where Q is the charge on the inner sphere. The capacitance is just

$$C = \frac{Q}{\Delta V} = 4\pi\epsilon_o \left[\frac{1}{r_1} - \frac{1}{r_2}\right]^{-1} \tag{5.2}$$

where $r_1$ and $r_2$ are the radii of the inner and outer spheres respectively. The reference capacitance or capacitance to infinity of the inner sphere is

$$C_\infty = 4\pi\epsilon_o r_1 \tag{5.3}$$

The relative capacitance can be computed from

$$\frac{C}{C_\infty} = \left[1 - \frac{r_1}{r_2}\right]^{-1} \tag{5.4}$$

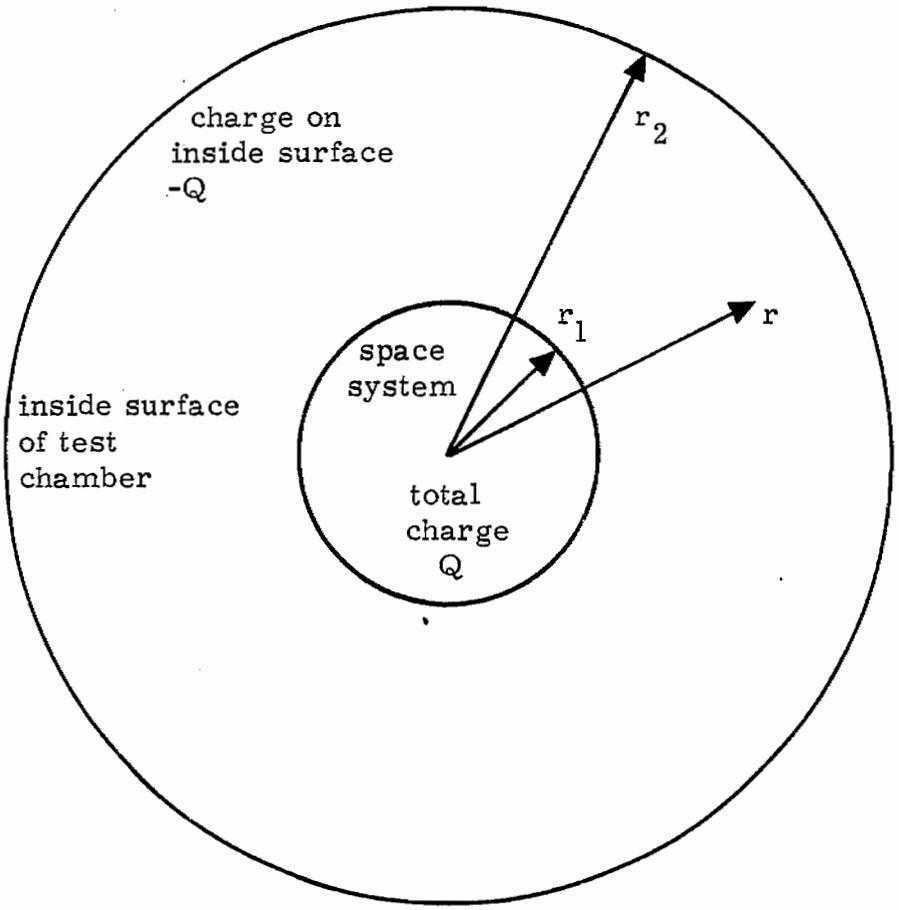


Figure 5.1 Spherical Capacitor Representation of Space System and Test Chamber

The relative capacitance increase is

$$\frac{\Delta C}{C_\infty} = \frac{C - C_\infty}{C_\infty} = \left[1 - \frac{r_1}{r_2}\right]^{-1} - 1$$

$$= \frac{r_1}{r_2}\left[1 - \frac{r_1}{r_2}\right]^{-1} = \left[\frac{r_2}{r_1} - 1\right]^{-1} \tag{5.5}$$

which for $r_1/r_2 \to 0$ is

$$\frac{\Delta C}{C_\infty} = \frac{r_1}{r_2} + o\left(\left(\frac{r_1}{r_2}\right)^2\right) \tag{5.6}$$

This relative capacitance increase is one figure of merit for this type of simulator; it should be kept small compared to 1.

The relative capacitance increase can be calculated for various shapes of space systems and inner chamber walls (including grids and damping structures). A useful approach to this problem is to approximately separate the space system geometry from the chamber geometry. To do this one can define effective values of $r_1$ and $r_2$ from two separate electrostatic boundary value problems. Consider the space system with some net charge in free space and calculate $C_\infty$, its capacitance to infinity. Use this to define

$$r_{1_{eff}} \equiv \frac{C_\infty}{4\pi\varepsilon_o} \tag{5.7}$$

This is a special type of mean radius for the space system.

As one goes farther away from a charged space system in free space the equipotentials are approximate spheres. Finding the best fit for the center of these approximate spheres in the limit of large radius for the equipotential surfaces defines an electrical center $\vec{r}_{c_1}$ for the space system. The electrical center can also be equivalently defined from

$$\vec{0} = \int_{\substack{\text{space}\\\text{system}}} (\vec{r} - \vec{r}_{c_1})\,\rho(\vec{r})\,dV \tag{5.8}$$

where $\rho(\vec{r})$ is the charge density on the system. Note then that for a coordinate system centered on $\vec{r}_{c1}$ the system has no electric dipole moment. The leading term in the potential and electric field expansion comes from the electric monopole moment (or total charge) given by

$$Q = \int_{\substack{\text{space} \\ \text{system}}} \rho(\vec{r})\, dV \tag{5.9}$$

The position of the electrical center of the space system is sometimes obvious from the symmetry of the space system or of the idealized shape representing it.

Having reduced the space system to an effective radius and an effective center let us do something similar for the test chamber. Assuming that the space system is very small compared to the inner test chamber dimensions (including grids, damping systems, etc.) then replace the space system by an arbitrarily small charged sphere of radius $r_o$. Move this test sphere inside the test chamber until its capacitance to the test chamber is minimized. Find the limit of this position as $r_o \to 0$. This defines $\vec{r}_{c2}$, the electrical center of the test chamber. In some cases of test chamber geometries the position of this minimum may not be unique and/or there may be relative minima in the test volume. However such cases are not very useful for test chamber design if one wishes to test only one space system at a time.

Having found the electrical center $\vec{r}_{c2}$ of the test chamber one can then find the effective radius $r_{2_{eff}}$ for the inside of the test chamber. With the small test sphere centered on $\vec{r}_{c2}$ calculate the capacitance and use

$$\frac{1}{r_{2_{eff}}} = \lim_{r_o \to 0} \left[ \frac{1}{r_o} - \frac{4\pi\varepsilon_o}{C} \right] \tag{5.10}$$

which comes by replacing $r_1$ by $r_o$ and $r_2$ by $r_{2_{eff}}$ in equation 4.2 and then taking the limiting case of a small test sphere. Note that the position $\vec{r}_{c2}$ of minimum capacitance for the small test sphere is that position which maximizes $r_{2_{eff}}$.

In calculating $r_{2_{eff}}$ one must include the various equipment attached to the inside of the tank walls. This includes the grids for electron capture and the electromagnetic damping system which may be also sparse like a grid so as to emit few electrons in the photon and electron environment incident on it. The innermost of these sparse structures is the most important

for determining $r_{2eff}$. As a first rough estimate of $r_{2eff}$ one could simply choose an average radius from the geometric center of the test chamber (assuming appropriate symmetry) to the innermost conducting (even finitely conducting) materials which would be placed inside the vacuum tank connected to the tank walls through various impedances, etc. Since these structures are somewhat sparse then $r_{2eff}$ is somewhat larger than an estimate which assumes these structures a conducting surface at the innermost position. The actual $r_{2eff}$ is increased and the extra distance can be estimated for grid like structures using various boundary value problems such as for two dimensional grids.[16]

By use of the technique of spherical inversion the interior boundary value problem for $r_{2eff}$ can be converted into an exterior boundary value problem in which the arbitrarily small test sphere centered on $\vec{r}_{c2}$ is converted into an arbitrarily large sphere approaching infinity.[17] The inversion is centered on $\vec{r}_{c2}$. By this procedure the calculation of $r_{2eff}$ is converted into a calculation for $r_{1eff}$ (with appropriate conversion factors) with a somewhat altered shape. One can then choose an appropriate geometry (such as an ellipsoid) for the inverted exterior geometry and invert it back to an interior problem of interest so as to tabulate $r_{2eff}$ for various interior chamber shapes.

For the exterior problem such as used for calculating $r_{1eff}$, the effective radius of a space system, there are many shapes that one could consider and tabulate. One of the simpler of these is the ellipsoid which has a closed form solution in terms of an elliptic integral.[17] An ellipsoid with three separate principal-axis radii gives some flexibility in trying to approximate objects of interest. By using such a shape to enclose a space system of interest one can obtain an upper bound on $r_{1eff}$. Such a shape inscribed inside the outer boundaries of a space system (if conducting) can be used to obtain a lower bound on $r_{1eff}$. An average of upper and lower bounds can be used as an approximation of $r_{1eff}$.

This low frequency capacitance between the space system and the test chamber is one of the definable parameters for the interaction of the two. There are various detailed boundary value problems to be solved and tabulated for $r_{1eff}$ and $r_{2eff}$ (as well as $\vec{r}_{c1}$ and $\vec{r}_{c2}$ in some cases). Various geometries such as ellipsoids, elliptic cylinders, rectangular parallelepipeds, etc. can be considered. For cases that the internal test chamber dimensions are not much larger than the external space system dimensions then the problem does not quite split into a separate consideration of the space system and test chamber parameters as outlined above. Such more complex mutual interaction problems can also be considered. Many specific boundary value problems need to be considered in detail to definitively understand this type of system-simulator interaction.

One effect of the capacitance increase is to allow more electrons to reach the cavity walls than would escape to infinity from an object in free space. The potential between the space system and the cavity walls is also less than the potential to infinity for the same object in free space. This effect can be partially compensated by giving the space system an initial positive charge. This charge can be introduced through a high value resistor string (with small cross section) from a power supply connected to the innermost electron trapping grid (and damping structure) or to the tank wall. The resistor string would have large enough resistance that no significant current can flow through it during times of interest for the simulated system generated EMP. This technique has a drawback, however, in that it alters the electron trajectories outside the space system at early times during the pulse, whereas a state of no initial charge would give a more realistic simulation at early times. Of course, one could test the space system with various different initial charges in the same simulator. After tests this charging system can also be used to discharge the space system.

Part of the charge (negative) that escapes to the tank walls should ideally return to the space system (if it were in space) at some time characteristic of the round trip time of electrons of less than, but near, the energy of the electrons that escape from the space system. One might do this through resistive paths to the space system, but this would have the significant disadvantage of only returning these electrons to chosen discrete positions on the space system conductors. Furthermore such resistive paths would complicate the design of either or both the equipment for placing an initial charge on the satellite and the paths for returning electrons to the space system. One could better place electron guns at various positions around the tank wall (or on the innermost electron trapping grid) to reintroduce electrons with an appropriate slowed down waveform and at appropriate energies.

Note that capacitance increase is only an approximate way to characterize the increase in electron loss to the tank wall. In the presence of space charge the capacitance changes. Thus one can define a capacitance change under space charge limited conditions. Such calculations would be a helpful addition to the usual capacitance calculations. However in the real transient situation such a steady state calculation with space charge will not be accurate either.

## VI. General Considerations for the Use of Discrete Loading Antennas on the Wall of the Test Chamber

Now move to somewhat higher frequencies, frequencies such that the associated wavelengths are of the order of the dimensions of the internal vacuum chamber dimensions. In such a frequency range a cavity is resonant at various discrete frequencies if the cavity is lossless. Among other problems to be considered the cavity resonances excited by the electrons emitted from the space system (and other sources such as the photon generator, electrons from the walls, etc.) need to be considered. These resonances should be damped to improve the simulation at late times (compared to the characteristic times associated with the cavity size). There are various detailed designs for the damping system one might use. However, all these designs must have the characteristic of not greatly interferring with the desired electromagnetic characteristics of the cavity at other significant frequencies, such as with the capacitance reduction at low frequencies or with the reflection reduction (from the cavity walls, damping structures, etc.) at higher frequencies. There are many desirable performance characteristics for the type of simulator under discussion. The optimum simulator design for given simulator and space system sizes is one which takes all of these performance features into account and compromises among them so as to obtain the best overall performance and minimizes the "errors" associated with the simulator across the entire frequency band of interest. What is best in one frequency band may be incompatible with good performance in other frequency bands and would then be discarded in favor of other approaches.

One way to introduce loss into the cavity resonances is by the addition of small electric and magnetic dipole antennas with lossy impedance loading onto the cavity walls. These would be placed so that the electric antennas would couple to the cavity modes at positions where the electric field perpendicular to the cavity wall is large. Similarly the magnetic antennas would be placed so that they are coupled to large magnetic fields tangential to the cavity wall. These types of damping structures are indicated in figure 6.1 for single electric and magnetic dipole antennas as well as combinations of these. Note that for any one location on the cavity wall (innermost grid for electron trapping) there are three field components of interest associated with the cavity modes, one electric and two magnetic. Correspondingly there are one electric and two magnetic dipole moment components of interest that can be induced in loading antennas on the cavity wall. For the lower order cavity modes with antennas small compared to the cavity dimensions the antennas can be considered electrically small. Various notes deal with the characteristics of such electrically small antennas.[18,19]

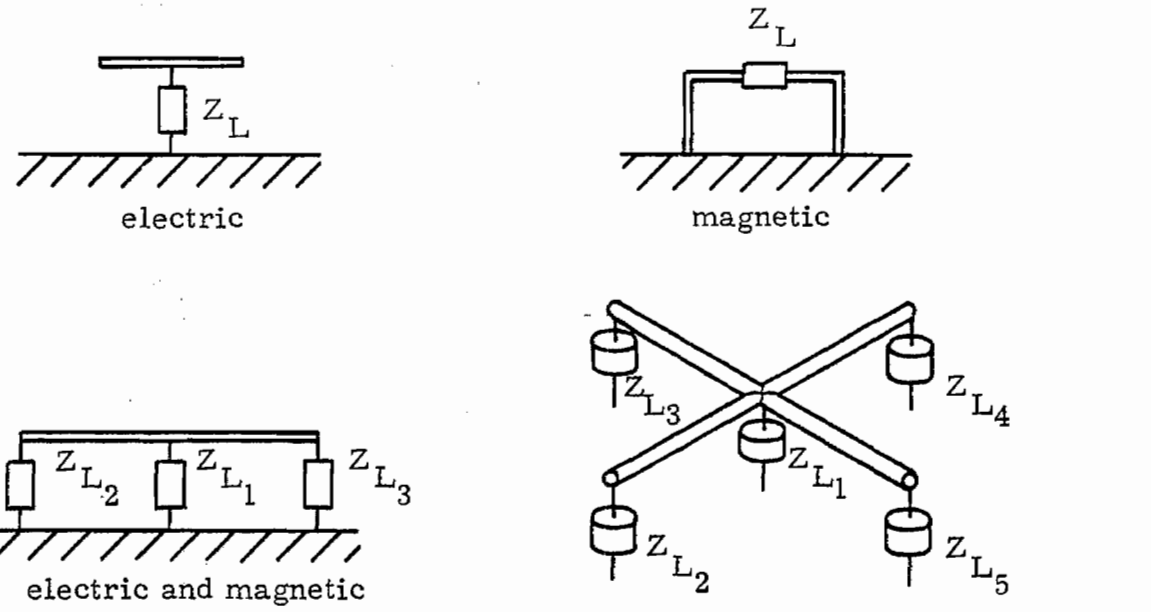


A. General types of loading antennas

Only one mode is shown here. This is the $E_{1,1}$ or $TM_{1,1}$ mode. This mode is degenerate so that more loads are needed to also damp the rotations of this mode. There are also many other mode patterns.

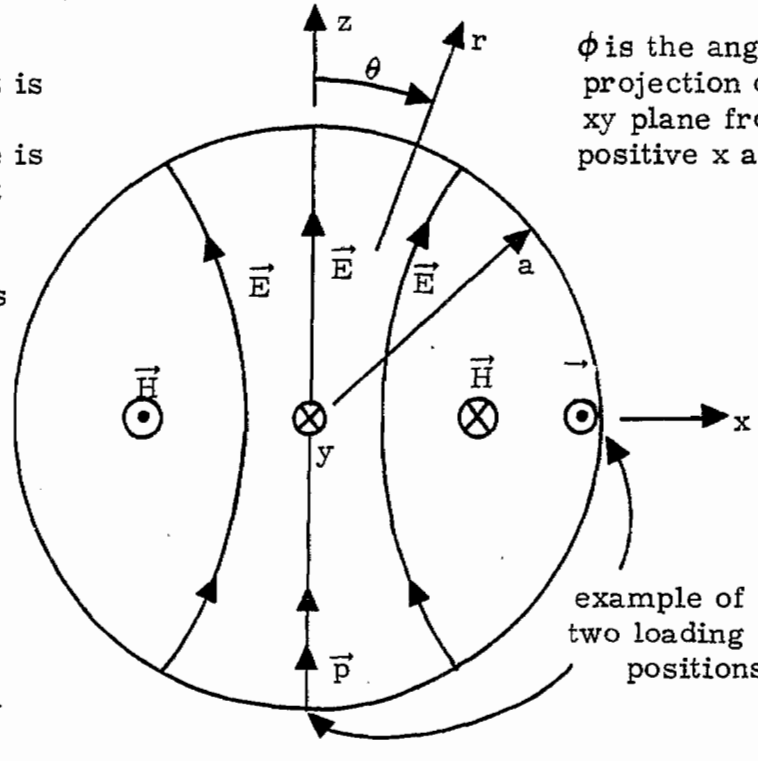


$\phi$ is the angle of the projection of r on the xy plane from the positive x axis.

B. Loading dipoles at discrete positions inside a spherical cavity

Figure 6.1 Discrete Loading on Cavity Walls

The load impedances ($Z_L$ in figure 6.1A) on the electrically small dipole antennas can have various characteristics. They might be frequency independent resistances. They could also be an inductor plus a resistor on the electric antennas or a capacitor plus a resistor on the magnetic antennas. The element values could be chosen to make the antenna with its loading impedance resonant at some desired frequency such as a cavity resonance frequency and thereby increase the damping of that cavity resonance if the resistance is optimally chosen. A damped cavity mode, however, has a complex resonance frequency and this prevents a lossy resonant coupler from attaining an arbitrarily large rate of energy extraction from the cavity fields. Using active devices in the load impedance one can perhaps increase the damping coefficient, but at a cost of complexity. Certainly it would be good to do some detailed calculations for such small loading antennas with various types of impedances. However, there is a fundamental problem with small antennas which leads to low damping efficiencies, namely the antennas are small leading to small coupling to the cavity fields. One can avoid this problem by making large distributed coupling structures as will be discussed later.

Another problem with resonant damping structures is that there is not only one mode to damp. There are many cavity modes (including degenerate modes) to damp. This leads to many resonant frequencies for even the lower order modes that one would consider in the response of such a cavity to a rather broadband EMP. It is not sufficient to damp only one mode. This requires that the individual damping antennas operate at many discrete frequencies or be broadband enough to cover the same frequency band, or that the various modes be damped by separate damping antennas thereby leading to a large number of such damping antennas.

One of the disadvantages of using discrete damping antennas on the cavity wall is mode conversion. If one determines the cavity modes and resonant frequencies for an unloaded cavity and then introduces a discrete load not only are the various resonances shifted but the original modes are coupled together. Equivalently this can be considered as shifting the mode distributions over the inner cavity surface. As an example the spherical symmetry of a spherical cavity is destroyed by the introduction of discrete damping antennas so that the individual spherical vector wave functions do not give the resulting natural modes of the cavity with damper(s). If there is only a little damping of the cavity modes due to small coupling to the small loading antennas, then the damping antennas can be considered as perturbations in using the undamped cavity modes. However, small damping is not what is wanted for a good simulator.

One would like the resonances to damp out in say a cycle or less. Thinking of the damped resonances as complex resonant

frequencies, then damping corresponds to moving poles off the $i\omega$ axis ($s = \Omega + i\omega$ being the complex frequency plane) so that the magnitude of the real part of s at the pole in the left half plane is of the order of (or larger than) the magnitude of the associated imaginary part of s. If $s_\alpha = \Omega_\alpha + i\omega_\alpha$ is the resonant (or natural) frequency then $\Omega_\alpha$ (or $-\Omega_\alpha$) is what is referred to as the damping constant. One would like to minimize $|\omega_\alpha/\Omega_\alpha|$ for each resonance $s_\alpha$ of concern.

If one wishes to damp many low order cavity modes using discrete small loading antennas then many antenna positions are needed. This results from the many mode patterns for the various resonances and the resulting variation among the modes of the positions on the cavity wall for maximum coupling and for the positions of nulls. To illustrate some of these problems consider the spherical cavity as illustrated in figure 6.1B. In this figure only the mode with smallest resonant frequency is shown; this is the $E_{1,1}$ or $TM_{1,1}$ mode. One can couple into this mode where the magnetic field is maximum or where the electric field is maximum as shown in figure 6.1B. However, this mode is degenerate and can be rotated through any angle about the coordinate center. One can find three independent orientations for this mode with say the electric field maximum (magnetic field null) positioned on the x, y and z axes to define the linearly independent modes. To couple to the electric field maxima of the three modes requires at least three electric dipole antenna dampers; for coupling to the magnetic field maxima requires at least two magnetic dipole damper positions with two magnetic dipole components for the loading antennas used at one of these positions (or magnetic dipole loading at more positions).

As one goes to higher order modes for a sphere the degeneracy is more severe requiring more discrete damping antennas for the higher order modes. The modes for the spherical cavity arise from the spherical wave functions given by[20]

$$\Xi^{(\ell)}_{n,m,\sigma}(\gamma\vec{r}) = f^{(\ell)}_n(\gamma r)Y_{n,m,\sigma}(\theta,\phi)$$

$$\vec{L}^{(\ell)}_{n,m,\sigma}(\gamma\vec{r}) = \frac{1}{\gamma}\nabla\Xi^{(\ell)}_{n,m,\sigma}(\gamma\vec{r})$$

$$= f^{(\ell)\,\prime}_n(\gamma r)\vec{P}_{n,m,\sigma}(\theta,\phi) + \frac{f^{(\ell)}_n(\gamma r)}{\gamma r}\vec{Q}_{n,m,\sigma}(\theta,\phi)$$

$$\vec{M}^{(\ell)}_{n,m,\sigma}(\gamma\vec{r}) = \nabla \times [\vec{r}\Xi^{(\ell)}_{n,m,\sigma}(\gamma\vec{r})]$$

$$= -\gamma\vec{r} \times \vec{L}^{(\ell)}_{n,m,\sigma}(\gamma\vec{r}) = -\frac{1}{\gamma}\nabla \times \vec{N}^{(\ell)}_{n,m,\sigma}(\gamma\vec{r}) \qquad (6.1)$$

$$= f^{(\ell)}_n(\gamma r)\vec{R}_{n,m,\sigma}(\theta,\phi)$$

$$\vec{N}^{(\ell)}_{n,m,\sigma}(\gamma\vec{r}) = \frac{1}{\gamma}\nabla \times \vec{M}^{(\ell)}_{n,m,\sigma}(\gamma\vec{r})$$

$$= n(n+1)\frac{f^{(\ell)}_n(\gamma r)}{\gamma r}\vec{P}_{n,m,\sigma}(\theta,\phi)$$

$$+ \frac{[\gamma r f^{(\ell)}_n(\gamma r)]'}{\gamma r}\vec{Q}_{n,m,\sigma}(\theta,\phi)$$

The spherical harmonics are

$$Y_{n,m,\begin{matrix}e\\o\end{matrix}}(\theta,\phi) = P^m_n(\cos(\theta))\begin{Bmatrix}\cos(m\phi)\\ \sin(m\phi)\end{Bmatrix} \qquad m = 0,\ 1,\ 2,\ \cdots$$

$$\vec{P}_{n,m,\sigma}(\theta,\phi) = Y_{n,m,\sigma}(\theta,\phi)\vec{e}_r$$

$$\vec{Q}_{n,m,\sigma}(\theta,\phi) = \nabla_s Y_{n,m,\sigma}(\theta,\phi) = \vec{e}_r \times \vec{R}_{n,m,\sigma}(\theta,\phi)$$

$$\vec{Q}_{n,m,\begin{matrix}e\\o\end{matrix}}(\theta,\phi) = \vec{e}_\theta \frac{dP^m_n(\cos(\theta))}{d\theta}\begin{Bmatrix}\cos(m\phi)\\ \sin(m\phi)\end{Bmatrix} + \vec{e}_\phi \frac{P^m_n(\cos(\theta))}{\sin(\theta)} m\begin{Bmatrix}-\sin(m\phi)\\ \cos(m\phi)\end{Bmatrix} \qquad (6.2)$$

$$\vec{R}_{n,m,\sigma}(\theta,\phi) = \nabla_s \times \vec{P}_{n,m,\sigma}(\theta,\phi) = -\vec{e}_r \times \vec{Q}_{n,m,\sigma}(\theta,\phi)$$

$$\vec{R}_{n,m,\begin{matrix}e\\o\end{matrix}}(\theta,\phi) = \vec{e}_\theta \frac{P^m_n(\cos(\theta))}{\sin(\theta)} m\begin{Bmatrix}-\sin(m\phi)\\ \cos(m\phi)\end{Bmatrix} - \vec{e}_\phi \frac{dP^m_n(\cos(\theta))}{d\theta}\begin{Bmatrix}\cos(m\phi)\\ \sin(m\phi)\end{Bmatrix}$$

where the index $\sigma$ stands for e (even) or o (odd) and $\vec{e}$ with a subscript is a unit vector for that coordinate. The Legendre functions are

$$P_n^m(\xi) \equiv (-1)^m(1 - \xi^2)^{m/2} \frac{d^m}{d\xi^m} P_n(\xi)$$

$$P_n(\xi) \equiv P_n^o(\xi) \equiv \frac{1}{2^n n!} \frac{d^n}{d\xi^n}(\xi^2 - 1)^n \tag{6.3}$$

The spherical Bessel functions are denoted by $f_n^{(\ell)}(\gamma r)$ where

$$f_n^{(1)}(\gamma r) = i_n(\gamma r) = i^n j_n(kr)$$

$$f_n^{(2)}(\gamma r) = k_n(\gamma r) = i^{-n-2} h_n^{(2)}(kr) \tag{6.4}$$

where the propagation constant is

$$\gamma = ik = \sqrt{s\mu(\sigma + s\varepsilon)} \tag{6.5}$$

where the permittivity $\varepsilon$, permeability $\mu$, and conductivity $\sigma$ depend on the specific uniform, isotropic medium under consideration. Other forms of spherical Bessel functions such as $y_n(kr)$ and $h_n^{(1)}(kr)$ can also be used as convenient. The spherical Bessel functions can be calculated from

$$i_n(\zeta) = \frac{e^{\zeta}}{2\zeta} \sum_{\beta=o}^{n} \frac{(n + \beta)!}{\beta!(n - \beta)!}(-2\zeta)^{-\beta} + (-1)^{n+1} \frac{e^{-\zeta}}{2\zeta} \sum_{\beta=o}^{n} \frac{(n + \beta)!}{\beta!(n - \beta)!}(2\zeta)^{-\beta}$$

$$k_n(\zeta) = \frac{e^{-\zeta}}{\zeta} \sum_{\beta=o}^{n} \frac{(n + \beta)!}{\beta!(n - \beta)!}(2\zeta)^{-\beta} \tag{6.6}$$

A prime superscript on a spherical Bessel function indicates the derivative with respect to the argument. Solutions of Maxwell's equations can be constructed in spherical coordinates by linear combinations of these wave functions. For solutions without sources only $\vec{M}$ and $\vec{N}$ functions are needed for the fields as

$$\tilde{\vec{E}}(\vec{r},s) = E_o \sum_{n,m,\sigma,\ell} a_{n,m,\sigma,\ell} \vec{M}^{(\ell)}_{n,m,\sigma}(\gamma\vec{r}) + b_{n,m,\sigma,\ell} \vec{N}^{(\ell)}_{n,m,\sigma}(\gamma\vec{r})$$

$$\tilde{\vec{H}}(\vec{r},s) = \frac{E_o}{Z} \sum_{n,m,\sigma,\ell} -a_{n,m,\sigma,\ell} \vec{N}^{(\ell)}_{n,m,\sigma}(\gamma\vec{r}) + b_{n,m,\sigma,\ell} \vec{M}^{(\ell)}_{n,m,\sigma}(\gamma\vec{r}) \qquad (6.7)$$

where a tilde ~ indicates the Laplace transform and where the wave impedance is

$$Z = \sqrt{\frac{s\mu}{\sigma + s\varepsilon}} \qquad (6.8)$$

Solutions for the interior modes of a perfectly conducting sphere are found by setting $\ell = 1$ (to constrain that the fields be well behaved at $r = 0$) and by constraining that the tangential electric field be zero on the spherical surface $r = a$. There are two types of modes. The $E_{n,n'}$ or $TM_{n,n'}$ modes are based on the electric field in terms of $\vec{N}$ functions; the $H_{n,n'}$ or $TE_{n,n'}$ modes are based on the electric field in terms of $\vec{M}$ functions. The $E_{1,1}$ mode in figure 6.1B is associated with $n = 1$ and $m = 1$ in the $\vec{N}$ functions. The resonant frequencies for the E modes are found from

$$[u_{n,n'} i_n(u_{n,n'})]' = 0 \qquad (6.9)$$

which has the first few zeros ($[0 i_n(0)]'$ being excluded) at

$$u_{1,1_o} \simeq i\,2.744\,, \quad u_{2,1_o} \simeq i\,3.870 \qquad (6.10)$$

which can be set equal to $\gamma a$ to obtain the resonant frequency. The H mode resonant frequencies are found from

$$i_n(v_{n,n'}) = 0 \qquad (6.11)$$

which has the first few zeros (the zero at $i_n(0)$ being excluded as giving identically zero fields) at

$$v_{1,1} \simeq \pm i\,4.493\,, \quad v_{2,1} \simeq \pm i\,5.763 \qquad (6.12)$$

which can be set equal to $\gamma a$ to obtain the resonant frequencies.

The mode functions on a spherical surface are vector spherical harmonics. The normal electric field applies only to the $\vec{N}$ vector wave functions and is contained in the $\vec{P}$ spherical harmonics. The $\vec{M}$ type electric fields have no radial electric field and so electric loading antennas on the cavity wall do not apply for $H_{n,n'}$ (or $TE_{n,n'}$) modes. The tangential magnetic field is given by the $\vec{R}$ spherical harmonics for E modes and by the $\vec{Q}$ spherical harmonics for H modes. One can consider the patterns of the fields at $r = a$ and some texts have a few plots of this for various modes.[21] For the higher order modes these patterns on $r = a$ become rather complex with many sign reversals for the various field components. Correspondingly they are highly degenerate and a linear combination of such degenerate modes (for a single resonant frequency $s_\alpha$) forms a "new" mode with shifted null positions (many of them) for a particular field component. For discrete damping antennas enough antenna positions are needed for each $s_\alpha$ to couple to all the degenerate modes so that there is no combination which gives nulls for the appropriate field component at all the positions of the coupling antennas for that $s_\alpha$.

As a convenient example the spherical cavity is being considered in this note. However, one might distort this geometry somewhat in a real simulator of the type presented by this note. This will remove some or all of the mode degeneracy and split the associated resonant frequency into several such resonant frequencies. This cavity distortion still leaves one with many modes and more resonant frequencies to damp. One should also note that the presence of the space system in the test chamber will also alter the resonant frequencies and modal distributions and each different shape and size of space system will alter these somewhat differently. Thus the optimum positions and impedances associated with resonant dampers can change between tests, thereby complicating matters.

In order to quantify the attainable damping for the various modes using discrete damping antennas on the cavity walls there need to be some detailed boundary value problems worked out; these are beyond the scope of the present note but will hopefully be done in the future. From the present discussion, however, it is clear that there are significant disadvantages in this technique. These disadvantages are removed somewhat by the use of continuous damping structures as are discussed next. The continuous damping structures at least have the advantages of being large and thereby coupling more efficiently to the modes, as well as coupling to most or all of the cavity modes. The use of a large number of discrete damping antennas becomes a continuous damping structure in the limit of an infinitely large number of damping antennas. One might note that some combination of discrete and continuous damping structures may also be useful but such designs require detailed calculations to determine their advantages, if any.

## VII. Impedance Loaded Shell Inside Cavity and Away from the Wall for Damping Cavity Resonances

Let us go on to consider simple continuous damping structures. With an assumed spherical cavity of radius r = a as indicated in figure 7.1 let us include a spherically symmetric damping structure inside the perfectly conducting surface at r = a. This use of spherical symmetry in the damping structure keeps the mode distribution unchanged with respect to $\theta$ and $\phi$; the r dependence of the modes is changed in general, however.

Consider a spherical shell of radius r = b and sheet impedance $Z_s$ as an example of a continuous damping structure as shown in figure 7.1. The cavity parameters are those of free space with

$$\gamma = \gamma_o = ik = \frac{s}{c} = s\sqrt{\mu_o \varepsilon_o}$$

$$Z = Z_o = \sqrt{\frac{\mu_o}{\varepsilon_o}} \tag{7.1}$$

With $Z_s/Z_o$ and b/a as parameters (although $Z_s$ may be frequency dependent) one may consider the damping of the cavity modes.

First consider the E modes which have the form for $0 \leq r < b$ as

$$\tilde{\vec{E}}(\vec{r},s) = E_o \vec{N}^{(1)}_{n,m,\sigma}(\gamma\vec{r})$$

$$\tilde{\vec{H}}(\vec{r},s) = \frac{E_o}{Z_o} \vec{M}^{(1)}_{n,m,\sigma}(\gamma\vec{r}) \tag{7.2}$$

and for $b < r < a$ as

$$\tilde{\vec{E}}(\vec{r},s) = E_o\left\{\alpha_1 \vec{N}^{(1)}_{n,m,\sigma}(\gamma\vec{r}) + \alpha_2 \vec{N}^{(2)}_{n,m,\sigma}(\gamma\vec{r})\right\}$$

$$\tilde{\vec{H}}(\vec{r},s) = \frac{E_o}{Z_o}\left\{\alpha_1 \vec{M}^{(1)}_{n,m,\sigma}(\gamma\vec{r}) + \alpha_2 \vec{M}^{(2)}_{n,m,\sigma}(\gamma\vec{r})\right\}. \tag{7.3}$$

Constraining the tangential electric field at r = a to be zero gives

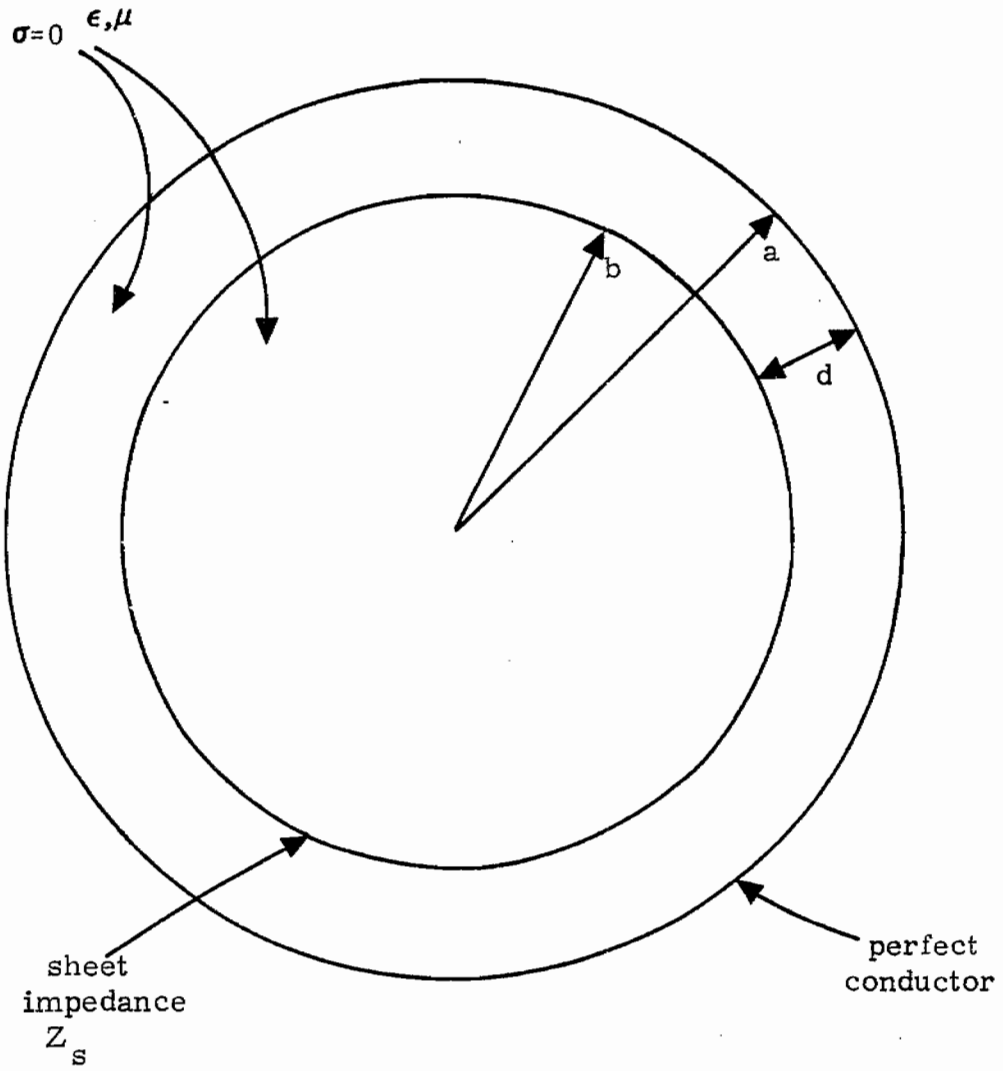


Figure 7.1 Impedance Loaded Shell for Damping Cavity Resonances

$$\alpha_1[\gamma a i_n(\gamma a)]' + \alpha_2[\gamma a k_n(\gamma a)]' = 0 \tag{7.4}$$

and constraining the tangential electric field to be continuous through r = b gives

$$(\alpha_1 - 1)[\gamma b i_n(\gamma b)]' + \alpha_2[\gamma b k_n(\gamma b)]' = 0 \tag{7.5}$$

The surface current density on the surface r = b is

$$\tilde{\vec{J}}_s(\theta,\phi,s) = \frac{1}{Z_s}\tilde{\vec{E}}(\vec{r},s)\Big|_{r=b} \tag{7.6}$$

and the tangential magnetic field is discontinuous through r = b according to

$$\vec{e}_r \times \{\tilde{\vec{H}}(\vec{r},s)\big|_{r=b+} - \tilde{\vec{H}}(\vec{r},s)\big|_{r=b-}\} = \tilde{\vec{J}}_s(\theta,\phi,s) \tag{7.7}$$

This gives another equation for the coefficients as

$$\frac{Z_s}{Z_o}\{(\alpha_1 - 1)i_n(\gamma b) + \alpha_2 k_n(\gamma b)\} = \frac{[\gamma b i_n(\gamma b)]'}{\gamma b} \tag{7.8}$$

For convenience we have the Wronskians

$$\begin{aligned} W\{i_n(\zeta),k_n(\zeta)\} &= i_n(\zeta)k_n'(\zeta) - i_n'(\zeta)k_n(\zeta) = -\zeta^{-2} \\ W\{\zeta i_n(\zeta),\zeta k_n(\zeta)\} &= \zeta i_n(\zeta)[\zeta k_n(\zeta)]' - [\zeta i_n(\zeta)]'\zeta k_n(\zeta) = -1 \end{aligned} \tag{7.9}$$

Let us combine equations 7.5 and 7.8. First substitute for $\alpha_1 - 1$ giving

$$\frac{Z_s}{Z_o}\alpha_2\{-\gamma b i_n(\gamma b)[\gamma b k_n(\gamma b)]' + [\gamma b i_n(\gamma b)]'\gamma b k_n(\gamma b)\}$$

$$= \{[\gamma b i_n(\gamma b)]'\}^2 \tag{7.10}$$

which reduces to

$$\alpha_2 = \frac{Z_o}{Z_s}\{[\gamma b i_n(\gamma b)]'\}^2 \tag{7.11}$$

Next substitute for $\alpha_2$ giving

$$\frac{Z_s}{Z_o}(\alpha_1 - 1)\{\gamma b i_n(\gamma b)[\gamma b k_n(\gamma b)]' - [\gamma b i_n(\gamma b)]'\gamma b k_n(\gamma b)\}$$

$$= [\gamma b k_n(\gamma b)]'[\gamma b i_n(\gamma b)]' \tag{7.12}$$

which reduces to

$$\alpha_1 = 1 - \frac{Z_o}{Z_s}[\gamma b k_n(\gamma b)]'[\gamma b i_n(\gamma b)]' \tag{7.13}$$

Combining equations 7.4, 7.11, and 7.13 then gives

$$[\gamma a i_n(\gamma a)]'\left\{1 - \frac{Z_o}{Z_s}[\gamma b k_n(\gamma b)]'[\gamma b i_n(\gamma b)]'\right\}$$

$$+ [\gamma a k_n(\gamma a)]'\frac{Z_o}{Z_s}\{[\gamma b i_n(\gamma b)]'\}^2 = 0 \tag{7.14}$$

Note for $Z_s = \infty$ so that the damper is removed this result reduces to

$$[\gamma a i_n(\gamma a)]' = 0 \ , \quad [ka j_n(ka)]' = 0 \tag{7.15}$$

as required for a lossless spherical cavity. For $Z_s = 0$ it reduces to

$$[\gamma b i_n(\gamma b)]' = 0 \quad (\text{or } [kb j_n(kb)]' = 0)$$

$$[\gamma a i_n(\gamma a)]'[\gamma b k_n(\gamma b)]' - [\gamma a k_n(\gamma a)]'[\gamma b i_n(\gamma b)]' = 0 \tag{7.16}$$

the first of these giving the interior resonances for a sphere of radius b and the second giving the resonances between two spherical shells (perfectly conducting) of radii b and a.

Let

$$z_s \equiv \frac{Z_s}{Z_o} \tag{7.17}$$

and rewrite equation 7.14 as

$$[\gamma a i_n(\gamma a)]'\{z_s - [\gamma b k_n(\gamma b)]'[\gamma b i_n(\gamma b)]'\}$$

$$+ [\gamma a k_n(\gamma a)]'\{[\gamma b i_n(\gamma b)]'\}^2 = 0 \tag{7.18}$$

Now if $\gamma a = u_{n,n_o'}$ is a solution for $z_s \to \infty$ and/or $b \to a$ (both of which give a cavity of radius a) then the shifted resonance can be written as $u_{n,n_o'} + \Delta u_{n,n'}$ or $u + \Delta$ for short. Note that (with zero excluded)

$$[u_{n,n_o'} i_n(u_{n,n_o'})]' = 0 \tag{7.19}$$

Then expand the various functions in a Taylor series for small d/a and small frequency shift $\Delta$ where

$$d \equiv a - b \tag{7.20}$$

noting that

$$\gamma b = (u + \Delta)\frac{b}{a} = (u + \Delta)\left(1 - \frac{d}{a}\right) = u + \Delta - \frac{d}{a}u - \frac{d}{a}\Delta \tag{7.21}$$

Then equation 7.18 can be expanded for small d/a and $\Delta$ as

$$\left\{\Delta[ui_n(u)]'' + \frac{\Delta^2}{2}[ui_n(u)]''' + O(\Delta^3)\right\}$$

$$\cdot \left\{z_s - \left\{[uk_n(u)]' + O\left(\Delta - \frac{d}{a}u - \frac{d}{a}\Delta\right)\right\}\right.$$

$$\left.\cdot \left\{\left[\Delta - \frac{d}{a}u - \frac{d}{a}\Delta\right][ui_n(u)]'' + O\left(\left(\Delta - \frac{d}{a}u - \frac{d}{a}\Delta\right)^2\right)\right\}\right\}$$

$$+ \left\{[uk_n(u)]' + O\left(\Delta - \frac{d}{a}u - \frac{d}{a}\Delta\right)\right\}\left\{\left[\Delta - \frac{d}{a}u - \frac{d}{a}\Delta\right]^2\{[ui_n(u)]''\}^2\right.$$

$$\left. + O\left(\left(\Delta - \frac{d}{a}u - \frac{d}{a}\Delta\right)^3\right)\right\}$$

$$= 0 \qquad (7.22)$$

Retaining only up through second order terms we have

$$\Delta[ui_n(u)]''z_s + \frac{\Delta^2}{2}[ui_n(u)]'''z_s - \Delta\left[\Delta - \frac{d}{a}u - \frac{d}{a}\Delta\right]\{[ui_n(u)]''\}^2[uk_n(u)]'$$

$$+ \left[\Delta - \frac{d}{a}u - \frac{d}{a}\Delta\right]^2\{[ui_n(u)]''\}^2[uk_n(u)]'$$

$$= O(\Delta^3) + O\left(\Delta^2\left(\Delta - \frac{d}{a}u - \frac{d}{a}\Delta\right)\right) + O\left(\Delta\left(\Delta - \frac{d}{a}u - \frac{d}{a}\Delta\right)^2\right) + O\left(\left(\Delta - \frac{d}{a}u - \frac{d}{a}\Delta\right)^3\right)$$

(7.23)

which can be shortened as

$$\Delta[ui_n(u)]''z_s + \frac{\Delta^2}{2}[ui_n(u)]'''z_s$$

$$+ \left[-\frac{d}{a}u - \frac{d}{a}\Delta\right]\left[\Delta - \frac{d}{a}u - \frac{d}{a}\Delta\right]\{[ui_n(u)]''\}^2[uk_n(u)]'$$

$$\simeq 0 \qquad (7.24)$$

Now neglect the $\Delta^2$ terms compared to $\Delta$ and neglect the $(d/a)\Delta$ terms with respect to $d/a$ or $\Delta$ to obtain the approximation

$$\Delta z_s - \frac{d}{a}u\left[\Delta - \frac{d}{a}u\right][ui_n(u)]''[uk_n(u)]' \simeq 0 \qquad (7.25)$$

as the equation for the change in natural frequency for small $d/a$ but any $z_s$. In another form we write this out more explicitly as

$$(\Delta u_{n,n'})\left\{z_s - \frac{d}{a}\, u_{n,n_o'}[u_{n,n_o'} i_n(u_{n,n_o'})]''[u_{n,n_o'} k_n(u_{n,n_o'})]'\right\}$$

$$+ \left[\frac{d}{a} u_{n,n_o'}\right]^2 [u_{n,n_o'} i_n(u_{n,n_o'})]''[u_{n,n_o'} k_n(u_{n,n_o'})]' \simeq 0 \quad (7.26)$$

from which $\Delta u_{n,n'}$ can be readily solved in terms of d/a and $z_s$. The $u_{n,n_o'}$ for the unloaded cavity are found for the first few modes (equations 6.10) as

$$\begin{aligned} u_{1,1_o} &\simeq i\,2.744\,, & u_{1,2_o} &\simeq i\,6.117 \\ u_{2,1_o} &\simeq i\,3.870\,, & u_{2,2_o} &\simeq i\,7.443 \\ u_{3,1_o} &\simeq i\,4.973\,, & u_{3,2_o} &\simeq i\,8.722 \end{aligned} \quad (7.27)$$

The approximate relation of $\Delta u_{n,n'}$ to $z_s$ and d/a can now be determined for the lower order modes. Note that as $z_s \to \infty$ we have $\Delta u_{n,n'} \to 0$ as is required physically. Also as $z_s \to 0$ we have $\Delta u_{n,n'} \to (d/a) u_{n,n_o'}$ which is also quite reasonable as a simple perturbation on the cavity radius from a to b. One would like to be able to choose an optimum $z_s$ for any given d/a. An optimum $z_s$ requires a definition of the optimum $\Delta u_{n,n'}$. Let us adopt as our definition of an optimum natural frequency one which has the maximum argument in the second quadrant of the complex frequency plane. This maximizes $|\Omega_\alpha|/|\omega_\alpha|$ for the complex frequency. For small $\Delta u_{n,n'}$, since $u_{n,n_o'}$ (unperturbed) is a pure imaginary number, the definition is approximately the same as minimizing $\mathrm{Re}[\Delta u_{n,n'}]$.

Now $z_s$ can be complex if one chooses. If one requires that it be realizable from passive elements then it is restricted somewhat. For the present let us make $z_s$ a real and positive number corresponding to a simple resistive shell. Write an equation for $\Delta u_{n,n'}$ as well as for its real part as

$$\frac{\Delta u_{n,n'}}{u_{n,n_o'}} \simeq -\left(\frac{d}{a}\right)^2 \alpha_{n,n'}\left\{z_s - \frac{d}{a}\,\alpha_{n,n'}\right\}^{-1}.$$

$$\alpha \equiv \alpha_{n,n'} \equiv u_{n,n_o'}[u_{n,n_o'} i_n(u_{n,n_o'})]''[u_{n,n_o'} k_n(u_{n,n_o'})]'$$

$$\mathrm{Re}[\Delta u_{n,n'}] \simeq -\left(z_s - \frac{d}{a}\alpha\right)^{-1}\left(z_s - \frac{d}{a}\bar{\alpha}\right)^{-1}\mathrm{Re}\left[\left(\frac{d}{a}\right)^2 u\alpha\left(z_s - \frac{d}{a}\bar{\alpha}\right)\right] \tag{7.28}$$

$$= -\left(z_s - \frac{d}{a}\alpha\right)^{-1}\left(z_s - \frac{d}{a}\bar{\alpha}\right)^{-1}\left(\frac{d}{a}\right)^2 z_s \mathrm{Re}[u\alpha]$$

Differentiating with respect to $z_s$ and factoring gives

$$0 \simeq \left[\left(z_s - \frac{d}{a}\alpha\right)^{-2}\left(z_s - \frac{d}{a}\alpha\right)^{-1} + \left(z_s - \frac{d}{a}\alpha\right)^{-1}\left(z_s - \frac{d}{a}\bar{\alpha}\right)^{-2}\right] z_s$$

$$- \left(z_s - \frac{d}{a}\alpha\right)^{-1}\left(z_s - \frac{d}{a}\bar{\alpha}\right)^{-1} \tag{7.29}$$

or

$$\left(z_s - \frac{d}{a}\alpha\right)\left(z_s - \frac{d}{a}\bar{\alpha}\right) \simeq \left(2z_s - \frac{d}{a}\alpha - \frac{d}{a}\bar{\alpha}\right) z_s \tag{7.30}$$

or

$$z_s^2 - \left(\frac{d}{a}\right)^2 \alpha\bar{\alpha} \simeq 0 \tag{7.31}$$

so that the optimum value for resistive $z_s$ is

$$z_s \simeq \frac{d}{a}\sqrt{\alpha\bar{\alpha}} = \frac{d}{a}|\alpha_{n,n'}| \tag{7.32}$$

which is a rather simple result with the optimum resistive $z_s$ directly proportional to d/a. Substituting this result back into equations 7.28 we have the small $\Delta u_{n,n'}$ resulting from optimum resistive $z_s$ as

$$\Delta u_{n,n'} \simeq \frac{d}{a} u_{n,n'_o} \alpha'_{n,n'}$$

$$\alpha'_{n,n'} \equiv -\alpha_{n,n'}\{|\alpha_{n,n'}| - \alpha_{n,n'}\}^{-1} = \left\{1 - \frac{|\alpha_{n,n'}|}{\alpha_{n,n'}}\right\}^{-1} \tag{7.33}$$

$$= \frac{|\alpha|^2 - \alpha|\alpha|}{2|\alpha|^2 - (\alpha+\bar{\alpha})|\alpha|} = \frac{1}{2} - \frac{i}{2}\,\mathrm{Im}[\alpha_{n,n'}]\{|\alpha_{n,n'}| - \mathrm{Re}[\alpha_{n,n'}]\}^{-1}$$

Thus for the optimum resistive $z_s$ the frequency shift is also proportional to d/a.

Starting with the differential equation

$$\zeta^2\left[\zeta f_n^{(\ell)}(\zeta)\right]'' - [\zeta^2 + n(n+1)]\zeta f_n^{(\ell)}(\zeta) = 0 \qquad (7.34)$$

then we can write

$$\alpha_{n,n'} = \frac{u_{n,n_o'}^2 + n(n+1)}{u_{n,n_o'}}\, u_{n,n_o'} i_n(u_{n,n_o'})\,[u_{n,n_o'} k_n(u_{n,n_o'})]' \qquad (7.35)$$

From a Wronskian (equations 7.9) we have

$$\alpha_{n,n'} = -\frac{u_{n,n_o'}^2 + n(n+1)}{u_{n,n_o'}}$$

$$= -u_{n,n_o'} - \frac{n(n+1)}{u_{n,n_o'}} \qquad (7.36)$$

since $[\zeta i_n(\zeta)]' = 0$ at $\zeta = u_{n,n_o'}$. Thus $\alpha_{n,n'}$ is pure imaginary.

The result for $\alpha'$ can be further simplified. Consider the spherical Bessel functions. We have the relations

$$i_n(\zeta) = i^n j_n(\xi)\ , \quad k_n(\zeta) = i^{-n-2} h_n^{(2)}(\xi)$$

$$\zeta \equiv i\xi$$

$$h_n^{(1)}(\xi) = j_n(\xi) + iy_n(\xi)\ , \quad h_n^{(2)}(\xi) = j_n(\xi) - iy_n(\xi) \qquad (7.37)$$

$$j_n(\xi) = \frac{1}{2}\left[h_n^{(2)}(\xi) + h_n^{(1)}(\xi)\right]\ , \quad y_n(\xi) = \frac{i}{2}\left[h_n^{(2)}(\xi) - h_n^{(1)}(\xi)\right]$$

By considering the small argument asymptotic forms

$$i_n(\zeta) = \frac{\zeta^n}{(2n+1)!!}[1+O(\zeta^2)] \ , \quad k_n(\zeta) = \zeta^{-n-1}(2n-1)!![1+O(\zeta)]$$

$$j_n(\xi) = \frac{\xi^n}{(2n+1)!!}[1+O(\xi^2)] \ , \quad y_n(\xi) = -\xi^{-n-1}(2n-1)!![1+O(\xi^2)]$$

$$h_n^{(1)}(\xi) = -i\xi^{-n-1}(2n-1)!![1+O(\xi)] \ , \tag{7.38}$$

$$h_n^{(2)}(\xi) = i\xi^{-n-1}(2n-1)!![1+O(\xi)]$$

one can find the signs of the functions for small arguments. For convenience we also have (to complement equations 6.6)

$$h_n^{(1)}(\xi) = i^{-n-1}\xi^{-1} \ e^{i\xi} \sum_{\beta=o}^{\infty} \frac{(n+\beta)!}{\beta!(n-\beta)!}(-i2\xi)^{-\beta}$$

$$= i^{-n} \ \frac{e^{\zeta}}{\zeta} \sum_{\beta=o}^{\infty} \frac{(n+\beta)!}{\beta!(n-\beta)!}(-2\zeta)^{-\beta}$$

$$= i^{-n-2}k_n(-\zeta) \tag{7.39}$$

so that

$$k_n(-\zeta) = i^{n+2}h_n^{(1)}(\xi) \tag{7.40}$$

gives the appropriate functions for incoming waves.

Now letting

$$u_{n,n'_o} \equiv ip_{n,n'} \tag{7.41}$$

we have

$$\alpha_{n,n'} = u_{n,n'_o}[u_{n,n'_o} i_n(u_{n,n'_o})]''[u_{n,n'_o} k_n(u_{n,n'_o})]'$$

$$= -p_{n,n'}[p_{n,n'} j_n(p_{n,n'})]''[p_{n,n'} h_n^{(2)}(p_{n,n'})]'$$

$$= ip_{n,n'}[p_{n,n'} j_n(p_{n,n'})]''[p_{n,n'} y_n(p_{n,n'})]' \qquad (7.42)$$

since

$$[p_{n,n'} j_{n,n'}(p_{n,n'})]' = 0 \qquad (7.43)$$

defines the roots $p_{n,n'}$ $(= -iu_{n,n'_o})$ for the unloaded cavity. All the $p_{n,n'}$ are real (the $u_{n,n'_o}$ being imaginary) as is required for a lossless cavity. The $j_n(\xi)$ and $y_n(\xi)$ are real functions for real $\xi$ (or imaginary $\zeta$) as well as all their derivatives. Therefore $\alpha_{n,n'}$ must be purely imaginary as observed above.

As discussed in another note[20] the zeros of spherical Bessel functions $f_n(\zeta)$ and combinations like $\zeta f_n(\zeta)$ and their derivatives have only simple zeros for $\zeta \neq 0$. Thus

$$[p_{n,n'} j_n(p_{n,n'})]'' \neq 0 \qquad (7.44)$$

and from a Wronskian one can also show (equations 7.9)

$$[p_{n,n'} y_n(p_{n,n'})]' \neq 0 \qquad (7.45)$$

so that

$$\alpha_{n,n'} \neq 0 \qquad (7.46)$$

Now the zeros of $[p_{n,n'} j_n(p_{n,n'})]''$ alternate between those for $[p_{n,n'} j_n(p_{n,n'})]'$ and so the sign of $[p_{n,n'} j_n(p_{n,n'})]''$ alternates between adjacent roots $p_{n,n'}$ as n' is varied. When $[\xi j_n(\xi)]'$ changes sign (at its zeros) then $[\xi y_n(\xi)]'$ cannot change sign (from the Wronskian) nor can $\xi j_n(\xi)$ change sign (from the differential equation); the same argument applies around the zeros of other similar combinations of three terms. Consider two adjacent zeros of $[\xi j_n(\xi)]'$ which we denote by p' and p". Write out the Wronskian[8]

$$W\{\xi j_n(\xi), \xi y_n(\xi)\} = \xi j_n(\xi)[\xi y_n(\xi)]' - [\xi j_n(\xi)]' \xi y_n(\xi) = 1 \qquad (7.47)$$

At the endpoints of our interval

$$j_n(\xi)[\xi y_n(\xi)]' = 1 \quad \text{for } \xi = p,p' \tag{7.48}$$

Since $j_n(\xi)$ has opposite sign at the two ends $p,p'$ then so must $[\xi y_n(\xi)]'$. Thus $[\xi y_n(\xi)]'$ must have at least one zero between $p$ and $p'$. Considering two adjacent zeros of $[\xi y_n(\xi)]'$ a similar argument shows that $[\xi j_n(\xi)]'$ must have at least one zero in this new interval. Combining the two results shows that the zeros of $[\xi j_n(\xi)]'$ and $[\xi y_n(\xi)]'$ must alternate on the real $\xi$ axis (neglecting $\xi = 0$). Thus the sign of $[p_{n,n'} y_n(p_{n,n'})]'$ must alternate for adjacent roots (successive $n'$). Since the expression for $\alpha_{n,n'}$ has a product of two terms with alternating signs then $\mathrm{Im}[\alpha_{n,n'}]$ must have the same sign for all $n'$ (for any given $n$). Considering the result for $\alpha_{n,n'}$ for large $u_{n,n'}$ for which it is negative imaginary for positive $\omega$ gives for all $n,n'$ (which are indexed for positive $\omega$)

$$\mathrm{Re}[\alpha_{n,n'}] = 0 \ , \quad \mathrm{Im}[\alpha_{n,n'}] < 0 \tag{7.49}$$

Using this result for $\alpha_{n,n'}$ in equations 7.33 gives

$$\alpha'_{n,n'} = [1 - i]^{-1} = \frac{1 + i}{2} \tag{7.50}$$

which holds for all $n,n'$ corresponding to the roots $p_{n,n'}$. Thus for optimum choice of $z_s$ (which does depend on $n,n'$) we have for small $d/a$ the result

$$\Delta u_{n,n'} \simeq \frac{1 + i}{2} \frac{d}{a} u_{n,n'_o} = \frac{-1 + i}{2} \frac{d}{a} |u_{n,n'_o}| \tag{7.51}$$

with real part negative and imaginary and real part positive as required physically where only positive $p_{n,n'}$ have been considered. For negative $p_{n,n'}$ the imaginary part is negative.

As examples and to obtain a few numbers we tabulate the first several $\alpha_{n,n'}$ as

$$\begin{aligned} \alpha_{1,1} &\simeq -i\,2.015 \ , \quad \alpha_{1,2} \simeq -i\,5.790 \\ \alpha_{2,1} &\simeq -i\,2.320 \ , \quad \alpha_{2,2} \simeq -i\,6.637 \\ \alpha_{3,1} &\simeq -i\,2.561 \ , \quad \alpha_{3,2} \simeq -i\,7.346 \end{aligned} \tag{7.52}$$

Considering the $E_{1,1}$ mode for d/a = .1 we have

$$z_s \simeq .1007 , \quad \Delta u_{1,1}/u_{1,1_o} \simeq .05 + i\,.05 \tag{7.53}$$

and for d/a = .2 we have

$$z_s \simeq .2015 , \quad \Delta u_{1,1}/u_{1,1_o} \simeq .1 + i\,.1 \tag{7.54}$$

Equation 7.51 readily extends these results to other E modes with optimum choices of resistive $z_s$ for the individual modes.

Second consider the H modes which have the form for $0 \leq r < b$ as

$$\begin{aligned} \tilde{\vec{E}}(\vec{r},s) &= E_o \vec{M}^{(1)}_{n,m,\sigma}(\gamma\vec{r}) \\ \tilde{\vec{H}}(\vec{r},s) &= -\frac{E_o}{Z_o}\vec{N}^{(1)}_{n,m,\sigma}(\gamma\vec{r}) \end{aligned} \tag{7.55}$$

and for $b < r < a$ as

$$\begin{aligned} \tilde{\vec{E}}(\vec{r},s) &= E_o\left\{\beta_1 \vec{M}^{(1)}_{n,m,\sigma}(\gamma\vec{r}) + \beta_2 \vec{M}^{(2)}_{n,m,\sigma}(\gamma\vec{r})\right\} \\ \tilde{\vec{H}}(\vec{r},s) &= -\frac{E_o}{Z_o}\left\{\beta_1 \vec{N}^{(1)}_{n,m,\sigma}(\gamma\vec{r}) + \beta_2 \vec{N}^{(2)}_{n,m,\sigma}(\gamma\vec{r})\right\} \end{aligned} \tag{7.56}$$

Constraining the tangential electric field at r = b to be zero gives

$$\beta_1 i_n(\gamma a) + \beta_2 k_n(\gamma a) = 0 \tag{7.57}$$

and constraining the tangential electric field to be continuous through r = b gives

$$(\beta_1 - 1) i_n(\gamma b) + \beta_2 k_n(\gamma b) = 0 \tag{7.58}$$

The surface current density on the surface r = b is

$$\tilde{\vec{J}}_s(\theta,\phi,s) = \frac{1}{Z_s}\tilde{\vec{E}}(\vec{r},s)\Big|_{r=b} \tag{7.59}$$

and the tangential magnetic field is discontinuous through r = b according to

$$\vec{e}_r \times \{\tilde{\vec{H}}(\vec{r},s)\big|_{r=b+} - \tilde{\vec{H}}(\vec{r},s)\big|_{r=b-}\} = \tilde{\vec{J}}_s(\theta,\phi,s) \tag{7.60}$$

This gives another equation for the coefficients as

$$\frac{Z_s}{Z_o}\left\{(\beta_1 - 1)\frac{[\gamma b i_n(\gamma b)]'}{\gamma b} + \beta_2 \frac{[\gamma b k_n(\gamma b)]'}{\gamma b}\right\} = i_n(\gamma b) \tag{7.61}$$

Combine equations 7.58 and 7.61. First substitute for $\beta_1 - 1$ giving

$$\frac{Z_s}{Z_o}\beta_2 \{-[\gamma b i_n(\gamma b)]'\gamma b k_n(\gamma b) + \gamma b i_n(\gamma b)[\gamma b k_n(\gamma b)]'\}$$

$$= \{\gamma b i_n(\gamma b)\}^2 \tag{7.62}$$

which a Wronskian relation (equations 7.9) reduces to

$$\beta_2 = -\frac{Z_o}{Z_s}\{\gamma b i_n(\gamma b)\}^2 \tag{7.63}$$

Next substitute for $\beta_2$ giving

$$\frac{Z_s}{Z_o}(\beta_1 - 1)\{[\gamma b i_n(\gamma b)]'\gamma b k_n(\gamma b) - \gamma b i_n(\gamma b)[\gamma b k_n(\gamma b)]'\}$$

$$= \gamma b k_n(\gamma b)\gamma b i_n(\gamma b) \tag{7.64}$$

which reduces to

$$\beta_1 = 1 + \frac{Z_o}{Z_s}\gamma b k_n(\gamma b)\gamma b i_n(\gamma b) \tag{7.65}$$

Combining equations 7.57, 7.63, and 7.65 then gives

$$i_n(\gamma a)\left\{1 + \frac{Z_o}{Z_s}\gamma b k_n(\gamma b)\gamma b i_n(\gamma b)\right\}$$

$$- k_n(\gamma a)\frac{Z_o}{Z_s}\{\gamma b i_n(\gamma b)\}^2 = 0 \qquad (7.66)$$

Note for $Z_s = \infty$ so that the damper is removed this result reduces to

$$i_n(\gamma a) = 0 , \quad j_n(ka) = 0 \qquad (7.67)$$

as required for a lossless spherical cavity. For $Z_s = 0$ it reduces to

$$i_n(\gamma b) = 0 \quad (\text{or } j_n(kb) = 0)$$

$$i_n(\gamma a)k_n(\gamma b) - k_n(\gamma a)i_n(\gamma b) = 0 \qquad (7.68)$$

the first of these giving the interior resonances for a sphere of radius b and the second giving the resonances between two spherical shells (perfectly conducting) of radii b and a.

Equation 7.66 can be rewritten as

$$\gamma a i_n(\gamma a)\{z_s + \gamma b k_n(\gamma b)\gamma b i_n(\gamma b)\}$$

$$- \gamma a k_n(\gamma a)\{\gamma b i_n(\gamma b)\}^2 = 0 \qquad (7.69)$$

Expand this solution around $v_{n,n'_o}$ which is a solution for $\gamma a \to \infty$ so that

$$i_n(v_{n,n'_o}) = 0 \qquad (7.70)$$

with zero excluded. Then expand the various functions in a Taylor series for small d/a and small frequency shift $\Delta$. Note that

$$\gamma b = (v+\Delta)\frac{b}{a} = v + \Delta - \frac{d}{a} \quad - \frac{d}{a}\Delta \tag{7.71}$$

where v is short for $v_{n,n'}$ and $\Delta$ for $\Delta v_{n,n'}$. Then expand equation 7.69 for small d/a and $\Delta$ as

$$\left\{\Delta[vi_n(v)]' + \frac{\Delta^2}{2}[vi_n(v)]'' + O(\Delta^3)\right\}$$

$$\cdot \left\{z_s + \left\{vk_n(v) + O\left(\Delta - \frac{d}{a}v - \frac{d}{a}\Delta\right)\right\}\right.$$

$$\left.\cdot \left\{\left[\Delta - \frac{d}{a}v - \frac{d}{a}\Delta\right][vi_n(v)]' + O\left(\left(\Delta - \frac{d}{a}v - \frac{d}{a}\Delta\right)^2\right)\right\}\right\}$$

$$- \left\{vk_n(v) + O\left(\Delta - \frac{d}{a}v - \frac{d}{a}\Delta\right)\right\}$$

$$\cdot \left\{\left[\Delta - \frac{d}{a}v - \frac{d}{a}\Delta\right]^2\{[vi_n(v)]'\}^2 + O\left(\left(\Delta - \frac{d}{a}v - \frac{d}{a}\Delta\right)^3\right)\right\}$$

$$= 0 \tag{7.72}$$

Retaining only up through second order terms we have

$$\Delta[vi_n(v)]'z_s + \frac{\Delta^2}{2}[vi_n(v)]''z_s + \Delta\left[\Delta - \frac{d}{a}v - \frac{d}{a}\Delta\right]\{[vi_n(v)]'\}^2 vk_n(v)$$

$$- \left[\Delta - \frac{d}{a}v - \frac{d}{a}\Delta\right]^2\{[vi_n(v)]'\}^2 vk_n(v)$$

$$= O(\Delta^3) + O\left(\Delta^2\left(\Delta - \frac{d}{a}v - \frac{d}{a}\Delta\right)\right) + O\left(\Delta\left(\Delta - \frac{d}{a}v - \frac{d}{a}\Delta\right)^2\right)$$

$$+ O\left(\left(\Delta - \frac{d}{a}v - \frac{d}{a}\Delta\right)^3\right) \tag{7.73}$$

which can be shortened as

$$\Delta[vi_n(v)]'z_s + \frac{\Delta^2}{2}[vi_n(v)]''z_s$$

$$+ \left[\frac{d}{a}v + \frac{d}{a}\Delta\right]\left[\Delta - \frac{d}{a}v - \frac{d}{a}\Delta\right]\{[vi_n(v)]'\}^2 vk_n(v)$$

$$\simeq 0 \qquad (7.74)$$

Now neglect $\Delta^2$ with respect to $\Delta$ and neglect $(d/a)\Delta$ with respect to $d/a$ or $\Delta$ to obtain the approximation

$$\Delta z_s + \frac{d}{a}v\left[\Delta - \frac{d}{a}v\right][vi_n(v)]'vk_n(v) \simeq 0 \qquad (7.75)$$

or

$$(\Delta v_{n,n'})\left\{z_s + \frac{d}{a}v_{n,n_o'}[v_{n,n_o'}i_{n,n'}(v_{n,n_o'})]'v_{n,n_o'}k_n(v_{n,n_o'})\right\}$$

$$-\left[\frac{d}{a}v_{n,n_o'}\right]^2[v_{n,n_o'}i_{n,n_o'}(v_{n,n'})]'v_{n,n_o'}k_n(v_{n,n_o'}) \simeq 0 \qquad (7.76)$$

from which $\Delta v_{n,n'}$ can be solved in terms of $d/a$ and $z_s$. The $v_{n,n_o'}$ for the unloaded cavity are found for the first few modes (equations 6.12) as

$$v_{1,1_o} \simeq i\,4.493\,, \quad v_{1,2_o} \simeq i\,7.725$$

$$v_{2,1_o} \simeq i\,5.763\,, \quad v_{2,2_o} \simeq i\,9.095 \qquad (7.77)$$

$$v_{3,1_o} \simeq i\,6.988\,, \quad v_{3,2_o} \simeq i\,10.417$$

The approximate relation of $\Delta v_{n,n'}$ to $z_s$ and $d/a$ can now be determined for the lower order modes. Note for $z_s \to \infty$ that $\Delta v_{n,n'} \to 0$. As $z_s \to 0$ we have $\Delta v_{n,n'} \to (d/a)v_{n,n_o'}$ consistent with the results for the E modes. Again let us consider an optimum $z_s$ for any given $d/a$ based on minimizing $\mathrm{Re}[\Delta v_{n,n'}]$ for small $\Delta v_{n,n'}$ as before.

Let $z_s$ be a real and positive number corresponding to a simple frequency independent resistive shell. Then we can write

$$\frac{\Delta v_{n,n'}}{v_{n,n'_o}} \simeq -\left(\frac{d}{a}\right)^2 \beta_{n,n'} \left\{ z_s - \frac{d}{a}\beta_{n,n'} \right\}^{-1}$$

$$\beta \equiv \beta_{n,n'} \equiv -v_{n,n'_o}[v_{n,n'_o} i_n(v_{n,n'_o})]' v_{n,n'_o} k_n(v_{n,n'_o}) \tag{7.78}$$

$$\mathrm{Re}[\Delta v_{n,n'}] \simeq -\left(z_s - \frac{d}{a}\beta\right)^{-1}\left(z_s - \frac{d}{a}\bar{\beta}\right)^{-1} \mathrm{Re}\left[\left(\frac{d}{a}\right)^2 u\beta\left(z_s - \frac{d}{a}\bar{\beta}\right)\right]$$

$$= -\left(z_s - \frac{d}{a}\beta\right)^{-1}\left(z_s - \frac{d}{a}\bar{\beta}\right)^{-1}\left(\frac{d}{a}\right)^2 z_s \mathrm{Re}[u\beta]$$

For the H modes this equation is of the same form as that for the E modes (equations 7.28) giving the optimum resistive $z_s$ as

$$z_s \simeq \frac{d}{a}|\beta_{n,n'}| \tag{7.79}$$

and a resulting frequency shift as

$$\Delta v_{n,n'} \simeq \frac{d}{a} v_{n,n'_o} \beta'_{n,n'}$$

$$\beta'_{n,n'} \equiv \left\{1 - \frac{|\beta_{n,n'}|}{\beta_{n,n'}}\right\}^{-1} = \frac{1}{2} - \frac{i}{2}\mathrm{Im}[\beta_{n,n'}]\{|\beta_{n,n'}| - \mathrm{Re}[\beta_{n,n'}]\}^{-1} \tag{7.80}$$

These results are the same as those for the E modes with different constants in the formulae.

From a Wronskian (equations 7.9) we can write

$$\beta_{n,n'} = -v_{n,n'_o} \tag{7.81}$$

since $v_{n,n'_o} i_n(v_{n,n'_o}) = 0$ at $\zeta = u_{n,n'_o}$. Thus $\beta_{n,n'}$ is pure imaginary. Considering only the roots for positive $\omega$ then we have

$$\mathrm{Re}[\beta_{n,n'}] = 0 \ , \quad \mathrm{Im}[\beta_{n,n'}] < 0 \tag{7.82}$$

Using this result for $\beta'_{n,n'}$ in equations 7.80 gives

$$\beta'_{n,n'} = [1 - i]^{-1} = \frac{1 + i}{2} \tag{7.83}$$

which holds for all n,n' (n = 1, 2, 3, ..., n' = 1, 2, 3, ...). For small d/a then we have (with optimum $z_s$)

$$\Delta v_{n,n'} \simeq \frac{1 + i}{2} \frac{d}{a} v_{n,n'_o} = \frac{-1 + i}{2} \frac{d}{a} |v_{n,n'_o}| \tag{7.84}$$

Note that

$$\beta'_{n,n'} = \alpha'_{n,n'} = \frac{1 + i}{2} \tag{7.85}$$

so that both E and H modes have the same optimum damping for small d/a. The values for optimum $z_s$ vary depending on n,n' and on whether E or H modes are being considered.

Considering the $H_{1,1}$ mode for d/a = .1 we have

$$z_s \simeq .4493 \text{ (.2247)}, \quad \Delta v_{1,1}/v_{1,1_o} \simeq .05 + i\,.05 \tag{7.86}$$

and for d/a = .2 we have

$$z_s \simeq .8986 \text{ (.4493)}, \quad \Delta v_{1,1}/v_{1,1_o} \simeq .1 + i\,.1 \tag{7.87}$$

Equation 7.84 readily extends these results to other H modes with optimum choices of resistive $z_s$ for the individual modes.

A rather interesting result is that both $\Delta u_{n,n'}/u_{n,n'_o}$ and $\Delta v_{n,n'}/v_{n,n'_o}$ have the same form with $z_s$ scaling with $\alpha_{n,n'}$ and $\beta_{n,n'}$ in the two cases respectively. For a given small d/a the trajectories of $\Delta u$ and $\Delta v$ are the same in the normalized complex frequency plane as $z_s$ is varied. Another interesting result for these trajectories, taking $\Delta u$ as an example, is found from equations 7.28 as

$$\frac{\Delta u}{u} - \frac{1}{2}\frac{d}{a} \simeq -\left(\frac{d}{a}\right)^2 \alpha \left\{ z_s - \frac{d}{a}\alpha \right\}^{-1} - \frac{1}{2}\frac{d}{a}$$

$$= -\frac{1}{2}\frac{d}{a}\left\{ 2\left\{ \frac{a}{d}\frac{z_s}{\alpha} - 1 \right\}^{-1} + 1 \right\}$$

$$= -\frac{1}{2}\frac{d}{a}\frac{\frac{a}{d}\frac{z_s}{\alpha} + 1}{\frac{a}{d}\frac{z_s}{\alpha} - 1} \qquad (7.88)$$

For resistive $z_s$ with $u_{n,n'_o}$ on the positive imaginary axis this result leads to

$$\left| \frac{\Delta u}{u} - \frac{1}{2}\frac{d}{a} \right| = \frac{1}{2}\frac{d}{a} \qquad (7.89)$$

so that the trajectories of $\Delta u_{n,n'}$ and $\Delta v_{n,n'}$ are circles in the normalized complex frequency plane for resistive $z_s$ and small d/a with radii $(1/2)(d/a)|u_{n,n'_o}|$ and $(1/2)(d/a)|v_{n,n'}|$ respectively.

Note that the simple results only apply for small d/a with frequency bounded. As one goes to higher order resonant modes then d/a must be made smaller so that it is still small compared to a (complex) radian wavelength. The value of d/a can be such as to place the resistive damper at a null of the tangential electric field of a given resonant mode and thus give no damping for that mode. One can find such unwanted values of d/a, or equivalently b/a, for the lower order modes by choosing two values of n' for a given n and given E or H mode and considering the ratios

$$\frac{b}{a} = \frac{u_{n,n''_o}}{u_{n,n'''_o}} \quad \text{or} \quad \frac{b}{a} = \frac{v_{n,n''_o}}{v_{n,n'''_o}} \qquad (7.90)$$

where $n''' > n'' \geq 1$. Some of these ratios for the lower order modes are

$$\frac{u_{1,1_o}}{u_{1,2_o}} \simeq .449 \ , \quad \frac{u_{2,1_o}}{u_{2,2_o}} \simeq .520 \ , \quad \frac{u_{3,1_o}}{u_{3,2_o}} \simeq .570$$

$$\frac{v_{1,1_o}}{v_{1,2_o}} \simeq .582 \ , \quad \frac{v_{2,1_o}}{v_{2,2_o}} \simeq .634 \ , \quad \frac{v_{3,1_o}}{v_{3,2_o}} \simeq .671 \tag{7.91}$$

For small d/a (or b/a near 1) these critical values can be avoided for the lower order modes. As one goes to higher frequencies then for small d/a one will get no damping if d is an integer number of half wavelengths for imaginary s (= $i\omega$). This points out a general limitation on the effectiveness of a resistive sheet damper for reducing reflections of the higher frequencies (say from space system resonances) from the cavity walls. The damping structure can be made of more than one shell, however, or given some thickness as a liner which is considered in the next section for comparison.

Note that $Z_s$ can have forms other than a simple resistance, but one must be careful because this damping and reflection reduction structure has to perform well for many modes and over a large frequency band. Simply concentrating on damping one resonant mode (say the lowest frequency one, the $E_{1,1}$ mode) does not lead to an optimum simulator design. However, other interesting forms of $Z_s$, including reactive elements, need further consideration in future notes from the viewpoint of making the damping structure more effectively broadband.

Another task left for a future note is a detailed numerical study of the mode damping for arbitrary b/a (in the range 0 to 1) from equations 7.18 and 7.69 for resistive $z_s$ with $0 \leq z_s \leq \infty$. These equations also are the starting point for considering other forms of $z_s$. Note that the approximate pole shifts considered in this section are for small shifts from the undamped modes with resonant frequencies on the $i\omega$ axis. Other poles may arise in the left half of the complex frequency plane with various forms of passive damping structures and these can also be found and their behavior studied. Additional indices on the poles (beyond n,n') may be useful in such cases.

## VIII. Impedance Loaded Liner Inside Cavity and in Contact with the Wall for Damping Cavity Resonances

As illustrated in figure 8.1 let the region for $b < r < a$ be a uniform isotropic medium with constitutive parameters $\varepsilon$, $\mu$, $\sigma$, wave impedance $Z$, and propagation constant $\gamma$. The medium for $0 \leq r < b$ has the parameters of free space which can be distinguished by a subscript 0 (including on $Z_o$ and $\gamma_o$).

Consider first the E modes which have the form for $0 \leq r < b$ as

$$\tilde{\vec{E}}(\vec{r},s) = E_o \vec{N}^{(1)}_{n,m,\sigma}(\gamma_o \vec{r})$$

$$\tilde{\vec{H}}(\vec{r},s) = \frac{E_o}{Z_o} \vec{M}^{(1)}_{n,m,\sigma}(\gamma_o \vec{r}) \tag{8.1}$$

and for $b < r < a$ as

$$\tilde{\vec{E}}(\vec{r},s) = E_o \left\{ \alpha_1 \vec{N}^{(1)}_{n,m,\sigma}(\gamma \vec{r}) + \alpha_2 \vec{N}^{(2)}_{n,m,\sigma}(\gamma \vec{r}) \right\}$$

$$\tilde{\vec{H}}(\vec{r},s) = \frac{E_o}{Z} \left\{ \alpha_1 \vec{M}^{(1)}_{n,m,\sigma}(\gamma \vec{r}) + \alpha_2 \vec{M}^{(2)}_{n,m,\sigma}(\gamma \vec{r}) \right\} \tag{8.2}$$

Constraining the tangential electric field at $r = a$ to be zero gives

$$\alpha_1 [\gamma a i_n(\gamma a)]' + \alpha_2 [\gamma a k_n(\gamma a)]' = 0 \tag{8.3}$$

At $r = b$ both tangential electric and magnetic fields must be continuous, thereby giving

$$\alpha_1 \frac{[\gamma b i_n(\gamma b)]'}{\gamma b} + \alpha_2 \frac{[\gamma b k_n(\gamma b)]'}{\gamma b} = \frac{[\gamma_o b i_n(\gamma_o b)]'}{\gamma_o b}$$

$$\alpha_1 i_n(\gamma b) + \alpha_2 k_n(\gamma b) = \frac{Z}{Z_o} i_n(\gamma_o b) \tag{8.4}$$

From these equations first eliminate $\alpha_1$ to give

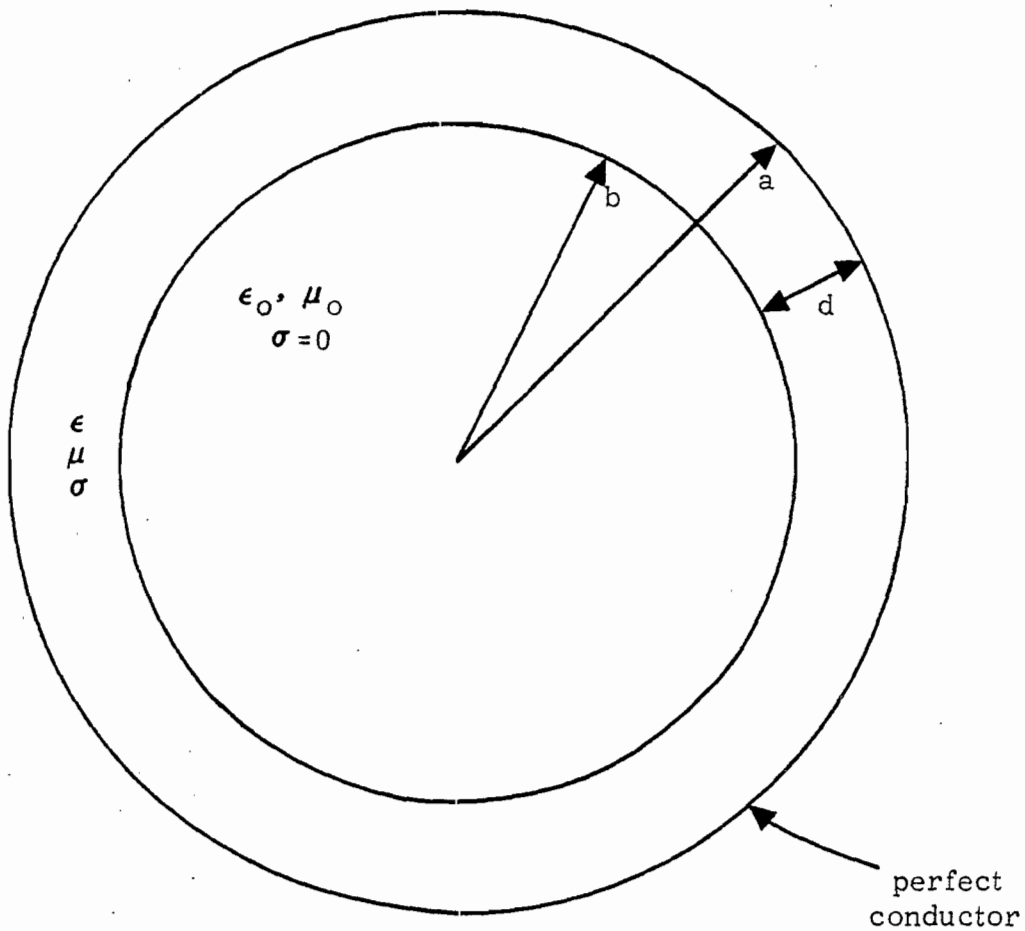


Figure 8.1 Impedance Loaded Liner in Contact with Cavity Wall for Damping Resonances

$$\alpha_2\{\gamma b i_n(\gamma b)[\gamma b k_n(\gamma b)]' - [\gamma b i_n(\gamma b)]'\gamma b k_n(\gamma b)\}$$

$$= \frac{(\gamma b)^2}{\gamma_o b} i_n(\gamma b)[\gamma_o b i_n(\gamma_o b)]' - \frac{Z}{Z_o}\gamma b[\gamma b i_n(\gamma b)]' i_n(\gamma_o b) \qquad (8.5)$$

which a Wronskian relationship reduces to

$$\alpha_2 = -\frac{(\gamma b)^2}{\gamma_o b} i_n(\gamma b)[\gamma_o b i_n(\gamma_o b)]' + \frac{Z}{Z_o}\gamma b[\gamma b i_n(\gamma b)]' i_n(\gamma_o b) \qquad (8.6)$$

Next eliminate $\alpha_2$ to give

$$\alpha_1\{[\gamma b i_n(\gamma b)]'\gamma b k_n(\gamma b) - \gamma b i_n(\gamma b)[\gamma b k_n(\gamma b)]'\}$$

$$= \frac{(\gamma b)^2}{\gamma_o b} k_n(\gamma b)[\gamma_o b i_n(\gamma_o b)]' - \frac{Z}{Z_o}\gamma b[\gamma b k_n(\gamma b)]' i_n(\gamma_o b) \qquad (8.7)$$

which reduces to

$$\alpha_1 = \frac{(\gamma b)^2}{\gamma_o b} k_n(\gamma b)[\gamma_o b i_n(\gamma_o b)]' - \frac{Z}{Z_o}\gamma b[\gamma b k_n(\gamma b)]' i_n(\gamma_o b) \qquad (8.8)$$

Note that if the parameters of the liner are the same as the inner cavity then $\alpha_2 = 0$ and $\alpha_1 = 1$ (the latter result coming from a Wronskian relation).

Combining equations 8.3, 8.6, and 8.8 gives

$$[\gamma a i_n(\gamma a)]'\left\{\gamma b k_n(\gamma b)[\gamma_o b i_n(\gamma_o b)]' - \frac{Z}{Z_o}[\gamma b k_n(\gamma b)]'\gamma_o b i_n(\gamma_o b)\right\}$$

$$+ [\gamma a k_n(\gamma a)]'\left\{-\gamma b i_n(\gamma b)[\gamma_o b i_n(\gamma_o b)]' + \frac{Z}{Z_o}[\gamma b i_n(\gamma b)]'\gamma_o b i_n(\gamma_o b)\right\}$$

$$= 0 \qquad (8.9)$$

For $\gamma = \gamma_o$ and $Z = Z_o$ so that the damper is removed this result reduces to

$$[\gamma_o a i_n(\gamma_o a)]' = 0 \tag{8.10}$$

as required. For $\sigma \to \infty$ with fixed $\varepsilon$, $\mu$, and s we have

$$\gamma = \sqrt{s\mu(\sigma + s\varepsilon)} = \sqrt{s\mu\sigma}\left\{1 + \frac{s\varepsilon}{\sigma}\right\}^{1/2}$$

$$= \sqrt{s\mu\sigma}\{1 + O(\sigma^{-1})\}^{-1} \tag{8.11}$$

Consider the asymptotic forms of the spherical Bessel functions for large arguments as for $|\zeta| \to \infty$ with $|\arg(\zeta)| \leq \pi/2 - \delta$ with $\delta > 0$. From equations 6.6 we have

$$\begin{aligned} \zeta i_n(\zeta) &= \frac{e^{\zeta}}{2}[1 + O(\zeta^{-1})] \\ \zeta k_n(\zeta) &= e^{-\zeta}[1 + O(\zeta^{-1})] \\ [\zeta i_n(\zeta)]' &= \frac{e^{\zeta}}{2}[1 + O(\zeta^{-1})] \\ [\zeta k_n(\zeta)]' &= -e^{-\zeta}[1 + O(\zeta^{-1})] \end{aligned} \tag{8.12}$$

For $|\zeta| \to \infty$ with $|\arg(\zeta)| = \pi/2$ we have

$$\begin{aligned} \zeta i_n(\zeta) &= \frac{1}{2}[e^{\zeta} + (-1)^{n+1} e^{-\zeta}][1 + O(\zeta^{-1})] \\ \zeta k_n(\zeta) &= e^{-\zeta}[1 + O(\zeta^{-1})] \\ [\zeta i_n(\zeta)]' &= \frac{1}{2}[e^{\zeta} + (-1)^{n} e^{-\zeta}][1 + O(\zeta^{-1})] \\ [\zeta k_n(\zeta)]' &= -e^{-\zeta}[1 + O(\zeta^{-1})] \end{aligned} \tag{8.13}$$

Define

$$z_\ell \equiv \frac{Z}{Z_o} \tag{8.14}$$

and rewrite equation 8.9 as

$$[\gamma a i_n(\gamma a)]'\{\gamma b k_n(\gamma b)[\gamma_o b i_n(\gamma_o b)]' - z_\ell[\gamma b k_n(\gamma b)]'\gamma_o b i_n(\gamma_o b)\}$$

$$+ [\gamma a k_n(\gamma a)]'\{-\gamma b i_n(\gamma b)[\gamma_o b i_n(\gamma_o b)]' + z_\ell[\gamma b i_n(\gamma b)]'\gamma_o b i_n(\gamma_o b)\}$$

$$= 0 \tag{8.15}$$

Now let $\gamma \to \infty$ (from $\sigma \to \infty$) with $|\arg(\gamma)| \leq \pi/2 - \delta$ with $\delta > 0$ giving

$$\frac{e^{\gamma a}}{2}[1 + O((\gamma a)^{-1})]\{-e^{-\gamma b}[1 + O((\gamma b)^{-1})][\gamma_o b i_n(\gamma_o b)]'$$

$$+ z_\ell\, e^{-\gamma b}[1 + O((\gamma b)^{-1})]\gamma_o b i_n(\gamma_o b)\}$$

$$- e^{-\gamma a}[1 + O((\gamma a)^{-1})]\left\{-\frac{e^{\gamma b}}{2}[1 + O((\gamma b)^{-1})][\gamma_o b i_n(\gamma_o b)]'\right.$$

$$\left. + z_\ell \frac{e^{\gamma b}}{2}[1 + O((\gamma b)^{-1})]\gamma_o b i_n(\gamma_o b)\right\}$$

$$= 0 \tag{8.16}$$

Neglecting terms proportional to $e^{\gamma(b-a)}$, but not those proportional to $e^{\gamma(a-b)}$ (since $a > b$) gives

$$\{-[\gamma_o b i_n(\gamma_o b)]' + z_\ell \gamma_o b i_n(\gamma_o b)\}[1 + O((\gamma b)^{-1})] = O(e^{-\gamma(a-b)}) \tag{8.17}$$

Note that

$$z_\ell = \frac{Z}{Z_o} = \sqrt{\frac{\varepsilon_o}{\mu_o}}\sqrt{\frac{s\mu}{\sigma + s\varepsilon}} = \frac{\mu}{\mu_o}\frac{\gamma_o}{\gamma} \tag{8.18}$$

so that as $|\gamma| \to \infty$ with $|\gamma_o|$ bounded we have in the limit

$$[\gamma_o b i_n(\gamma_o b)]' = 0 \tag{8.19}$$

as the equation for the E mode resonant frequencies corresponding to a perfectly conducting cavity of radius b.

As an aid to considering the solution of equation 8.15 for small d/a consider first the effective impedance at r = b. Neglect the form of the fields for r < b for the moment and consider the ratio of the tangential electric and magnetic fields at r = b. For this purpose equations 8.2 can be written as

$$\tilde{\vec{E}}(\vec{r},s)\Big|_{r=b} = E_o\Bigg\{n(n+1)\left\{\alpha_1 \frac{i_n(\gamma b)}{\gamma b} + \alpha_2 \frac{k_n(\gamma b)}{\gamma b}\right\}\vec{P}_{n,m,\sigma}(\theta,\phi) + \left\{\alpha_1 \frac{[\gamma b i_n(\gamma b)]'}{\gamma b} + \alpha_2 \frac{[\gamma b k_n(\gamma b)]'}{\gamma b}\right\}\vec{Q}_{n,m,\sigma}(\theta,\phi)\Bigg\}$$

$$\tilde{\vec{H}}(\vec{r},s)\Big|_{r=b} = \frac{E_o}{Z}\{\alpha_1 i_n(\gamma b) + \alpha_2 k_n(\gamma b)\}\vec{R}_{n,m,\sigma}(\theta,\phi) \tag{8.20}$$

Then choosing $\vec{E}$ and $\vec{H}$ polarities such that $\vec{E} \times \vec{H}$ is in the $\vec{e}_r$ direction and noting that $\vec{R} = -\vec{e}_r \times \vec{Q}$ (so that the tangential components of $\vec{E}$ and $\vec{H}$ are simply related for all $\theta,\phi$) then we have an effective wave impedance at r = b as

$$z_b \equiv \frac{Z_b}{Z} = -\frac{\alpha_1 \frac{[\gamma b i_n(\gamma b)]'}{\gamma b} + \alpha_2 \frac{[\gamma b k_n(\gamma b)]'}{\gamma b}}{\alpha_1 i_n(\gamma b) + \alpha_2 k_n(\gamma b)} \tag{8.21}$$

Using equation 8.3 for the boundary condition at r = a gives

$$z_b = -\frac{[\gamma a i_n(\gamma a)]'[\gamma b k_n(\gamma b)]' - [\gamma a k_n(\gamma a)]'[\gamma b i_n(\gamma b)]'}{[\gamma a i_n(\gamma a)]'\gamma b k_n(\gamma b) - [\gamma a k_n(\gamma a)]'\gamma b i_n(\gamma b)} \tag{8.22}$$

Using the relation

$$\zeta = i\xi$$

$$i_n(\zeta) = i^n j_n(\xi) = \frac{i^n}{2}\left\{h_n^{(2)}(\xi) + h_n^{(1)}(\xi)\right\}$$

$$= \frac{1}{2}\left\{i^{2n+2}k_n(\zeta) + i^{-2}k_n(-\zeta)\right\} \tag{8.23}$$

$$= \frac{1}{2}\left\{(-1)^{n+1}k_n(\zeta) - k_n(-\zeta)\right\}$$

we can write for the impedance at r = b

$$z_b = \frac{-[-\gamma a k_n(-\gamma a)]'[\gamma b k_n(\gamma b)]' + [\gamma a k_n(\gamma a)]'[-\gamma b k_n(-\gamma b)]'}{[-\gamma a k_n(-\gamma a)]'[\gamma b k_n(\gamma b)] + [\gamma a k_n(\gamma a)]'[-\gamma b k_n(-\gamma b)]} \tag{8.24}$$

where a prime indicates the derivative with respect to the argument ($\gamma a$, $-\gamma a$, etc.) of the Bessel function.

For large $|\gamma a|$ (and thus large $|\gamma b|$ since d/a is taken as a constant (small)) we have

$$z_b = \frac{-e^{\gamma a}[1 + O((\gamma a)^{-1})]e^{-\gamma b}[1 + O((\gamma b)^{-1})] + e^{-\gamma a}[1 + O((\gamma a)^{-1})]e^{\gamma b}[1 + O((\gamma b)^{-1})]}{-e^{\gamma a}[1 + O((\gamma a)^{-1})]e^{-\gamma b}[1 + O((\gamma b)^{-1})] - e^{-\gamma a}[1 + O((\gamma a)^{-1})]e^{\gamma b}[1 + O((\gamma b)^{-1})]}$$

$$= \frac{e^{\gamma d}[1 + O((\gamma a)^{-1})] - e^{-\gamma d}[1 + O((\gamma a)^{-1})]}{e^{\gamma d}[1 + O((\gamma a)^{-1})] + e^{-\gamma d}[1 + O((\gamma a)^{-1})]} \tag{8.25}$$

If $|e^{\gamma d} + e^{-\gamma d}|$ is bounded away from 0 then this result reduces to

$$z_b = \frac{e^{\gamma d} - e^{-\gamma d}}{e^{\gamma d} + e^{-\gamma d}}[1 + O((\gamma a)^{-1})]$$

$$= \frac{1 - e^{-2\gamma d}}{1 + e^{-2\gamma d}}[1 + O((\gamma a)^{-1})] \tag{8.26}$$

Note that for a plane wave incident perpendicular to a slab of thickness d with a perfectly conducting backing this result is exact so the result is physically quite reasonable. Also note that while $|\gamma a|$ is large for this estimate $|\gamma d|$ need not be large since d/a is small. For small $|\gamma d|$ this reduces to

$$z_b = \frac{Z_b}{Z} = \left\{\gamma d - \frac{1}{3}(\gamma d)^3 + O((\gamma d)^5)\right\}[1 + O((\gamma a)^{-1})]$$

$$z_b = s\mu d\left\{1 - \frac{1}{3}(\gamma d)^2 + O((\gamma d)^4)\right\}[1 + O((\gamma a)^{-1})] \tag{8.27}$$

For comparison consider the result for small $|\gamma a|$. For this we have

$$\zeta k_n(\zeta) = (2n-1)!!\zeta^{-n} + O(\zeta^{-n+1})$$

$$[\zeta k_n(\zeta)]' = -n(2n-1)!!\zeta^{-n-1} + O(\zeta^{-n})$$

$$\zeta i_n(\zeta) = \frac{\zeta^{n+1}}{(2n+1)!!} + O(\zeta^{n+3}) \tag{8.28}$$

$$[\zeta i_n(\zeta)]' = \frac{n+1}{(2n+1)!!}\zeta^n + O(\zeta^{n+2})$$

From equation 8.22 we then have

$$z_b = \frac{Z_b}{Z} = -\frac{-\frac{n(n+1)}{2n+1}(\gamma a)^n(\gamma b)^{-n-1}[1+O(\gamma a)] + \frac{n(n+1)}{2n+1}(\gamma a)^{-n-1}(\gamma b)^n[1+O(\gamma a)]}{\frac{n+1}{2n+1}(\gamma a)^n(\gamma b)^{-n}[1+O(\gamma a)] + \frac{n}{2n+1}(\gamma a)^{-n-1}(\gamma b)^{n+1}[1+O(\gamma a)]}$$

$$= \frac{1}{\gamma b}\frac{n(n+1)\left(\frac{b}{a}\right)^{-n} - n(n+1)\left(\frac{b}{a}\right)^{n+1}}{(n+1)\left(\frac{b}{a}\right)^{-n} + n\left(\frac{b}{a}\right)^{n+1}}[1+O(\gamma a)]$$

$$= \frac{n(n+1)}{\gamma b}\left\{\frac{1 + n\frac{d}{a} - 1 + (n+1)\frac{d}{a} + O\left(\left(\frac{d}{a}\right)^2\right)}{(n+1)\left[1+n\frac{d}{a}\right] + n\left[1-(n+1)\frac{d}{a}\right] + O\left(\left(\frac{d}{a}\right)^2\right)}\right\}[1+O(\gamma a)] \tag{8.29}$$

$$= \frac{n(n+1)}{\gamma b}\frac{d}{a}\left[1+O\left(\frac{d}{a}\right)\right][1+O(\gamma a)] = \frac{n(n+1)}{\gamma a}\frac{d}{a}\left[1+O\left(\frac{d}{a}\right)\right][1+O(\gamma a)]$$

$$z_b = \frac{n(n+1)}{(\sigma+s\varepsilon)b}\frac{d}{a}\left[1+O\left(\frac{d}{a}\right)\right][1+O(\gamma a)] = \frac{n(n+1)}{(\sigma+s\varepsilon)a}\frac{d}{a}\left[1+O\left(\frac{d}{a}\right)\right][1+O(\gamma a)]$$

This result is quite different from that for large $|\gamma a|$ (but not necessarily large $|\gamma d|$) in equations 8.27. Note that this result is for E modes and for small $\gamma a$ the Bessel functions correspond to near fields of electric antennas with large E/H ratios. The result of equations 8.27 corresponds to the far field form of the functions for which E/H is like the wave impedance of free space (before the perfectly conducting boundary is introduced).

In our case of interest $|\gamma_o a|$ is of order one, so if $|\gamma| >> |\gamma_o|$ the results of equations 8.26 apply. The results of equations 8.29 apply for small $|\gamma a|$ which requires even smaller $|\gamma_o a|$ so one is considering frequencies for which cavity resonances are not of concern, but capacitance is of concern (section V).

For convenience the equation for the cavity resonances can be written for the E modes in terms of the impedance at r = b as

$$\frac{Z_b}{Z_o} = -\frac{[\gamma_o b i_n(\gamma_o b)]'}{\gamma_o b i_n(\gamma_o b)} \tag{8.30}$$

or in terms of $z_\ell$

$$\frac{Z_b}{Z}\frac{Z}{Z_o} \equiv z_b z_\ell = -\frac{[\gamma_o b i_n(\gamma_o b)]'}{\gamma_o b i_n(\gamma_o b)} \tag{8.31}$$

Now expand equation 8.31 around $u_{n,n'_o}$ which satisfies

$$[u_{n,n'_o} i_n(u_{n,n'_o})]' = 0 \tag{8.32}$$

for which we have (as in the previous section)

$$\begin{aligned} \gamma_o a &= u_{n,n'_o} + \Delta u_{n,n'} \\ \gamma_o b &= \gamma_o a\left[1 - \frac{d}{a}\right] = u_{n,n'_o} + \Delta u_{n,n'} - \frac{d}{a} u_{n,n'_o} - \frac{d}{a}\Delta u_{n,n'} \end{aligned} \tag{8.33}$$

Abbreviating these terms as u and $\Delta$ we have

$$\frac{Z_b}{Z_o} = -\left\{\left[\Delta - \frac{d}{a}u - \frac{d}{a}\Delta\right][ui_n(u)]'' + \frac{1}{2}\left[\Delta - \frac{d}{a}u - \frac{d}{a}\Delta\right]^2 [ui_n(u)]''' + o\left(\left(\Delta - \frac{d}{a}u - \frac{d}{a}\Delta\right)^3\right)\right\}$$

$$\cdot \left\{ui_n(u) + o\left(\left(\Delta - \frac{d}{a}u - \frac{d}{a}\Delta\right)^2\right)\right\}^{-1} \qquad (8.34)$$

For $Z_b$ let us use the approximation for large $|\gamma a|$ (corresponding to large $\sigma$) without assuming the size of $|\gamma d|$. Also then expand

$$\gamma a = [s\mu(\sigma + s\varepsilon)]^{1/2} a = (s\mu\sigma)^{1/2} a[1 + O(\sigma^{-1})]$$

$$= (\gamma_o a)^{1/2}\left(\frac{\mu\sigma a}{\sqrt{\mu_o\varepsilon_o}}\right)^{1/2}[1 + O(\sigma^{-1})]$$

$$= u^{1/2}\left[1 + \frac{1}{2}\frac{\Delta}{u} + O(\Delta^2)\right]\left(\frac{\mu\sigma a}{\mu_o\varepsilon_o}\right)^{1/2}[1 + O(\sigma^{-1})]$$

$$\gamma d = \gamma a \frac{d}{a} = \frac{d}{a}u^{1/2}\left[1 + \frac{1}{2}\frac{\Delta}{u} + O(\Delta^2)\right]\left(\frac{\mu\sigma a}{\sqrt{\mu_o\varepsilon_o}}\right)^{1/2}[1 + O(\sigma^{-1})] \qquad (8.35)$$

$$= \left(\frac{d}{a}\right)^{1/2} u^{1/2}\left[1 + \frac{1}{2}\frac{\Delta}{u} + O(\Delta^2)\right]\left(\frac{\mu\sigma d}{\sqrt{\mu_o\varepsilon_o}}\right)^{1/2}[1 + O(\sigma^{-1})]$$

$$z_\ell = \frac{\mu}{\mu_o}\frac{\gamma_o}{\gamma} = \frac{\mu}{\mu_o}\frac{\gamma_o a}{\gamma d}\frac{d}{a}$$

$$= \frac{d}{a}\frac{\mu}{\mu_o}\frac{u + \Delta}{\gamma d}$$

Define a combination for $\gamma d$ at the unperturbed resonances as

$$\Gamma \equiv \gamma d\big|_{s=s_{n,n_o'}} = (s_{n,n_o'}\mu(\sigma + s_{n,n_o'}\varepsilon))^{1/2} d = \left(\frac{d}{a}\right)^{1/2} u^{1/2} \left(\frac{\mu\sigma d}{\sqrt{\mu_o \varepsilon_o}}\right)^{1/2} [1 + O(\sigma^{-1})] \tag{8.36}$$

$$\gamma d - \Gamma = \frac{1}{2}\frac{\Delta}{u}\Gamma\,[1 + O(\sigma^{-1})]$$

Now expand

$$\frac{Z_b}{Z_o} = \frac{1 - e^{-2\gamma d}}{1 + e^{-2\gamma d}}[1 + O(\sigma^{-1})]\frac{d}{a}\frac{\mu}{\mu_o}\frac{u + \Delta}{\gamma d}$$

$$= \frac{e^{2\gamma d - 2\Gamma} - e^{-2\Gamma}}{e^{2\gamma d - 2\Gamma} + e^{2\Gamma}}[1 + O(\sigma^{-1})]\frac{d}{a}\frac{\mu}{\mu_o}\frac{u + \Delta}{\Gamma + (\gamma d - \Gamma)} \tag{8.37}$$

Dropping the $O(\sigma^{-1})$ terms for simplicity and expanding in terms of $\Delta$ we have

$$\frac{Z_b}{Z_o} \simeq \frac{1 + \frac{\Delta}{u}\Gamma + O(\Delta^2) - e^{-2\Gamma}}{1 + \frac{\Delta}{u}\Gamma + O(\Delta^2) + e^{-2\Gamma}}\frac{d}{a}\frac{\mu}{\mu_o}\frac{u + \Delta}{\Gamma + \frac{1}{2}\frac{\Delta}{u}\Gamma + O(\sigma^2)}$$

$$= \frac{1 - e^{-2\Gamma}}{1 + e^{-2\Gamma}}\left\{1 + \frac{\Delta}{u}\Gamma[1 - e^{-2\Gamma}]^{-1}\right\}\left\{1 - \frac{\Delta}{u}\Gamma[1 + e^{-2\Gamma}]^{-1}\right\}$$

$$\frac{d}{a}\frac{\mu}{\mu_o}\left\{1 + \frac{\Delta}{u}\right\}\frac{u}{\Gamma}\left\{1 - \frac{1}{2}\frac{\Delta}{u}\Gamma\right\} + O(\Delta^2)$$

$$= \frac{1 - e^{-2\Gamma}}{1 + e^{-2\Gamma}}\frac{d}{a}\frac{\mu}{\mu_o}\frac{u}{\Gamma} + O(\Delta) \tag{8.38}$$

Then we can write

$$\frac{1 - e^{-2\Gamma}}{1 + e^{-2\Gamma}}\frac{d}{a}\frac{\mu}{\mu_o}\frac{u}{\Gamma} \simeq -\left[\Delta - \frac{d}{a}u\right]\frac{[ui_n(u)]''}{ui_n(u)} \tag{8.39}$$

From the differential equation for the spherical Bessel function terms (equation 7.34) we have

$$\frac{[u_{n,n'_o} i_n(u_{n,n'_o})]''}{u_{n,n'_o} i_n(u_{n,n'_o})} = \frac{u^2_{n,n'_o} + n(n+1)}{u^2_{n,n'_o}} = 1 + \frac{n(n+1)}{u^2_{n,n'_o}} = -\frac{\alpha_{n,n'}}{u_{n,n'_o}} \tag{8.40}$$

where $\alpha_{n,n'}$ was introduced in the previous section (equation 7.36). Then we have

$$\frac{\Delta u_{n,n'}}{u_{n,n'_o}} \simeq \frac{d}{a}\left\{1 + \frac{u_{n,n'_o}}{\alpha_{n,n'}} \frac{\mu}{\mu_o} \frac{1}{\Gamma} \frac{1 - e^{-2\Gamma}}{1 + e^{-2\Gamma}}\right\} \tag{8.41}$$

Note that this can also be written in terms of a general impedance at r = b as

$$\frac{Z_b}{Z_o} \simeq \left[\Delta - \frac{d}{a} u\right]\frac{\alpha}{u}$$

$$\frac{\Delta u_{n,n'}}{u_{n,n'_o}} \simeq \frac{d}{a} + \frac{1}{\alpha_{n,n'}} \frac{Z_b}{Z_o} \tag{8.42}$$

where $Z_b$ is evaluated at the frequency corresponding to $u_{n,n'}$. Note that this assumes $|Z_b/Z_o| << 1$ so that the change in the effective wall impedance from zero is sufficiently small that the shift in resonant frequency is also small and that $|Z_b|$ does not get too large at (or too near) this resonant frequency. There are various forms of $Z_b$ that one might choose so as to optimize the shift of the resonant frequency. Equations 8.42 show how much damping they achieve for small d/a (and small $|Z_b/Z_o|$) with a somewhat simpler form than that in equation 8.40.

In using a form of $Z_b$ in equations 8.42 one should be careful that approximations for $Z_b$ are accurate. For example section VII considers the case of $\gamma = \gamma_o$ but with a surface impedance added at r = b. Such can be found from equation 8.24 (with $\gamma = \gamma_o$) with the parallel addition of $Z_s$. In such a case $Z_b$ would be approximated by expanding $\gamma_o b$ as a small perturbation from $\gamma_o a$. This would not give the simple form of result for $Z_b$ as in equation 8.26 since $\gamma_o a$ is of the order of a constant (unless we consider the result for large n' and thus large $|u_{n,n'_o}|$). For the present we are considering $|\gamma| >> |\gamma_o|$ so that the result of equation 8.26 applies. Equation 8.41 then gives the result for small d/a.

Now $\alpha_{n,n'}$ is negative imaginary (equation 7.49) for positive imaginary $u_{n,n'_o}$ giving

$$-1 < \frac{u_{n,n'_o}}{\alpha_{n,n'}} < 0 \tag{8.43}$$

In order to minimize the real part of $\Delta u_{n,n'}$ we then need

$$\frac{\mathrm{Re}[\Delta u_{n,n'}]}{|u_{n,n'_o}|} = \frac{d}{a}\left|\frac{u_{n,n'_o}}{\alpha_{n,n'}}\right| \mathrm{Im}\left[\frac{\mu}{\mu_o}\,\frac{1}{\Gamma}\,\frac{1-e^{-2\Gamma}}{1+e^{-2\Gamma}}\right] \tag{8.44}$$

Let $\mu$ be real (and typically equal $\mu_o$). Then we need to minimize $\mathrm{Im}[\nu]$ where

$$\nu = \frac{1}{\Gamma}\,\frac{1-e^{-2\Gamma}}{1+e^{-2\Gamma}} = \frac{1}{\Gamma}\tanh(\Gamma) \tag{8.45}$$

For this purpose approximate

$$\begin{aligned}\Gamma &= (s\mu(\sigma + s\varepsilon))^{1/2} d \\ &= (s\mu\sigma)^{1/2} d[1 + O(\sigma^{-1})] \\ &\simeq (s\mu\sigma)^{1/2} d \\ &= \left(\frac{u\mu\sigma}{a\sqrt{\mu_o\varepsilon_o}}\right)^{1/2} d\end{aligned} \tag{8.46}$$

With $(s_{n,n'_o}a)/c = u_{n,n'_o}$ then we have

$$\begin{aligned}\Gamma &\simeq \frac{1+i}{\sqrt{2}}(|s|\mu\sigma)^{1/2} d \equiv (1+i)\psi \\ \psi &\equiv \left(\frac{|s|\mu\sigma}{2}\right)^{1/2} d\end{aligned} \tag{8.47}$$

giving

$$\frac{d}{d\psi}\nu = \frac{d}{d\psi}\mathrm{Re}[\nu] + i\frac{d}{d\psi}\mathrm{Im}[\nu]$$

$$= (1 + i)\left\{-\frac{1}{\Gamma^2}\tanh(\Gamma) + \frac{1}{\Gamma}\mathrm{sech}^2(\Gamma)\right\}$$

$$= \frac{1 + i}{\Gamma}\left\{\mathrm{sech}^2(\Gamma) - \frac{1}{\Gamma}\tanh(\Gamma)\right\}$$

$$= \frac{1}{\psi}\left\{\mathrm{sech}^2(\Gamma) - \frac{1}{\Gamma}\tanh(\Gamma)\right\} \qquad (8.48)$$

Since $\psi$ is real we wish to find $\Gamma_o$ such that

$$\mathrm{Im}\left[\mathrm{sech}^2(\Gamma_o) - \frac{1}{\Gamma_o}\tanh(\Gamma_o)\right] = 0 \qquad (8.49)$$

with

$$\Gamma_o = (1 + i)\psi_o$$

$$\nu_o = \frac{1}{\Gamma_o}\tanh(\Gamma_o) \qquad (8.50)$$

The numerical solution to these equations is

$$\psi_o \simeq 1.127$$

$$\Gamma_o \simeq 1.127 + i\,1.127 \qquad (8.51)$$

$$\nu_o \simeq .582 - i\,.417$$

Figure 8.2 shows $\nu$ plotted as a function of $\psi$. Note that $\mathrm{Im}[\nu]$ has a single minimum and smoothly rises toward zero on both sides of this minimum. Also note that $\mathrm{Re}[\nu]$ starts at 1 and monotonically decays to zero as $\psi$ varies from 0 to $\infty$.

Next then we define

$$\mu_{n,n'} \equiv 1 + \frac{u_{n,n'_o}}{\alpha_{n,n'}}\nu_o \qquad (8.52)$$

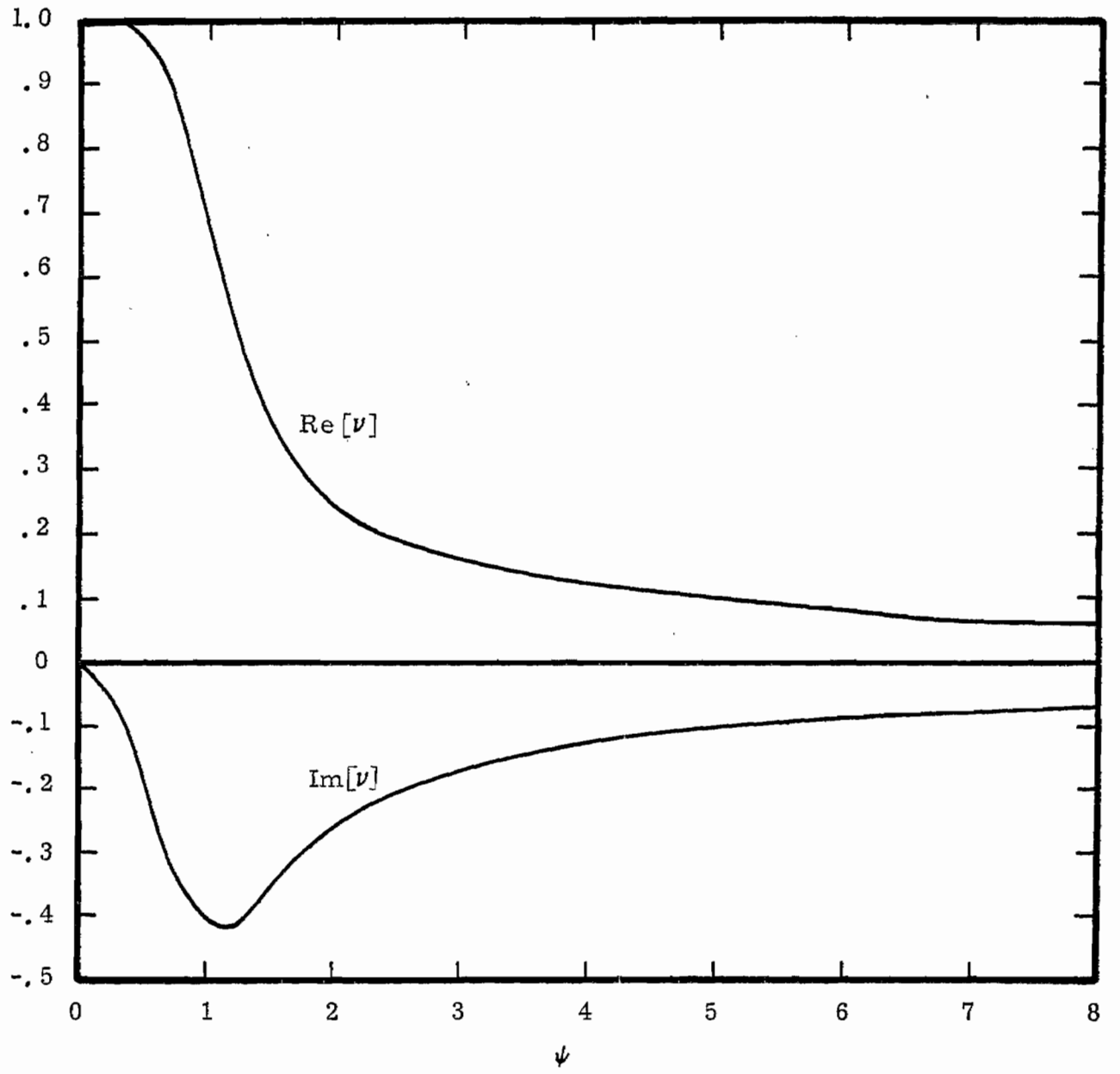


Figure 8.2 Factor in Impedance of Liner

which for the various n,n' has values

$$\mu_{1,1} \simeq .208 + i\,.568\,, \quad \mu_{1,2} \simeq .386 + i\,.441$$

$$\mu_{2,1} \simeq .0297 + i\,.696\,, \quad \mu_{2,2} \simeq .348 + i\,.468 \tag{8.53}$$

$$\mu_{3,1} \simeq -.130 + i\,.810\,, \quad \mu_{3,2} \simeq .309 + i\,.495$$

Given a particular $u_{n,n'_o}$ we can find the conductivity for optimum damping (with real $\mu$) from

$$\sigma_o = \frac{2}{|s_{n,n'_o}|\mu}\left(\frac{\psi_o}{d}\right)^2 \tag{8.54}$$

$$= \frac{2a}{|u_{n,n'_o}|c\mu}\left(\frac{\psi_o}{d}\right)^2$$

or

$$\sigma_o dZ_o = \frac{a}{d}\frac{\mu_o}{\mu}\frac{2\psi_o^2}{|u_{n,n'_o}|} \simeq \frac{a}{d}\frac{\mu_o}{\mu}\frac{2.541}{|u_{n,n'_o}|} \tag{8.55}$$

The resulting resonant frequency shift (for real $\mu$) is

$$\frac{\Delta u_{n,n'}}{u_{n,n'_o}} \simeq \frac{d}{a}\left\{1 + \frac{\mu}{\mu_o}\frac{u_{n,n'_o}}{\alpha_{n,n'}}\nu_o\right\} \tag{8.56}$$

which for $\mu = \mu_o$ is

$$\frac{\Delta u_{n,n'}}{u_{n,n'_o}} \simeq \frac{d}{a}\mu_{n,n'} \tag{8.57}$$

As examples consider the conductivity and frequency shift for $\mu = \mu_o$. Consider the $E_{1,1}$ mode for $d/a = .1$ for which we have

$$\sigma_o dZ_o \simeq 9.260 , \quad \Delta u_{1,1}/u_{1,1_o} \simeq .0208 + i\,.0568 \qquad (8.58)$$

and for d/a = .2 for which we have

$$\sigma_o dZ_o \simeq 4.630 , \quad \Delta u_{1,1}/u_{1,1_o} \simeq .0416 + i\,.1136 \qquad (8.59)$$

Equations 8.55 and 8.57 readily extend these results to other E modes.

Compare the liner results (equations 8.53 and 8.57) for the optimum damping for each E mode to the corresponding results for the shell (equation 7.51). Note for the shell that the magnitude of the damping coefficient is $.5(d/a)|u|$ for small d/a. However, for the liner the optimum damping is different for each mode and the magnitude of the damping coefficient is greater than .5 for small n' while it is less than .5 for large n'. For small n' (say n' = 1) also note that the damping is greater for larger n. In all, the optimum damping with the liner is about the same as with the shell. For the lowest order mode, the $E_{1,1}$ mode, the liner gives a coefficient of .568, or about a 14% improvement (again for small d/a and $\mu = \mu_o$).

Second consider the H modes which have the form for $0 \leq r < b$

$$\tilde{\vec{E}}(\vec{r},s) = E_o \vec{M}^{(1)}_{n,m,\sigma}(\gamma_o \vec{r})$$

$$\tilde{\vec{H}}(\vec{r},s) = -\frac{E_o}{Z_o} \vec{N}^{(1)}_{n,m,\sigma}(\gamma_o \vec{r}) \qquad (8.60)$$

and for $b < r < a$ as

$$\tilde{\vec{E}}(\vec{r},s) = E_o \left\{ \beta_1 \vec{M}^{(1)}_{n,m,\sigma}(\gamma \vec{r}) + \beta_2 \vec{M}^{(2)}_{n,m,\sigma}(\gamma \vec{r}) \right\}$$

$$\tilde{\vec{H}}(\vec{r},s) = -\frac{E_o}{Z} \left\{ \beta_1 \vec{N}^{(1)}_{n,m,\sigma}(\gamma \vec{r}) + \beta_2 \vec{N}^{(2)}_{n,m,\sigma}(\gamma \vec{r}) \right\} \qquad (8.61)$$

Constraining the tangential electric field at r = a to be zero gives

$$\beta_1 i_n(\gamma a) + \beta_2 k_n(\gamma a) = 0 \qquad (8.62)$$

At r = b both tangential electric and magnetic fields must be continuous, thereby giving

$$\beta_1 i_n(\gamma b) + \beta_2 k_n(\gamma b) = i_n(\gamma_o b)$$

$$\beta_1 \frac{[\gamma b i_n(\gamma b)]'}{\gamma b} + \beta_2 \frac{[\gamma b k_n(\gamma b)]'}{\gamma b} = \frac{Z}{Z_o} \frac{[\gamma_o b i_n(\gamma_o b)]'}{\gamma_o b} \tag{8.63}$$

Eliminating $\beta_1$ gives

$$\beta_2\{[\gamma b i_n(\gamma b)]'\gamma b k_n(\gamma b) - \gamma b i_n(\gamma b)[\gamma b k_n(\gamma b)]'\}$$

$$= [\gamma b i_n(\gamma b)]'\gamma b i_n(\gamma_o b) - \frac{Z}{Z_o}\frac{(\gamma b)^2}{\gamma_o b} i_n(\gamma b)[\gamma b i_n(\gamma_o b)]' \tag{8.64}$$

which reduces to

$$\beta_2 = [\gamma b i_n(\gamma b)]'\gamma b i_n(\gamma_o b) - \frac{Z}{Z_o}\frac{(\gamma b)^2}{\gamma_o b} i_n(\gamma b)[\gamma b i_n(\gamma_o b)]' \tag{8.65}$$

Eliminating $\beta_2$ gives

$$\beta_1\{\gamma b i_n(\gamma b)[\gamma b k_n(\gamma b)]' - [\gamma b i_n(\gamma b)]'\gamma b k_n(\gamma b)\}$$

$$= [\gamma b k_n(\gamma b)]'\gamma b i_n(\gamma_o b) - \frac{Z}{Z_o}\frac{(\gamma b)^2}{\gamma_o b} k_n(\gamma b)[\gamma_o b i_n(\gamma_o b)]' \tag{8.66}$$

which reduces to

$$\beta_1 = -[\gamma b k_n(\gamma b)]'\gamma b i_n(\gamma_o b) + \frac{Z}{Z_o}\frac{(\gamma b)^2}{\gamma_o b} k_n(\gamma b)[\gamma_o b i_n(\gamma_o b)]' \tag{8.67}$$

Note that if the parameters of the liner are the same as the inner cavity then $\beta_2 = 0$ and $\beta_1 = 1$ (the latter due to a Wronskian relation).

Combining equations 8.62, 8.65, and 8.67 gives

$$\gamma a i_n(\gamma a)\left\{-[\gamma b k_n(\gamma b)]'\gamma_o b i_n(\gamma_o b) + \frac{Z}{Z_o}\gamma b k_n(\gamma b)[\gamma_o b i_n(\gamma_o b)]'\right\}$$

$$+ \gamma a k_n(\gamma a)\left\{[\gamma b i_n(\gamma b)]'\gamma_o b i_n(\gamma_o b) - \frac{Z}{Z_o}\gamma b i_n(\gamma b)[\gamma_o b i_n(\gamma_o b)]'\right\}$$

$$= 0 \tag{8.68}$$

For $\gamma = \gamma_o$ and $Z = Z_o$ so that the damper is removed the result reduces to

$$i_n(\gamma_o a) = 0 \tag{8.69}$$

as required. For $\sigma \to \infty$ with fixed $\varepsilon$, $\mu$, and s we can use the asymptotic forms of equations 8.11 through 8.13 to give

$$\frac{e^{\gamma a}}{2}[1 + O((\gamma a)^{-1})]\left\{e^{-\gamma b}[1 + O((\gamma b)^{-1})]\gamma_o b i_n(\gamma_o b)\right.$$

$$\left. + z_\ell\, e^{-\gamma b}[1 + O((\gamma b)^{-1})][\gamma_o b i_n(\gamma_o b)]'\right\}$$

$$+ e^{-\gamma a}[1 + O((\gamma a)^{-1})]\left\{\frac{e^{\gamma b}}{2}[1 + O((\gamma b)^{-1})]\gamma_o b i_n(\gamma_o b)\right.$$

$$\left. - z_\ell \frac{e^{\gamma b}}{2}[1 + O((\gamma b)^{-1})][\gamma_o b i_n(\gamma_o b)]'\right\}$$

$$= 0 \tag{8.70}$$

Neglecting terms proportional to $e^{\gamma(b-a)}$, but not those proportional to $e^{\gamma(a-b)}$ gives in the limit

$$i_n(\gamma_o b) = 0 \tag{8.71}$$

as the equation for the H mode resonant frequencies corresponding to a perfectly conducting cavity of radius b. In terms of the normalized liner wave impedance $z_\ell$ we have

$$\gamma a i_n(\gamma a)\{-[\gamma b k_n(\gamma b)]'\gamma_o b i_n(\gamma_o b) + z_\ell \gamma b k_n(\gamma b)[\gamma_o b i_n(\gamma_o b)]'\}$$

$$+ \gamma a k_n(\gamma a)\{[\gamma b i_n(\gamma b)]'\gamma_o b i_n(\gamma_o b) - z_\ell \gamma b i_n(\gamma b)[\gamma_o b i_n(\gamma_o b)]'\}$$

$$= 0 \tag{8.72}$$

This is the equation for determining the natural frequencies for the H modes for arbitrary d/a (with $0 \leq d/a \leq 1$).

For the H modes the wave impedance at r = b can be found from the fields there which are

$$\tilde{\vec{E}}(\vec{r},s)\big|_{r=b} = E_o\{\beta_1 i_n(\gamma b) + \beta_2 k_n(\gamma b)\}\vec{R}_{n,m,\sigma}(\theta,\phi)$$

$$\tilde{\vec{H}}(\vec{r},s)\big|_{r=b} = -\frac{E_o}{Z}\left\{n(n+1)\left\{\beta_1 \frac{i_n(\gamma b)}{\gamma b} + \beta_2 \frac{k_n(\gamma b)}{\gamma b}\right\}\vec{P}_{n,m,\sigma}(\theta,\phi)\right.$$

$$\left. + \left\{\beta_1 \frac{[\gamma b i_n(\gamma b)]'}{\gamma b} + \beta_2 \frac{[\gamma b k_n(\gamma b)]'}{\gamma b}\right\}\vec{Q}_{n,m,\sigma}(\theta,\phi)\right\} \tag{8.73}$$

Comparing $\vec{e}_r \times \vec{E}$ to $\vec{H}$ and noting that $\vec{e}_r \times \vec{R} = \vec{Q}$ we have

$$z_b \equiv \frac{Z_b}{Z} = -\frac{\beta_1 i_n(\gamma b) + \beta_2 k_n(\gamma b)}{\beta_1 \dfrac{[\gamma b i_n(\gamma b)]'}{\gamma b} + \beta_2 \dfrac{[\gamma b k_n(\gamma b)]'}{\gamma b}} \tag{8.74}$$

Using equation 8.62 for the boundary condition at r = a gives

$$z_b = -\frac{\gamma a i_n(\gamma a)\gamma b k_n(\gamma b) - \gamma a k_n(\gamma a)\gamma b i_n(\gamma b)}{\gamma a i_n(\gamma a)[\gamma b k_n(\gamma b)]' - \gamma a k_n(\gamma a)[\gamma b i_n(\gamma b)]'} \tag{8.75}$$

Converting the $i_n$ functions to $k_n$ functions from equations 8.23 gives another form for the impedance at r = b as

$$z_b = \frac{-[-\gamma a k_n(-\gamma a)][\gamma b k_n(\gamma b)] + [\gamma a k_n(\gamma a)][-\gamma b k_n(-\gamma b)]}{[-\gamma a k_n(-\gamma a)][\gamma b k_n(\gamma b)]' + [\gamma a k_n(\gamma a)][-\gamma b k_n(-\gamma b)]'} \tag{8.76}$$

where again a prime indicates the derivative with respect to the argument $(\gamma b, -\gamma b)$ of the Bessel function.

For large $|\gamma a|$ with small d/a we have

$$z_b = \frac{-e^{\gamma a}[1+O((\gamma a)^{-1})]e^{-\gamma b}[1+O((\gamma b)^{-1})] + e^{-\gamma a}[1+O((\gamma a)^{-1})]e^{\gamma b}[1+O((\gamma b)^{-1})]}{-e^{\gamma a}[1+O((\gamma a)^{-1})]e^{-\gamma b}[1+O((\gamma b)^{-1})] - e^{-\gamma a}[1+O((\gamma a)^{-1})]e^{\gamma b}[1+O((\gamma b)^{-1})]}$$

$$= \frac{e^{\gamma d}[1+O((\gamma a)^{-1})] - e^{-\gamma d}[1+O((\gamma a)^{-1})]}{e^{\gamma d}[1+O((\gamma a)^{-1})] + e^{-\gamma d}[1+O((\gamma a)^{-1})]} \qquad (8.77)$$

If $|e^{\gamma d} + e^{-\gamma d}|$ is bounded away from zero then this result reduces to

$$z_b = \frac{e^{\gamma d} - e^{-\gamma d}}{e^{\gamma d} + e^{-\gamma d}}[1 + O((\gamma a)^{-1})]$$

$$= \frac{1 - e^{-2\gamma d}}{1 + e^{-2\gamma d}}[1 + O((\gamma a)^{-1})] \qquad (8.78)$$

which is the same result (equations 8.26 and 8.27) as for the E modes.

For small $|\gamma a|$ the normalized impedance at r = b reduces (from equation 8.75) to

$$z_b = \frac{Z_b}{Z} = -\frac{\frac{1}{2n+1}(\gamma a)^{n+1}(\gamma b)^{-n}[1+O(\gamma a)] - \frac{1}{2n+1}(\gamma a)^{-n}(\gamma b)^{n+1}[1+O(\gamma a)]}{-\frac{1}{2n+1}(\gamma a)^{n+1}(\gamma b)^{-n-1}[1+O(\gamma a)] - \frac{n+1}{2n+1}(\gamma a)^{-n}(\gamma b)^{n}[1+O(\gamma a)]}$$

$$= \gamma b \frac{\left(\frac{b}{a}\right)^{-n-1} - \left(\frac{b}{a}\right)^{n}}{n\left(\frac{b}{a}\right)^{-n-1} + (n+1)\left(\frac{b}{a}\right)^{n}}[1+O(\gamma a)]$$

$$= \gamma b \left\{ \frac{1 + (n+1)\frac{d}{a} - 1 + n\frac{d}{a} + O\left(\left(\frac{d}{a}\right)^2\right)}{n\left[1 + (n+1)\frac{d}{a}\right] + (n+1)\left[1 - n\frac{d}{a}\right] + O\left(\left(\frac{d}{a}\right)^2\right)} \right\}[1+O(\gamma a)]$$

$$= \gamma b \frac{d}{a}\left[1 + O\left(\frac{d}{a}\right)\right][1+O(\gamma a)] = \gamma d\left[1 + O\left(\frac{d}{a}\right)\right][1+O(\gamma a)]$$

(8.79)

$$Z_b = s\mu b \frac{d}{a}\left[1 + O\left(\frac{d}{a}\right)\right][1 + O(\gamma a)] = s\mu d\left[1 + O\left(\frac{d}{a}\right)\right][1 + O(\gamma a)]$$

Note that the result for small $|\gamma a|$ differs from that for large $|\gamma a|$. For small $|\gamma a|$ the H modes have $Z_b$ inductive while the E modes (equations 8.29) have $Z_b$ conductive and capacitive (in parallel). This result is quite similar to that for large $|\gamma a|$ in equation 8.78, particularly if $|\gamma d|$ is small for which we have

$$z_b = \gamma d[1 + O(\gamma d)][1 + O((\gamma a)^{-1})] \tag{8.80}$$

This result for the H modes is quite different than that for the E modes. Note that the E modes differ from the H modes in that the E modes have large radial electric fields near the cavity wall (or damper).

As in the case of the E modes let $|\gamma_o a|$ be of order one (bounded above and below) with $|\gamma| >> |\gamma_o|$ so that the result of equation 8.78 applies for the H modes. In terms of a general impedance at r = b the equation for the cavity resonances can be written for the H modes as

$$\frac{Z_b}{Z_o} = \frac{Z_b}{Z}\frac{Z}{Z_o} = z_b z_\ell = -\frac{\gamma_o b i_n(\gamma_o b)}{[\gamma_o b i_n(\gamma_o b)]'} \tag{8.81}$$

Expand this equation around $\nu_{n,n'_o}$ which satisfies

$$i_n(\nu_{n,n'_o}) = 0 \tag{8.82}$$

for which we have

$$\begin{aligned} \gamma_o a &= \nu_{n,n'_o} + \Delta\nu_{n,n'} \\ \gamma_o b &= \gamma_o a\left[1 - \frac{d}{a}\right] = \nu_{n,n'_o} + \Delta\nu_{n,n'} - \frac{d}{a}\nu_{n,n'_o} - \frac{d}{a}\Delta\nu_{n,n'} \end{aligned} \tag{8.83}$$

Abbreviating these terms as u and $\Delta$ we have

$$\frac{Z_b}{Z_o} = -\left\{\left[\Delta - \frac{d}{a}v - \frac{d}{a}\Delta\right][vi_n(v)]' + \left[\Delta - \frac{d}{a}v - \frac{d}{a}\Delta\right]^2 [vi_n(v)]'' + O\left(\left(\Delta - \frac{d}{a}v - \frac{d}{a}\Delta\right)^3\right)\right\}$$

$$\cdot \left\{[vi_n(v)]' + O\left(\left(\Delta - \frac{d}{a}v - \frac{d}{a}\Delta\right)^3\right)\right\}^{-1} \qquad (8.84)$$

where the second derivative term in the denominator is zero because of the differential equation (equation 7.34).

The results of equations 8.35 through 8.38 for $Z_b$ can be carried over for the H mode case with v replacing u giving

$$\frac{Z_b}{Z_o} \simeq \frac{1 - e^{-2\Gamma}}{1 + e^{-2\Gamma}} \frac{d}{a} \frac{\mu}{\mu_o} \frac{v}{\Gamma} + O(\Delta) \qquad (8.85)$$

Then we can write

$$\frac{1 - e^{-2\Gamma}}{1 + e^{-2\Gamma}} \frac{d}{a} \frac{\mu}{\mu_o} \frac{v}{\Gamma} \simeq -\left[\Delta - \frac{d}{a}v\right] \qquad (8.86)$$

For a general impedance at r = b we have

$$\frac{Z_b}{Z_o} \simeq -\left[\Delta - \frac{d}{a}v\right]$$

$$\frac{\Delta v_{n,n'}}{v_{n,n'_o}} \simeq \frac{d}{a} - \frac{1}{v_{n,n'_o}} \frac{Z_b}{Z_o} \qquad (8.87)$$

For the special impedance form in equation 8.85 we have

$$\frac{\Delta v_{n,n'}}{v_{n,n'_o}} \simeq \frac{d}{a}\left\{1 - \frac{\mu}{\mu_o} \frac{1}{\Gamma} \frac{1 - e^{-2\Gamma}}{1 + e^{-2\Gamma}}\right\}$$

$$= \frac{d}{a}\left\{1 - \frac{\mu}{\mu_o} \nu\right\} \qquad (8.88)$$

where $\nu$ has been considered in equations 8.45 through 8.51. The minimum real part of $\Delta v$ is found at $\Gamma = \Gamma_o$ for which $\nu = \nu_o$. For $\mu = \mu_o$ the optimum $\Delta v$ for small d/a is then found from

$$\frac{\Delta v_{n,n'}}{v_{n,n'_o}} \simeq \frac{d}{a}[1 - \nu_o] \simeq [.418 + i\ .417]\frac{d}{a} \tag{8.89}$$

which is conveniently independent of n,n' for the relative frequency shift. Note that the damping coefficient magnitude is $.417(d/a)|v|$. This is less damping under optimum choice of $\sigma$ than is achieved for the E mode damping for small d/a. For the H modes the liner gives less damping than the shell (equation 7.84) for which the magnitude of the damping coefficient for small d/a and $\mu = \mu_o$ is $.5(d/a)|v|$.

The optimum choice of liner conductivity is found from equation 8.55 with u replaced by v giving

$$\sigma_o dZ_o = \frac{a}{d}\frac{\mu_o}{\mu}\frac{2\psi_o^2}{|v_{n,n'_o}|} \simeq \frac{a}{d}\frac{\mu_o}{\mu}\frac{2.541}{|v_{n,n'_o}|} \tag{8.90}$$

As examples consider the conductivity and frequency shift for $\mu = \mu_o$. Consider the $H_{1,1}$ mode for d/a = .1 giving

$$\sigma_o dZ_o \simeq 5.654\ , \quad \Delta v_{1,1}/v_{1,1_o} \simeq .0418 + i\ .0417 \tag{8.91}$$

and for d/a = .2 giving

$$\sigma_o dZ_o \simeq 2.827\ , \quad \Delta v_{1,1}/v_{1,1_o} \simeq .8367 + i\ .8345 \tag{8.92}$$

Equations 8.89 and 8.90 readily extend these results to other H modes.

The results for small d/a for the liner of thickness d apply only for frequency low enough or d small enough that d is small compared to a radian wavelength. Note that the liner cannot be placed at a position of zero electric field for an unperturbed mode since the liner has finite thickness. In this respect the liner is superior to the sheet considered in section VII. The liner can be used to give a more uniform reflection coefficient for high frequency waves incident on the cavity wall from inside the cavity. This is considered further in the next section.

The liner parameters $\varepsilon$, $\mu$, $\sigma$ can have various more complex forms if desired. Again, however, one should be careful to choose these parameters to give good mode damping over a large range of frequencies corresponding to many modes. This question needs further detailed study.

A future note will hopefully numerically study the mode damping characteristics for arbitrary b/a from equations 8.15 and 8.72. Various forms of $\varepsilon$, $\mu$, and $\sigma$ can then be considered. One must also be concerned with the realizability of these parameters using three dimensional arrays of lumped elements. There is some advantage in also using only passive elements in such an array.

## IX. Impedance Loaded Liner Inside Cavity and in Contact with the Wall for Reducing High Frequency Reflections

Having considered the resonances of the test chamber as well as sheet and liner dampers for damping these resonances let us consider this phenomenon from another viewpoint, that of reflections from the cavity wall (including sheets, liners, etc.). Cavity resonances correspond to a combination of outward and inward propagating waves which are related to each other such that the fields are well behaved at r = 0 (satisfy Maxwell's equations with no singularity there).

With a space system in the test chamber as indicated in figure 9.1 the cavity modes are changed. Some of the resonances are associated with the resonances (natural frequencies) of the space system. The reflections from the walls of the test chamber alter the natural frequencies of the space system. A convenient way to consider the reduction of the effect of the cavity walls on the space system resonances is to minimize the reflection coefficients of the outgoing waves from the space system at the cavity walls.

Considering a spherical test chamber with a space system at the center of the test chamber, let us represent the fields radiated from the space system in terms of outward propagating spherical waves and consider the reflection coefficients for converting the outward propagating waves into inward propagating waves. This does not include the nonlinear effects associated with the electron cloud which extends out toward the chamber walls. It is a limited, but useful, view of the problem.

Since the space system ideally has linear dimensions small compared to 2b, then the radian wavelengths corresponding to resonances of the space system are also small compared to b. The cavity resonances without the space system present are also closely spaced between resonances, in the sense that $|\Delta s/s|$ is small between adjacent resonances for large resonant frequencies $|s|$ for which there are many wavelengths across the cavity. As the natural frequencies become closer together then a consideration of a continuous frequency dependence of the reflection from the cavity walls is more significant. The viewpoint of reflection reduction is then most appropriate at high frequencies.

Consider first the E waves (those with a radial component of the electric field) for $0 < r < b$ as

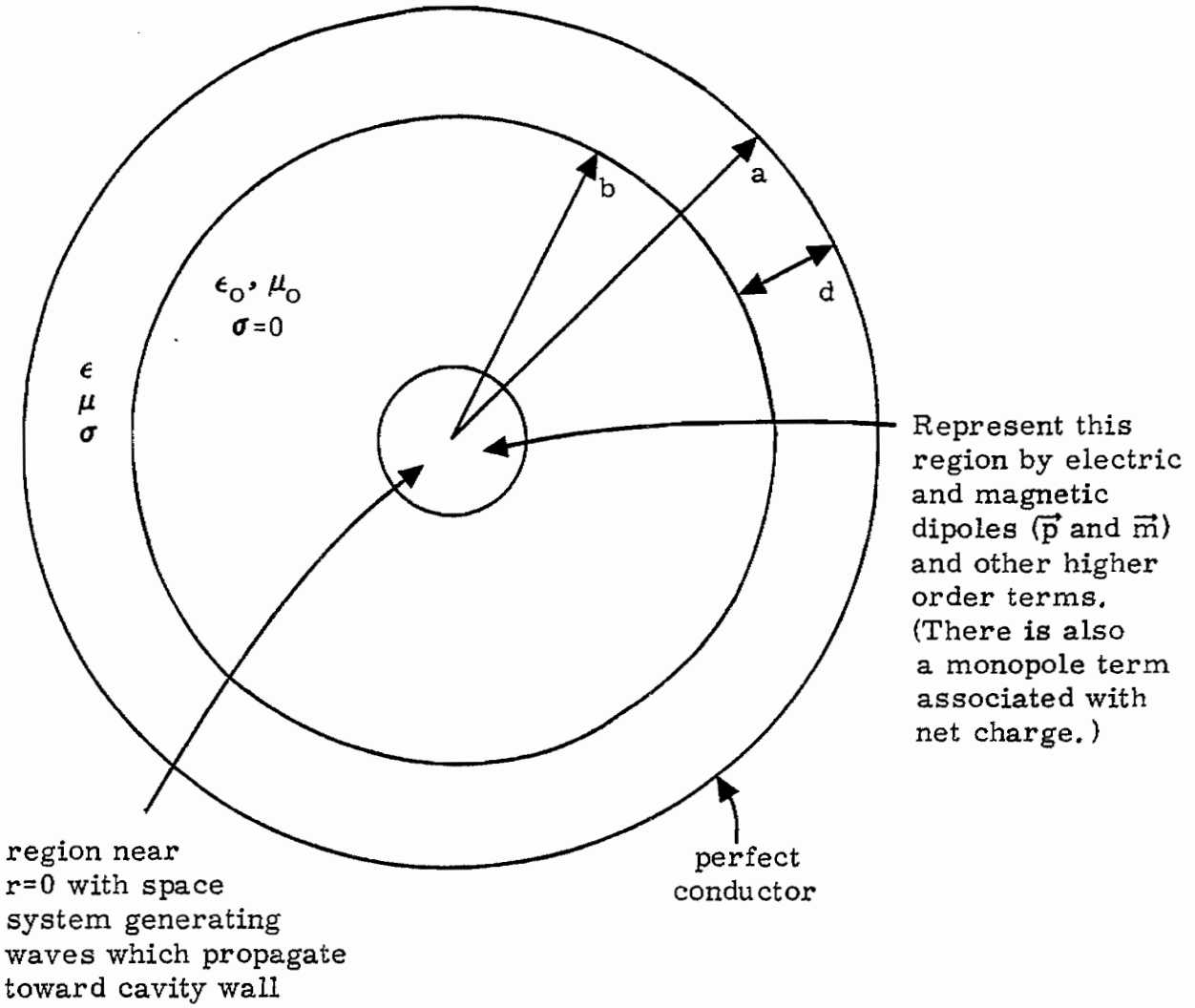


Figure 9.1 Impedance Loaded Liner in Contact with Cavity Wall for Reduction of Reflection of Waves Back Toward the Space System

$$\tilde{\vec{E}}(\vec{r},s) = E_o\left\{\vec{N}^{(2)}_{n,m,\sigma}(\gamma_o\vec{r}) + r_e\vec{N}^{(2)}_{n,m,\sigma}(-\gamma_o\vec{r})\right\}$$

$$\tilde{\vec{H}}(\vec{r},s) = \frac{E_o}{Z_o}\left\{\vec{M}^{(2)}_{n,m,\sigma}(\gamma_o\vec{r}) + r_e\vec{M}^{(2)}_{n,m,\sigma}(-\gamma_o\vec{r})\right\} \qquad (9.1)$$

where the $-\gamma_o\vec{r}$ argument indicates the incoming wave and $r_e$ is a reflection coefficient for the E waves. Note that at $r = b$ the reflection coefficient can be written somewhat differently so that it can be directly related to the impedance $Z_b$ considered in the previous section. Note that in the definition of the spherical vector wave functions (equations 6.1) the $k_n(-\gamma_o r)$ functions can be used, but the functions $f_n(\gamma r)$ and their derivatives use $\gamma r$ as the argument. In the case of $k_n(-\gamma_o r)$ it is convenient to shift the derivatives to those with respect to $-\gamma r$ so that derivatives are with respect to the argument of the Bessel function.

Equating the ratio of tangential electric and magnetic fields at $r = b$ (with $\vec{e}_r \times \vec{Q} = -\vec{R}$) gives

$$\frac{Z_b}{Z_o} = z_b z_\ell = -\frac{\dfrac{[\gamma_o b k_n(\gamma_o b)]'}{\gamma_o b} + r_e\dfrac{[-\gamma_o b k_n(-\gamma_o b)]'}{\gamma_o b}}{k_n(\gamma b) + r_e k_n(-\gamma b)}$$

$$= -\frac{[\gamma_o b k_n(\gamma_o b)]' + r_e[-\gamma_o b k_n(-\gamma_o b)]'}{\gamma_o b k_n(\gamma_o b) - r_e[-\gamma_o b k_n(-\gamma_o b)]} \qquad (9.2)$$

where the primes indicate derivatives with respect to the Bessel function argument, $\gamma b$ or $-\gamma b$ in this case. Solving for $r_e$ gives

$$r_e = -\frac{[\gamma_o b k_n(\gamma_o b)]' + \dfrac{Z_b}{Z_o}\gamma_o b k_n(\gamma_o b)}{[-\gamma_o b k_n(-\gamma_o b)]' - \dfrac{Z_b}{Z_o}[-\gamma_o b k_n(-\gamma_o b)]} \qquad (9.3)$$

From section VIII the appropriate impedance for the liner plus perfectly conducting wall, $Z_b$, is given by equations 8.22 and 8.24 for E waves. Note that the propagation constant in this case is $\gamma$ instead of $\gamma_o$ so that the net result is rather complex. Note for $\sigma \to \infty$ (large $\mathrm{Re}[\gamma]$) with $s = i\omega$ that $Z_b \to 0$. With $Z_b = 0$ we have

$$r_e = - \frac{[\gamma_o b k_n(\gamma_o b)]'}{[\gamma_o b k_n(-\gamma_o b)]'} \tag{9.4}$$

corresponding to a perfectly conducting wall at r = b. For $s = i\omega$ and noting that

$$\bar{k}_n(\zeta) = k_n(\bar{\zeta}) \tag{9.5}$$

then on the imaginary frequency axis for $Z_b = 0$ we have

$$r_e = - \frac{[ik_o b k_n(ik_o b)]'}{[ik_o b k_n(ik_o b)]'} \tag{9.6}$$

$$|r_e| = 1$$

Similarly if $\gamma_o = \gamma$ so that there is no added liner one can substitute from equation 8.24 and obtain

$$r_e = - \frac{[\gamma_o b k_n(\gamma_o b)]'}{[-\gamma_o b k_n(-\gamma_o b)]'} \tag{9.7}$$

which also has magnitude 1 on the $i\omega$ axis. Note that $r_e$ could be defined so that for $\sigma \to \infty$ one would have $r_e \to -1$, thereby referencing the reflection coefficient to r = b. This would be accomplished by replacing $r_e$ by $r_e[-\gamma_o b k_n(-\gamma_o b)]'/[\gamma_o b k_n(\gamma_o b)]'$ in equations 9.2 and 9.3. Suppose then we define

$$\rho_e \equiv r_e \frac{[-\gamma_o b k_n(-\gamma_o b)]'}{[\gamma_o b k_n(\gamma_o b)]'} \tag{9.8}$$

This removes the phase delay from r = 0 to r = b and back and is convenient to use in some cases.

For small $|\gamma_o b|$ the reflection coefficient reduces to

$$r_e = -\frac{-n(\gamma_o b)^{-n-1}[1+O(\gamma_o b)] + \frac{Z_b}{Z_o}(\gamma_o b)^{-n}[1+O(\gamma_o b)]}{-n(-\gamma_o b)^{-n-1}[1+O(\gamma_o b)] - \frac{Z_b}{Z_o}(-\gamma_o b)^{-n}[1+O(\gamma_o b)]}$$

$$= (-1)^n(1 + O(\gamma_o b)] \qquad (9.9)$$

$$\rho_e = (-1)^{n+1}[1 + O(\gamma_o b)]r_e$$

$$= -1 + O(\gamma_o b)$$

Note that this assumes fixed $\sigma > 0$ so that small $|\gamma_o b|$ implies small $|s|$ and thus a constant non zero $Z_b$ from equations 8.29.

For large $|\gamma_o b|$ the reflection coefficient reduces to

$$r_e = -\frac{-e^{\gamma_o b}[1 + O((\gamma_o b)^{-1})] + \frac{Z_b}{Z_o}e^{-\gamma_o b}[1 + O((\gamma_o b)^{-1})]}{-e^{\gamma_o b}[1 + O((\gamma_o b)^{-1})] - \frac{Z_b}{Z_o}e^{-\gamma_o b}[1 + O((\gamma_o b)^{-1})]} \qquad (9.10)$$

Referenced to r = b we have

$$\rho_e = -\frac{1 + \frac{Z_b}{Z_o}\frac{\gamma_o b k_n(\gamma_o b)}{[\gamma_o b k_n(\gamma_o b)]'}}{1 - \frac{Z_b}{Z_o}\frac{[-\gamma_o b k_n(-\gamma_o b)]}{[-\gamma_o b k_n(-\gamma_o b)]'}} \qquad (9.11)$$

For large $|\gamma_o b|$ this is

$$\rho_e = -\frac{1 - \frac{Z_b}{Z_o}[1 + O((\gamma_o b)^{-1})]}{1 + \frac{Z_b}{Z_o}[1 + O((\gamma_o b)^{-1})]}$$

$$\simeq -\frac{1-\frac{Z_b}{Z_o}}{1+\frac{Z_b}{Z_o}} = \frac{Z_b - Z_o}{Z_b + Z_o} \tag{9.12}$$

This last result is exactly what one would expect for a plane wave normally incident on a plane stratified structure with an impedance $Z_b$ at its front (input) surface. This last form will be later used with the high frequency form of $Z_b$ in order to discuss minimizing $\rho_e$ in a broadband sense.

Consider next the H waves (those with a radial component of the magnetic field) for $0 < r < b$ as

$$\begin{aligned}
\tilde{\vec{E}}(\vec{r},s) &= E_o\left\{\vec{M}^{(2)}_{n,m,\sigma}(\gamma_o\vec{r}) + r_h\vec{M}^{(2)}_{n,m,\sigma}(-\gamma_o\vec{r})\right\} \\
\tilde{\vec{H}}(\vec{r},s) &= -\frac{E_o}{Z_o}\left\{\vec{N}^{(2)}_{n,m,\sigma}(\gamma_o\vec{r}) + r_h\vec{N}^{(2)}_{n,m,\sigma}(-\gamma_o\vec{r})\right\}
\end{aligned} \tag{9.13}$$

Equating the ratio of tangential electric and magnetic fields at $r = b$ (with $\vec{e}_r \times \vec{R} = \vec{Q}$) gives

$$\begin{aligned}
\frac{Z_b}{Z_o} = z_b z_\ell &= -\frac{k_n(\gamma_o b) + r_h k_n(-\gamma_o b)}{\frac{[\gamma_o b k_n(\gamma_o b)]'}{\gamma_o b} + r_h\frac{[-\gamma_o b k_n(-\gamma_o b)]'}{\gamma_o b}} \\
&= -\frac{\gamma_o b k_n(\gamma_o b) - r_h[-\gamma_o b k_n(-\gamma_o b)]}{[\gamma_o b k_n(\gamma_o b)]' + r_h[-\gamma_o b k_n(-\gamma_o b)]'}
\end{aligned} \tag{9.14}$$

Solving for $r_h$ gives

$$r_h = -\frac{\gamma_o b k_n(\gamma_o b) + \frac{Z_b}{Z_o}[\gamma_o b k_n(\gamma_o b)]'}{-[-\gamma_o b k_n(-\gamma_o b)] + \frac{Z_b}{Z_o}[-\gamma_o b k_n(-\gamma_o b)]'} \tag{9.15}$$

For $\sigma \to \infty$ (large $\mathrm{Re}[\gamma]$) with $s = i\omega$ there results $Z_b \to 0$. With $Z_b = 0$ we have

$$r_h = \frac{\gamma_o b k_n'(\gamma_o b)}{[-\gamma_o b k_n'(-\gamma_o b)]} \tag{9.16}$$

corresponding to a perfectly conducting wall at r = b. For $s = i\omega$ and noting the conjugate symmetry of the $k_n$ functions

$$r_h = \frac{ik_o b k_n'(ik_o b)}{[-ik_o b k_n'(-ik_o b)]} \tag{9.17}$$

$$|r_h| = 1$$

Similarly if $\gamma_o = \gamma$ so that there is no added liner one can substitute from equation 8.76 and obtain

$$r_h = \frac{\gamma_o a k_n'(\gamma_o a)}{[-\gamma_o a k_n'(-\gamma_o a)]} \tag{9.18}$$

which also has magnitude 1 on the $i\omega$ axis. One can reference the reflection to r = b by defining

$$\rho_h \equiv -r_h \frac{[-\gamma_o b k_n'(-\gamma_o b)]}{\gamma_o b k_n'(\gamma_o b)} \tag{9.19}$$

For small $|\gamma_o b|$ the reflection coefficient reduces to

$$r_h = -\frac{(\gamma_o b)^{-n}[1 + O(\gamma_o b)] - \frac{Z_b}{Z_o} n(\gamma_o b)^{-n-1}[1 + O(\gamma_o b)]}{-(-\gamma_o b)^{-n}[1 + O(\gamma_o b)] - \frac{Z_b}{Z_o} n(-\gamma_o b)^{-n-1}[1 + O(\gamma_o b)]}$$

$$= (-1)^n[1 + O(\gamma_o b)] \tag{9.20}$$

$$\rho_h = (-1)^{n+1}[1 + O(\gamma_o b)]r_h$$

$$= -1 + O(\gamma_o b)$$

Note that this assumes that $|\gamma a|$ is also small. If d/a is also small then $Z_b$ from equations 8.79 is proportional to s cancelling one of the $\gamma_o b$ terms in the above expression for $r_h$.

For large $|\gamma_o b|$ the reflection coefficient reduces to

$$r_h = - \frac{e^{-\gamma_o b}[1 + O((\gamma_o b)^{-1})] - \frac{Z_b}{Z_o} e^{-\gamma_o b}[1 + O((\gamma_o b)^{-1})]}{-e^{\gamma_o b}[1 + O((\gamma_o b)^{-1}] - \frac{Z_b}{Z_o} e^{\gamma_o b}[1 + O((\gamma_o b)^{-1})]} \qquad (9.21)$$

Referenced to r = b we have

$$\rho_h = - \frac{1 + \frac{Z_b}{Z_o} \frac{[\gamma_o b k_n(\gamma_o b)]'}{\gamma_o b k_n(\gamma_o b)}}{1 - \frac{Z_b}{Z_o} \frac{[-\gamma_o b k_n(-\gamma_o b)]'}{[-\gamma_o b k_n(-\gamma_o b)]}} \qquad (9.22)$$

For large $|\gamma_o b|$ this is

$$\rho_h = - \frac{1 - \frac{Z_b}{Z_o}[1 + O((\gamma_o b)^{-1})]}{1 + \frac{Z_b}{Z_o}[1 + O((\gamma_o b)^{-1})]}$$

$$\simeq - \frac{1 - \frac{Z_b}{Z_o}}{1 + \frac{Z_b}{Z_o}} = \frac{Z_b - Z_o}{Z_b + Z_o} \qquad (9.23)$$

This result is the same as that for $\rho_e$ for large $|\gamma_o b|$. It is the result for a plane wave normally incident on a plane stratified structure with an impedance $Z_b$ at its front (input) surface.

For small d/a with a uniform liner with large $|\gamma a|$ (implied by large $|\gamma_o b|$) equations 8.26 and 8.78 give for both E and H waves

$$\frac{Z_b}{Z_o} = \frac{Z_b}{Z}\frac{Z}{Z_o} = z_b z_\ell \simeq \frac{Z}{Z_o}\frac{1 - e^{-2\gamma d}}{1 + e^{-2\gamma d}} \tag{9.24}$$

for large $|\gamma a|$ which is given by several alternative conditions, including large $\varepsilon$, $\mu$, $\sigma$, and $|\gamma_o a|$. The reflection coefficient for large $|\gamma_o a|$ for both E and H waves is

$$\rho \simeq -\frac{1 - \frac{Z_b}{Z_o}}{1 + \frac{Z_b}{Z_o}} \tag{9.25}$$

Consider some cases to obtain approximate forms for the reflection coefficients. First let $|\gamma_o d|\mu/\mu_o << 1$ with $\gamma_o$ imaginary and $\mu$ real. Let $\sigma >> |s|\varepsilon$ so that we have

$$\frac{Z_b}{Z_o} \simeq \nu\frac{d}{a}\frac{sa}{c}\frac{\mu}{\mu_o} = \frac{\mu}{\mu_o}\frac{sd}{c} = \frac{\mu}{\mu_o}\gamma_o d\nu$$

$$\nu = \frac{1}{\Gamma}\frac{1 - e^{-2\Gamma}}{1 + e^{-2\Gamma}} \tag{9.26}$$

$$\Gamma \simeq (1 + i)\left(\frac{|s|\mu\sigma}{2}\right)^{1/2} d \equiv (1 + i)\psi$$

with $\psi$ real. Then we have

$$\rho \simeq -\frac{1 - \frac{\mu}{\mu_o}\gamma_o d\nu}{1 + \frac{\mu}{\mu_o}\gamma_o d\nu}$$

$$= -1 + \frac{\mu}{\mu_o} 2\gamma_o d\nu + O\left(\left(\frac{\mu}{\mu_o}\gamma_o d\right)^2\right)$$

$$\simeq -1 + 2\frac{\mu}{\mu_o}\gamma_o d\nu \tag{9.27}$$

With $\gamma_o d$ positive imaginary the magnitude of $\rho$ is minimized for small $|\gamma_o d|$ by minimizing the imaginary part of $\nu$. As considered in section VIII (equations 8.44 through 8.51) for which we have the optimum choice of $\psi$, $\Gamma$, and $\nu$ as

$$\psi_o \simeq 1.127$$

$$\Gamma_o \simeq 1.127 + i\,1.127 \tag{9.28}$$

$$\nu_o \simeq .582 - i\,.417$$

For a given frequency one can choose an optimum conductivity from equations 9.26. The magnitude of the reflection coefficient is

$$|\rho| \simeq 1 + 2\frac{\mu}{\mu_o}|\gamma_o d|\,\mathrm{Im}[\nu] \tag{9.29}$$

which for optimum choice of conductivity gives

$$|\rho| \simeq 1 - .834\frac{\mu}{\mu_o}|\gamma_o d| \tag{9.30}$$

This shows that until $|\gamma_o d|\mu/\mu_o$ approaches 1 only small reductions of the reflection coefficient are achievable. Large $\mu/\mu_o$ lowers the frequency for which a certain reduction of $|\rho|$ is achievable but the most interesting case has $\mu = \mu_o$ since the reflection reduction (damping) structure should be sparse to avoid photon and electron collisions thereby precluding large volumes of magnetic materials.

Now let $|\gamma_o d| >> 1$ so that we also have $|\gamma d| >> 1$, at least on the $i\omega$ axis. Let $\sigma << |s|\varepsilon$ so that we have

$$\gamma = [s\mu(\sigma + s\varepsilon)]^{1/2} = s\sqrt{\mu\varepsilon}\left[1 + \frac{1}{2}\frac{\sigma}{s\varepsilon} + O\left(\left(\frac{\sigma}{s\varepsilon}\right)^2\right)\right]$$

$$Z = \left[\frac{s\mu}{\sigma + s\varepsilon}\right]^{1/2} = \sqrt{\frac{\mu}{\varepsilon}}\left[1 - \frac{1}{2}\frac{\sigma}{s\varepsilon} + O\left(\left(\frac{\sigma}{s\varepsilon}\right)^2\right)\right] \tag{9.31}$$

$$\frac{Z_b}{Z_o} \simeq \left(\frac{\mu}{\mu_o}\frac{\varepsilon_o}{\varepsilon}\right)\left[1 - \frac{1}{2}\frac{\sigma}{s\varepsilon}\right]\frac{1 - e^{-2s\sqrt{\mu\varepsilon}d}\; e^{-\sigma d\sqrt{\mu/\varepsilon}}}{1 + e^{-2s\sqrt{\mu\varepsilon}d}\; e^{-\sigma d\sqrt{\mu/\varepsilon}}}$$

In order to minimize $|\rho|$ one would like $Z_b/Z_o$ to approach 1. By constraining

$$\sqrt{\frac{\mu}{\varepsilon}} = \sqrt{\frac{\mu_o}{\varepsilon_o}} = Z_o \tag{9.32}$$

the coefficient of $Z_b/Z_o$ is nearly 1. By making $\sigma d Z_o$ large the exponential terms are made small. Note that we can still have $|\gamma d| >> 1$ and $\sigma << |s|\varepsilon$ under this condition. Then we have

$$\frac{Z_b}{Z_o} \simeq \left[1 - \frac{1}{2}\frac{\sigma}{s\varepsilon}\right][1 - 2e^{-2\gamma d} + O(e^{-4\gamma d})]$$

$$|e^{-\gamma d}| \simeq e^{-\sigma d Z_o} \tag{9.33}$$

and the reflection coefficient is

$$\rho \simeq \frac{1}{4}\frac{\sigma}{s\varepsilon} + e^{-\gamma d} \simeq \frac{1}{4}\frac{\sigma}{s\varepsilon} + e^{-2s\sqrt{\mu\varepsilon}d}\, e^{-\sigma d Z_o} \tag{9.34}$$

This last result confirms the need for small $\sigma/s\varepsilon$ and large $\sigma d Z_o$ in a proportion that makes the magnitudes of these two terms about the same. One would like large attenuation along the round trip path through the liner, but not with the disadvantage of a large change of $Z_b$ away from $Z_o$. In another form we have

$$\rho \simeq \frac{1}{4}\frac{\sigma d Z_o}{s\sqrt{\mu\varepsilon}d} + e^{-2s\sqrt{\mu\varepsilon}d}\, e^{-\sigma d Z_o} \tag{9.35}$$

so that for some large $|\gamma d| = |s\sqrt{\mu\varepsilon}d|$ one can estimate the size of $\sigma d Z_o$ to make the two terms have about equal magnitudes for imaginary s and real $\mu$, $\varepsilon$, and $\sigma$.

At high frequencies then one can achieve a small reflection coefficient. This is commonly achieved in anechoic chambers. However, at low frequencies a small reflection coefficient is difficult to achieve. In this section we have considered a uniform slab in front of a perfectly conducting wall. Other profiles are possible and some profiles would likely be better than the present uniform $\varepsilon$, $\mu$, $\sigma$ for minimizing reflections. Of course the optimum distribution functions for these parameters as a function of r are likely different in different

frequency bands. At high frequencies approximate techniques such as a WKBJ solution of Maxwell's equations are appropriate.

An interesting form of distribution for the constitutive parameters for r between b and a is

$$\vec{\vec{\sigma}} + s\vec{\vec{\varepsilon}} = y_r(r,s)\vec{e}_r\vec{e}_r + y_t(r,s)[\vec{\vec{I}} - \vec{e}_r\vec{e}_r]$$

$$s\vec{\vec{\mu}} = z_r(r,s)\vec{e}_r\vec{e}_r + z_t(r,s)[\vec{\vec{I}} - \vec{e}_r\vec{e}_r] \qquad (9.36)$$

where the identity dyadic is

$$\vec{\vec{I}} = \vec{e}_r\vec{e}_r + \vec{e}_\theta\vec{e}_\theta + \vec{e}_\phi\vec{e}_\phi \qquad (9.37)$$

This form of inhomogeneous anisotropic medium as the damping and reflection reduction liner still preserves the spherical symmetry of the cavity so that the E and H modes still have the same form as before for $r < b$ and do not couple to each other. For many practical cases one can simply use $\mu = \mu_o$ while $\sigma + s\varepsilon$ has the more general form in equations 9.36 where $y_r(r,s)$ and $y_t(r,s)$ are chosen so as to be approximately realizable by arrays of passive elements.

This general form of liner given by equations 9.36 needs to be considered in detail from the viewpoints of shifting the natural frequencies (damping resonances) and reducing reflection magnitudes. Given forms for $y_r(r,s)$ and $y_t(r,s)$ one needs to consider the approximation of these by arrays of discrete elements. Such arrays do not give the same results as continuous distributions and the differences between the two need to be quantified. Figure 9.2 indicates such a three dimensional array. If there is no mutual coupling between elements then $Y_r$ is directly associated with $y_r(r,s)$ for currents in the r direction and $Y_t$ is directly associated with $y_t(r,s)$ for transverse currents. Note that displacement current ($\vec{D}$) has to be added to the current through $Y_r$ and $Y_t$ when designing $Y_r$ and $Y_t$ to approximate the desired $y_r$ and $y_t$.

Note that the use of discrete elements in a damper array also complicates the calculation of the low frequency capacitance of the space system with respect to the test chamber. Some effective position of the surface of the liner can be calculated for such capacitance purposes.

In placing a liner inside a cavity the array of elements will need to allow for the wall curvature which will make the element spacing vary as one looks at different positions around

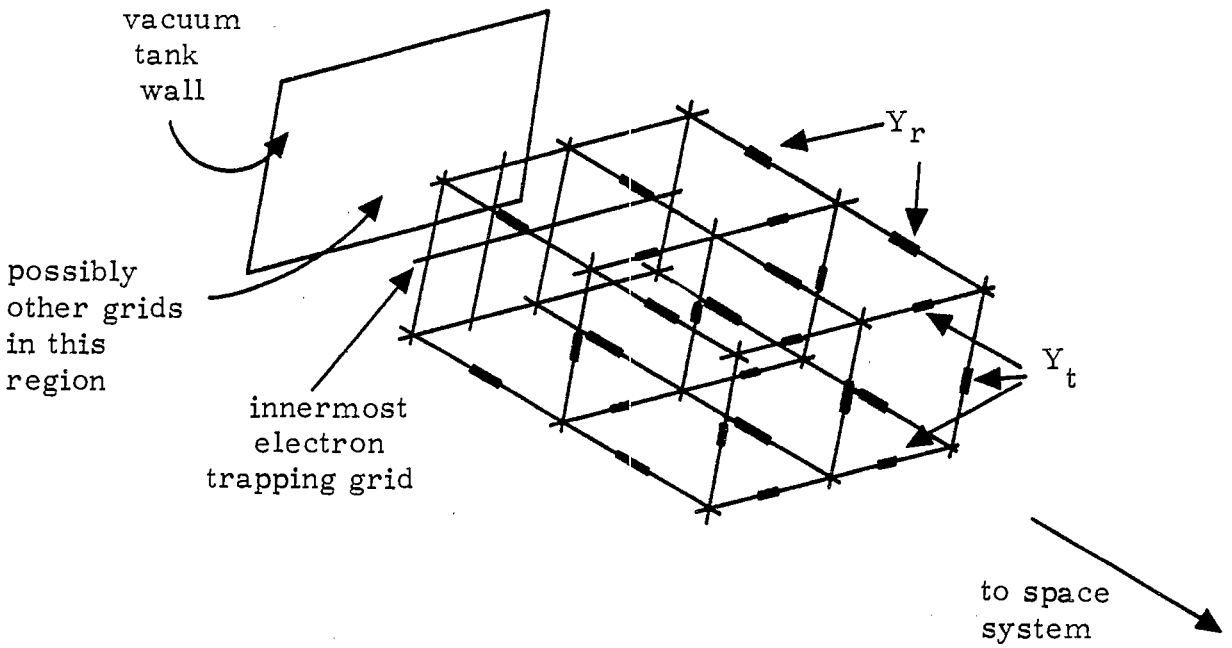


Figure 9.2 Three Dimensional Array of Admittances Connected to Innermost Electron Trapping Grid For Reflection Reduction and Damping of Resonances

the liner. The pattern of the element interconnections may also need to be changed at various locations to allow for this curvature. As the pattern and spacing change the element values $Y_r$ and $Y_t$ need to be changed so that $y_r(r,s)$ and $y_t(r,s)$ are correctly approximated. One should account for the shape of the small volume associated with each $Y_r$ and $Y_t$ so as to have the proper relation between the current density averaged over the appropriate cross section and the electric field. Note that the $Y_r$ and $Y_t$ elements should be small so as to minimize collisions of the photons and electrons from the space vehicle with these elements. These elements also need sufficient radiation hardness so that their circuit values do not appreciably change and noise signals are reasonably small. In some cases these elements might be simple resistive wire.

In a spherical cavity with the space system in the center, waves from the space system reflect back to the space system because of the symmetry. One might move the space system off center to reduce this reflection problem. Alternatively one might distort the cavity shape so as to break up any focusing action back toward the space system. Other cavity shapes such as finite circular cylinders, rectangular parallelepipeds, and ellipsoids are then of interest. The damper design may become more complex in some of these geometries. Various such problems need to be considered in detail so as to optimize the test chamber design.

## X. Inclusion of Some Other Nuclear and Space Environmental Effects and Instrumentation in the Simulator

There are various requirements on the design of a simulator for the system generated EMP on space systems besides those associated with the quality of the EMP environment generated. The space system has to be able to function in its normal operational configuration. This implies various features for the simulator facility depending on each specific space system. For power some space systems depend on solar energy so the simulator should have light with an appropriate spectrum illuminating the solar panels. Normal operational telemetry is also needed so that the space system can function as designed. This presents special problems for telemetry antennas near the tank walls and reflections of the telemetry signals from various parts of the simulator.

The space system needs to be positioned properly with respect to the incident photons. This requires special insulating supports which do not significantly interact with the photon and electron environment. Such dielectric supports must be rather sparse. The temperature (and associated heat flow) appropriate to the space system configuration needs to be achieved. This is also influenced by the space vacuum conditions being simulated. As discussed previously the vacuum conditions are important for the electron transport; likewise the earth's magnetic field is also important.

There are various other nuclear effects that one might include in a system generated EMP simulator. One might include late arriving particles (compared to photons) such as neutrons, electrons, and other charged and neutral particles. These would be provided by separate sources near the photon source and would be time tied to the photon source to have the various particle fluxes arrive at the proper times relative to the other particles and with the proper waveforms. One might also include the low energy photons in what is considered the thermal range as an appropriate thermal flash with a special generator.

Instrumentation is important both for simulator performance and space system response. Electromagnetic fields and related electromagnetic quantities can be monitored near the innermost electron trapping grid and vacuum tank wall without too much difficulty, although transformers with high voltage insulation may be needed in some cases. For monitoring currents and charges on the space system one needs telemetry for transmitting pulse waveforms using an appropriate modulation scheme. Such a telemetry channel or channels must operate without significant errors right through the pulse. In other words it must be radiation hard. Furthermore the portions of such a telemetry link on the space system must be small enough and so

configured that they do not significantly affect the electromagnetic response of the space system and in particular those quantities being measured. Other instrumentation includes monitors on the performance of the photon pulser and sensors for the photon environment produced. Various recording instruments and associated recording and control rooms (or other substitutes) are also needed.

## XI. Overall Simulator Geometry

Having considered many features of this type of system generated EMP simulator, some in more detail than others, let us consider what such a simulator might look like from an overall viewpoint. There are some features which constitute large portions of such a simulator. First there is the test chamber consisting of vacuum tank, electron and photon trapping structures, and damping and reflection reduction structures. The space system is placed roughly in the center of this test chamber. Second there is a pulsed photon generator. If a point source type of photon generator is used a conical volume is needed to expand the photons into the test volume. A distributed source photon generator can be placed right next to the test chamber without a large extension as in the case of the point source. Of course one might construct a point source with conical extension and later convert it to a distributed source with lower photon energy and perhaps use the conical extension of the vacuum tank to house the distributed source photon generator. One might also have two photon generators, say with different photon spectra, connected onto the test chamber from two different directions. These pulse generators might be used for separate tests. Note that an entry position into the test chamber is needed to take in and remove the space system. There may also be several electron pulse generators around the boundary of the test chamber for replacing electrons (at a later time) lost from the test volume to the test chamber walls.

Various supporting features, some of it rather large, are also needed. Coils with power supplies of some type are needed around the vacuum tank to control the simulation of the earth's magnetic field in the test chamber. One or more instrumentation rooms are needed for controlling the photon pulser, simulated earth's magnetic field, vacuum in the test chamber, solar power to the space system, etc. The space system normal operating functions need to be monitored and associated telemetry provided. This instrumentation room or rooms must also record various transient test data for both the simulator and the space system. Part of the overall simulator structure might be large mechanical supports for various items. There is also a large vacuum pump system to be included. Radiation shielding is also needed for personnel safety.

There are some optional items that one might include in such a simulation facility. Some of these could be for simulating other nuclear effects. These might involve very low energy photons, electrons, neutrons, etc. One might be wary of introducing neutrons, however, due to the associated activation problem.

Figure 11.1 shows a few options for the overall simulator layout including the test chamber, pulser, space system entry, and instrumentation (and control) room(s). As figure 11.1A

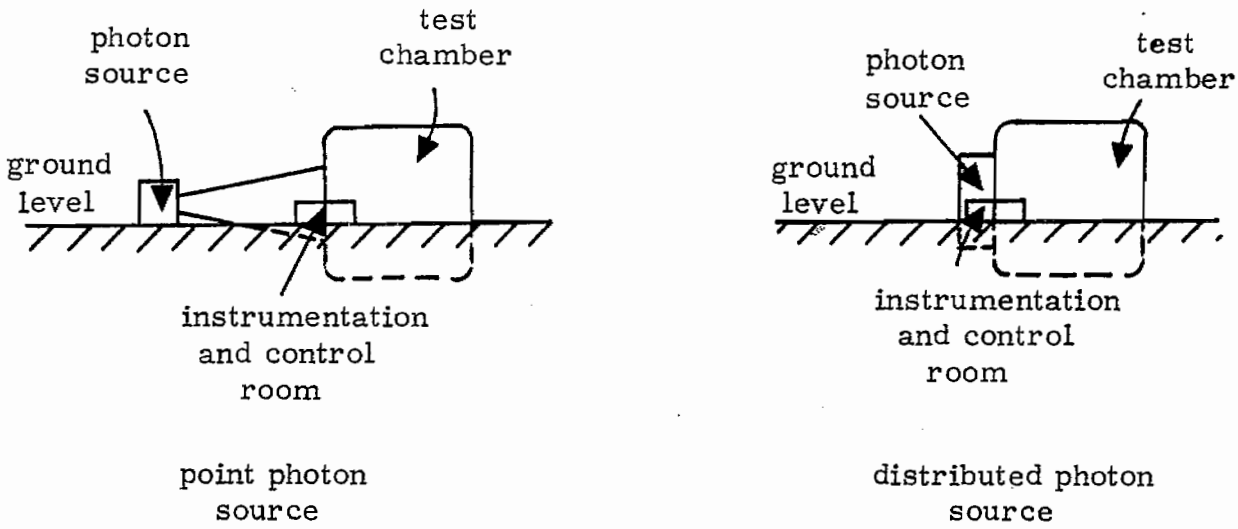


A. Photons propagating horizontally

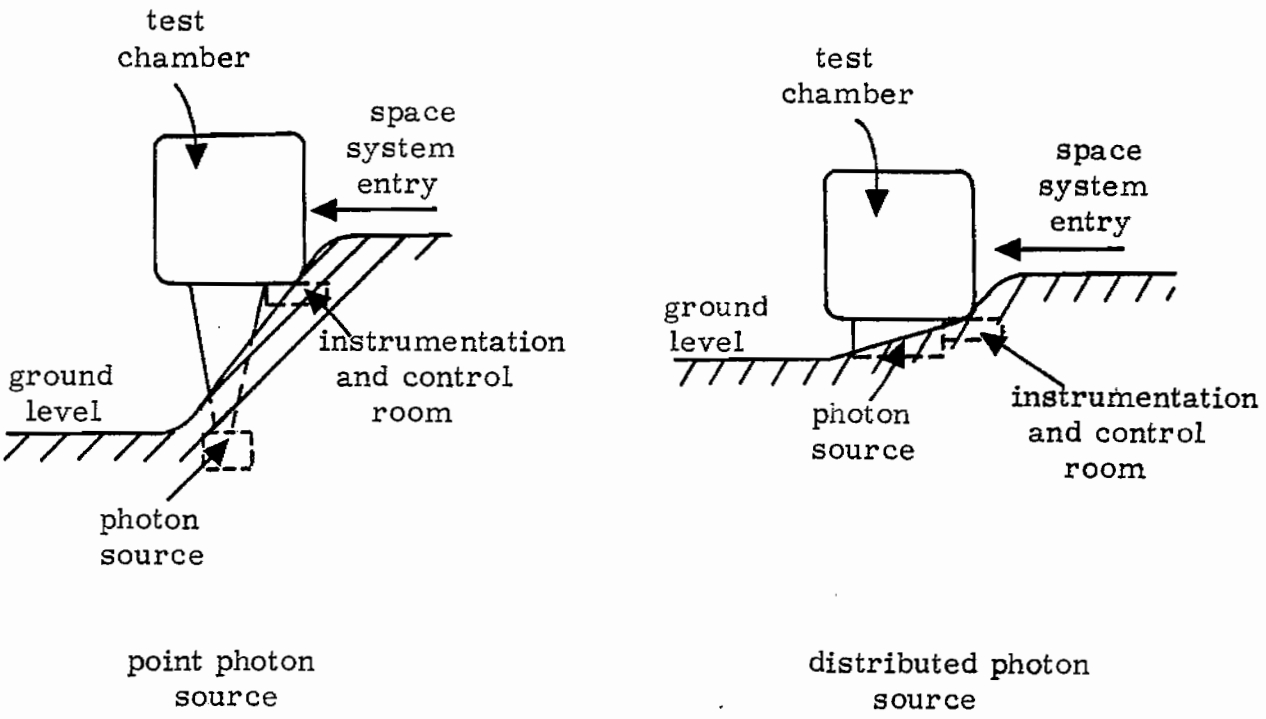


B. Photons propagating vertically

Figure 11.1 Some Overall Configurations for the Simulator

indicates one might have the direction of photon travel parallel to the earth surface. With the simulator laid out like this, other photon machines can be added which also propagate photons parallel to the earth toward the space system, but at some angle other than that of the first photon machine with respect to the test chamber and space system. If there is a single instrumentation and control room it could be placed adjacent to the test chamber at a position which minimizes its distance to the main photon pulser.

As indicated in figure 11.1B one might have the direction of photon travel upward away from the earth surface. In such a configuration one might place the simulator on the side of a hill so that the pulser, instrumentation and control room, and space system entry into the test chamber could take place on different levels, all of which would have access to earth surface on their own levels. Additional photon pulsers can be added which propagate photons horizontally. Such pulsers could be placed on a level about the same as the center of the test volume so as to have ready access from the earth surface on the hillside.

## XII. Summary

This type of simulator for the system generated EMP is quite different from the common EMP simulators which do not have nuclear radiation as part of the environment. Its major components are a pulsed photon source (with appropriate collimation) and a test chamber which should not significantly backscatter photons and electrons (in which respect it is partially a large vacuum tube) and should not significantly alter the space system response to the system generated EMP (in which respect it is partially an anechoic chamber). There are many detailed design calculations needed to optimize the various electromagnetic characteristics of this type of simulator; this note considers some of these calculations. There are other design details to be considered in depth which are not linear classical electromagnetics such as nuclear radiation transport, atomic physics, and nonlinear interaction of electrons (and other charged particles) with the system generated EMP fields.

There is considerable flexibility in the simulator design in the sense that there are alternative designs of pulsers, test chamber shape, and physical layout in connecting the various major parts together. Such a simulator also can be modified after its initial construction in that new radiation pulsers can be added or changed at later times.

The present note deals with simulation of the system generated EMP on space systems such as satellites. The techniques discussed here can be modified to apply to EMP simulation for nuclear source regions in air. In such a case one still needs a pulsed photon machine but the test chamber design and the required air density are somewhat different, but similar considerations in the test chamber design are still required.[1]

## XIII. References


1. Carl E. Baum, Sensor and Simulation Note 151, EMP Simulators for Various Types of Nuclear EMP Environments: An Interim Categorization, July 1972.

2. Capt Carl E. Baum, Interaction Note 76, Electromagnetic Pulse Interaction Close to Nuclear Bursts and Associated EMP Environment Specification, July 1971.

3. W. J. Karzas and R. Latter, Theoretical Note 27, Electromagnetic Radiation from a Nuclear Explosion in Space, October 1961.

4. B. R. Suydam, Theoretical Note 86, Electromagnetic Signal from a Bomb Burst in Vacuo, August 1959.

5. S. Glasstone, ed., The Effects of Nuclear Weapons, gov't printing office, 1964.

6. Conrad L. Longmire, Theoretical Note 124 (including classified appendix), External System Generated EMP on Some Types of Satellite Structure, August 1971.

7. R. P. Feynman, R. B. Leighton, and M. Sands, The Feynman Lectures on Physics, vol. 1, Addison Wesley, 1966, pp. 41-47.

8. M. Abramowitz and I. A. Stegun, ed., Handbook of Mathematical Functions, AMS 55, National Bureau of Standards, 1964.

9. R. D. Evans, The Atomic Nucleus, McGraw Hill, 1955, chapters 23 through 25.

10. Capt Clovis R. Hale, ed., Theoretical Note 121, A Review of Internal EMP Technology, April 1971.

11. Lt Jerry A. Sawyer, Calculation of High-Energy Secondary Electron Emission, AFSWC-TDR-63-50, August 1963.

12. T. H. Martin, K. R. Prestwich, and D. L. Johnson, Radiation Production Note 3, Summary of the Hermes Flash X-Ray Program, October 1969.

13. L. G. Kelly, L. D. Posey, and J. A. Halbeib, A Magnetic Compton Spectrometer for High Intensity Pulsed Gamma-Ray Environments, IEEE Trans. on Nuclear Science, NS-18 no. 1, February 1971, pp. 131-141.

14. L. D. Posey, private communication, November 1971.

15. Lt Carl E. Baum, Sensor and Simulation Note 15, Radiation and Conductivity Constraints on the Design of a Dipole Electric Field Sensor, February 1965.

16. Lt Carl E. Baum, Sensor and Simulation Note 21, Impedance and Field Distributions for Parallel Plate Transmission Line Simulators, June 1966.

17. W. R. Smythe, Static and Dynamic Electricity, 3rd ed., McGraw Hill, 1968, chapter V.

18. Capt Carl E. Baum, Sensor and Simulation Note 38, Parameters for Some Electrically-Small Electromagnetic Sensors, March 1967.

19. Capt Carl E. Baum, Sensor and Simulation Note 125, Some Characteristics of Electric and Magnetic Dipole Antennas for Radiating Transient Pulses, January 1971.

20. Carl E. Baum, Interaction Note 88, On the Singularity Expansion Method for the Solution of Electromagnetic Interaction Problems, appendix B, December 1971.

21. J. A. Stratton, Electromagnetic Theory, McGraw Hill, 1941, chapter IX.